

N O T I C E

THIS DOCUMENT HAS BEEN REPRODUCED FROM
MICROFICHE. ALTHOUGH IT IS RECOGNIZED THAT
CERTAIN PORTIONS ARE ILLEGIBLE, IT IS BEING RELEASED
IN THE INTEREST OF MAKING AVAILABLE AS MUCH
INFORMATION AS POSSIBLE

PHASE I OF THE NEAR TERM
HYBRID PASSENGER VEHICLE DEVELOPMENT
PROGRAM

(NASA-CR-163225) PHASE I OF THE NEAR TEAM
HYBRID PASSENGER VEHICLE DEVELOPMENT
PROGRAM. APPENDIC C: PRELIMINARY DESIGN
DATA PACKAGE. VOLUME 2: APPENDICES Final
Report (Fiat Research Center) 124 p

N80-28251

Unclas
G3/85 22368

FINAL REPORT

APPENDIX C: PRELIMINARY DESIGN DATA PACKAGE

Volume II: Appendices

Prepared for
JET PROPULSION LABORATORY
by
CENTRO RICERCHÉ FIAT S.p.A.
Orbassano (Turin) - ITALY



The research described in this publication represents the third of the several Tasks of the "Phase I of the Near Term Hybrid Passenger Vehicle Development Program" being carried-on by Centro Ricerche FIAT (CRF) on Contract No. 955187 from the Jet Propulsion Laboratory, California Institute of Technology.

Turin, September 11, 1979

This Report, prepared by:

R. Piccolo of CRF

has been issued in conformance to the following specifications:

JPL Contract No. 955187

Exhibit No. I Jan 16, 78

Exhibit No. II Dec. 1, 77

Contract Documentation - Phase I

Data Requirement Description No. 3

LIST OF CONTENTS

A.1 APPENDICES (SECTION 1: BACKGROUND INFORMATION)

Subcontractors Final Report on the Phase I

A.1-1	Brown Boveri & Cie A.G.	
	Final Report No. ZFL/L1/Mar., July 19, 1979	Page A.1-1
A.1-2a	(Fabbrica Italiana) Magneti Marelli S.p.A.	
	Final Report No. 0566, July 13, 1979	Page A.1-12
A.1-2b	(Fabbrica Italiana) Magneti Marelli S.p.A.	
	Final Report No. 103, July 21, 1979	Page A.1-18
A.1-3	Pininfarina S.p.A.	
	Final Report No. CS 167/79, May 24, 1979	Page A.1-32
A.1-4	(Industrie) Pirelli S.p.A.	
	Final Report No. RT 143, May 24, 1979	Page A.1-51

A.3 APPENDICES (SECTION 3: METHODOLOGY DESCRIPTION)

A.3-1	HANDLING Computer Simulation Model	Page A.3-1
A.3-2	CURVMAGN Computer Simulation Model	Page A.3-49
A.3-3	CURVMAGNCAR Computer Simulation Model	Page A.3-50
A.3-4	PRESTMCC Comput : Simulation Model	Page A.3-51

LIST OF TABLES

Table A.1-1.1	Time Schedule for the Na-S Battery Production	Page A.1-10
---------------	---	-------------

LIST OF FIGURES

Fig. A.1-1.1	Experimental Battery with 96 Cells	Page A.1-3
" A.1-1.2	Vertical Acceleration in Relation to Frequency Car Speed: 60 km/h on Macadam Road	" A.1-5
" A.1-1.3	Specific Power in Relation to Discharge Time of a Cell	" A.1-6
Fig. A.1-2.1	Battery Sizes	Page A.1-14
" A.1-2.2	Maximum Power vs Useable Specific Energy as a Function of Average Power	" A.1-16
" A.1-2.3	Armature Chopper Electric Diagram	" A.1-20
" A.1-2.4	Power Control Logic Block Diagram	" A.1-22
" A.1-2.5	Armature Chopper Electric Diagram Regenerative Braking Configuration for Speeds Greater than the Basic one	" A.1-24
" A.1-2.6	Armature Chopper Electric Diagram Regenerative Braking Configuration for Speeds Lower than the Basic One	" A.1-25
" A.1-2.7	Armature and Field Chopper Circuit	" A.1-28
" A.1-2.8	Battery Charger Circuit	" A.1-30

Fig. A.1-3.1	Body Shape - The First Solution	Page A.1-33
" A.1-3.2	Body Shape - The Selected Solution	" A.1-34
" A.1-3.3	Body Shape - Side View	" A.1-36
" A.1-3.4	Body Shape - Front and Rear Views	" A.1-37
" A.1-3.5	Body Shape - Three Quarter Front and Rear Views	" A.1-38
" A.1-3.6	Body Shape - Typical Sections	" A.1-39
" A.1-3.7	Hood/Wing Section on Front Wheel Center Line (Disregarding Shock-Absorber)	" A.1-40
" A.1-3.8	Hood Trailing Edge/Lower Windshield Section (at Side of Air Intake)	" A.1-41
" A.1-3.9	Upper Windshield Center Section	" A.1-42
" A.1-3.10	"A" Pillar Section	" A.1-43
" A.1-3.11	Front Door Lower Pillar Section	" A.1-44
" A.1-3.12	Lower Center Pillar Section	" A.1-45
" A.1-3.13	Sill/Rocker Panel & Lower Door Edge Section	" A.1-46
" A.1-3.14	Roof/Upper Door Edge Section	" A.1-47
" A.1-3.15	Fifth Door Side Section	" A.1-48
" A.1-3.16	Rear Wing Section on Rear Wheel Center Line	" A.1-49
" A.1-3.17	Fifth Door Center Section	" A.1-50

Fig. A.1-4.1	Dynamic Vertical Stiffness vs Speed for Two Different Tires	Page A.1-53
" A.1-4.2	Inflation Pressure Effect on Rolling Resistance Coefficient	" A.1-54
" A.1-4.3	Time Evolution of Cornering Stiffness/ Vertical Load Ratio for Different Tire Type	" A.1-56
" A.1-4.4	Tire Radius Effect Rolling Resistance Coefficient	" A.1-58
" A.1-4.5	Rolling Resistance Coefficient vs Year as a Function of Ply Tire Type	" A.1-59
" A.1-4.6	Rolling Resistance Coefficient vs Speed for Different Vehicles	" A.1-61
" A.1-4.7	Cornering Stiffness Characteristics for Hybrid Vehicle Tires	" A.1-63

APPENDIX A.1-1

HYBRID VEHICLE SODIUM-SULPHUR-BATTERY

Contribution of BBC for JPL Hybrid Vehicle

Contract No. 955187

K. Liemert

Brown Boveri & Cie A.G.

Central Research Laboratory, Heidelberg

1. INTRODUCTION

Na-S/batteries, when fully developed, are believed to be suitable for the propulsion of electric vehicles because of

- High energy density (Wh/kg and Wh/l)
- High power density (W/kg and W/l)
- Low price
- High cycle life
- High availability of the reactants.

A Na-S/battery consists of many series-parallel connected cells, a heat insulation and a temperature control system. A single cell contains the two molten reactants Sodium and Sulphur (or Na_2S_x if discharged), the beta-alumina solid electrolyte tube separating the reactants and the cell case. The operating temperature amounts to 285 °C to 350 °C. The design and the problems of Na-S/cells and Na-S/batteries are described in more detail in (1) (*).

2. STATE OF DEVELOPMENT

Our present cells show the following characteristics:

Length of ceramic tube:	200 mm
Ceramic outer diameter:	25 mm
Length of the cell:	235 mm
outer diameter of the cell:	37 mm
Cell weight:	460 g
Capacity:	40 Ah
Open circuit voltage:	2 V
Internal resistance:	≤ 25 m
Maximum current:	40 A

(*) Numbers in parentheses designate Reference at end of section.

Maximum power:	40 W
Energy at maximum power:	40 Wh
Current at 5 hours discharge:	8 A
Power at 5 hours discharge:	14.4 W
Energy at 5 hours discharge:	72 Wh
Efficiency ($E_{out} : E_{in}$) at 10 hours charge:	0.88

A battery with 96 of an earlier type of cells has been built (Fig. A.1-1.1) (2).

The performance of the battery was as expected from single cell experiments. Batteries with the new type of cells will be built and tested in 1979/80. Further efforts will be directed towards improving the following properties:

- Life cycle of single cells
- Electrolyte tube and cell dimensions
- Safety
- Energy and power density
- Efficiency of heat insulation
- Advanced technology for mass production.

3. Na-S BATTERY FOR A HYBRID VEHICLE

The dimensions for a battery to be installed between the back wheels of a hybrid vehicle should not exceed the following dimensions:

Length:	900 mm
Width:	1200 mm
Height:	400 mm

The following electrical data should be achieved:

Peak power:	≥ 32 kW for 1 minute
Power:	15 kW for 10 minutes
Open circuit voltage:	≤ 84 V

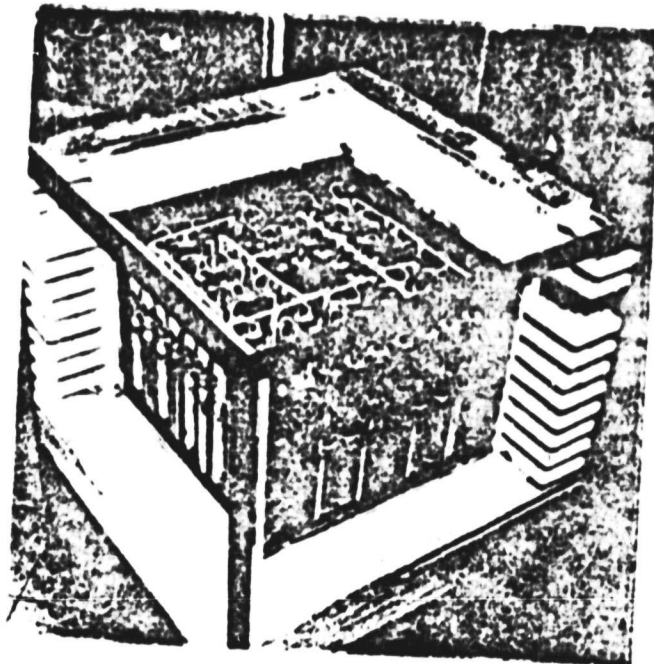


FIG. A.1 - 1.1 - EXPERIMENTAL BATTERY WITH 96 CELLS

ORIGINAL PAGE IS
OF POOR QUALITY

The weight should not exceed 300 kg.

If possible the battery should contain 12 separate strings. The connections for the different strings should be leaded separately to the outside of the battery and it should be possible to switch them off after charging or discharging.

The battery has to resist the normal stress which occurs during operation of the vehicle.

The normal accelerations during operation at the car do not exceed 1 g as can be seen from Fig. A.1-1.2 (3).

4. BATTERY DESIGN FOR THE HYBRID VEHICLE

4.1 Cell

The cell design for the hybrid vehicle battery is based on the cell described in chapter 2.

The dimensions of the cell were chosen in a way that high power density results at low discharge times of less than one hour (curve Δ of Fig. A.1-1.3).

By extrapolation of the cell data mentioned above, which have been already achieved and by assuming that a slight improvement with respect to internal resistance can be attained ($2 \Omega \text{ cm}^2$) the following data for a hybrid vehicle cell will be obtained:

Length of ceramic tube:	250 mm
Outer diameter of ceramic tube:	25 mm
Length of the cell:	285 mm
Outer diameter of the cell:	37 mm
Cell weight:	560 g
Capacity:	52.5 Ah
Open circuit voltage:	2 V
Internal resistance:	13.3 m Ω
Maximum current:	75 A
Maximum power:	75 W

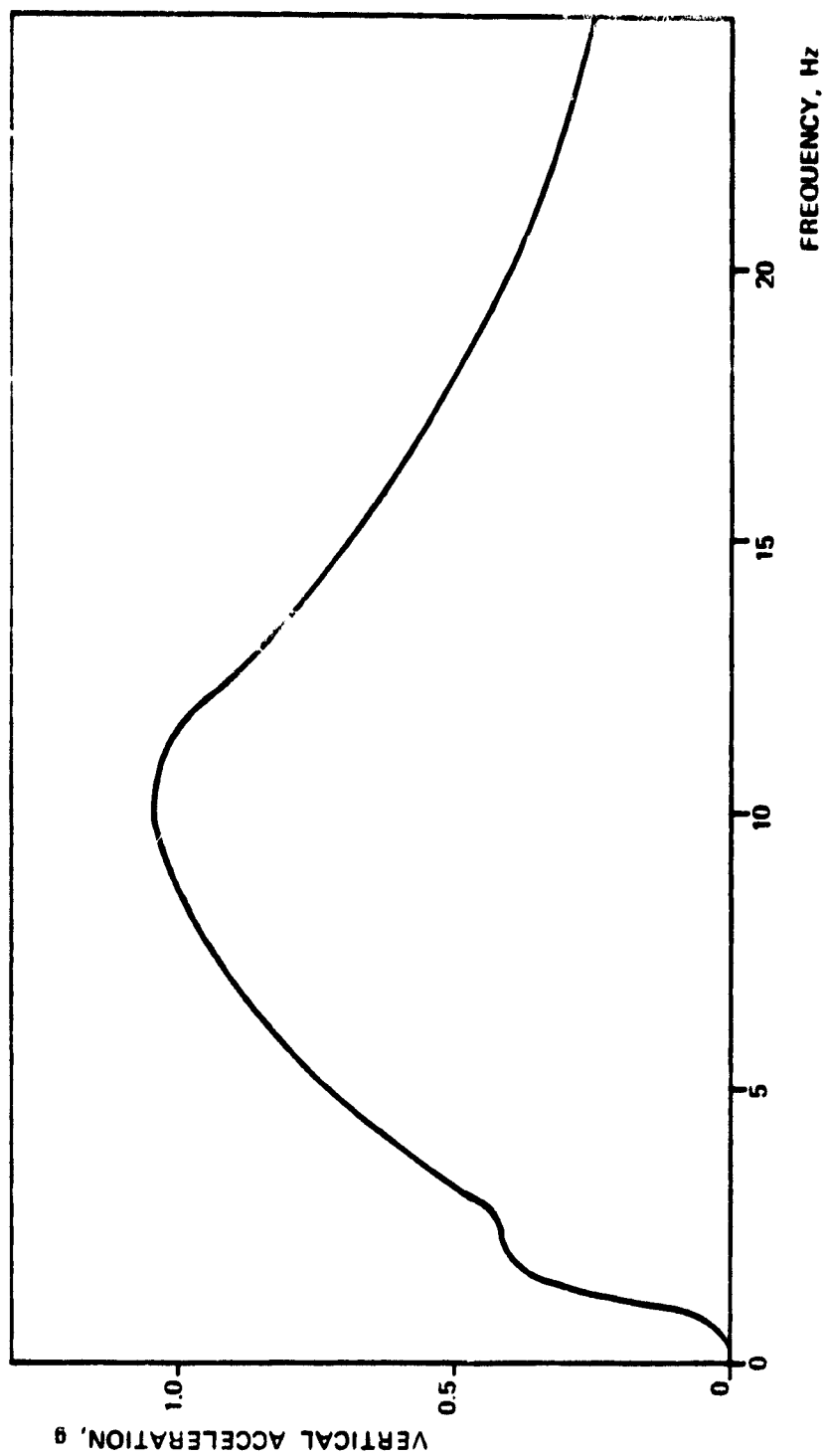


FIG.A.1-12 - VERTICAL ACCELERATION IN RELATION TO FREQUENCY.
CAR SPEED: 60 km/h ON MACADAM ROAD

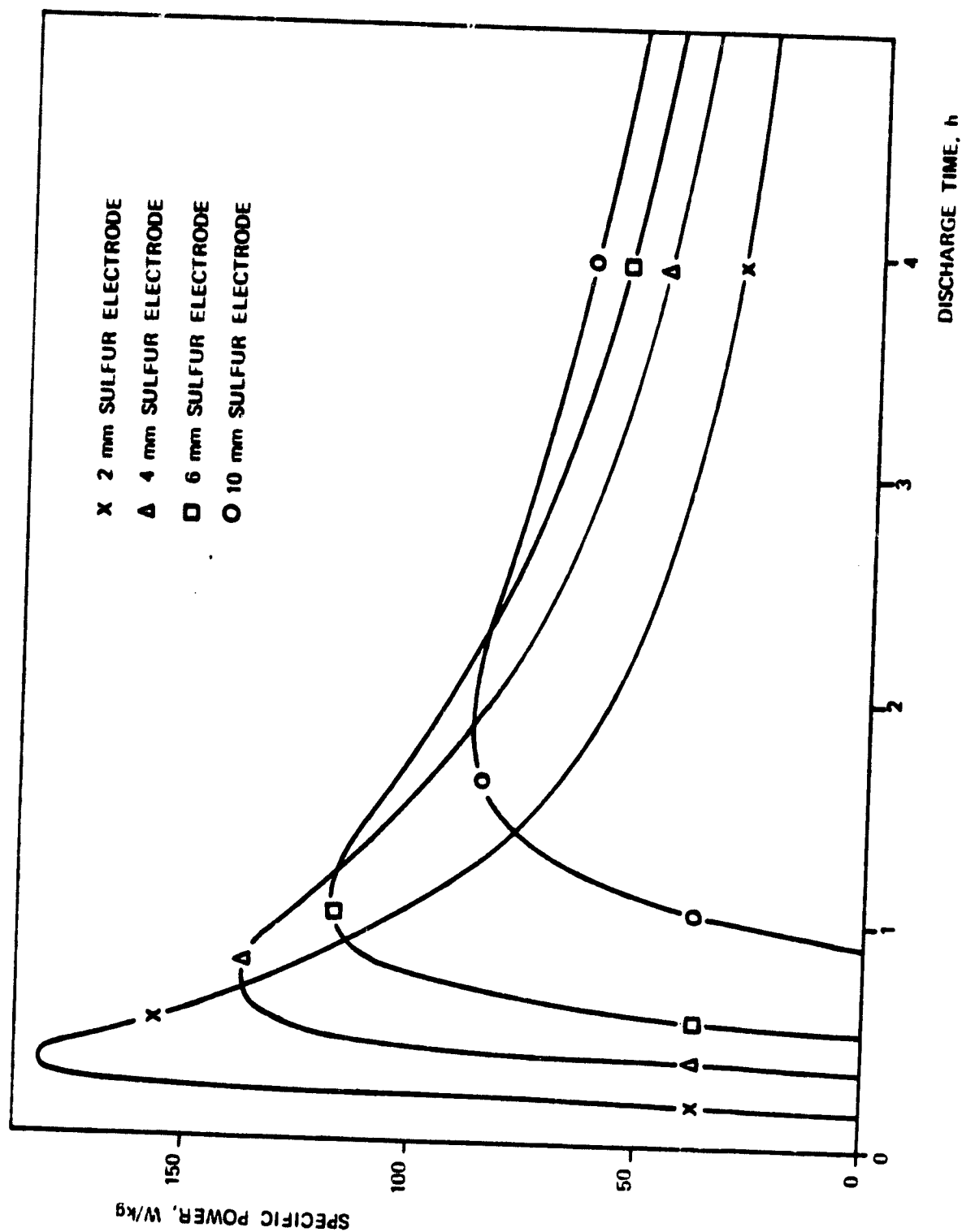


FIG.A.1-1.3 - SPECIFIC POWER IN RELATION TO DISCHARGE TIME OF A CELL

Discharge time at max. power:	0.7 h
Energy at max. power:	52.5 Wh
Efficiency ($E_{out} : E_{in}$) at charging times of about 10 hours:	0.45
Current at 5 hours discharge:	10.5 A
Power at 5 hours discharge:	19.5 W
Operating voltage at 5 hours discharge:	1.86 V
Energy at 5 hours discharge:	97.7 Wh

4.2 Battery

The battery consists of 24 modules. Each module contains 18 series connected cells. Two series connected modules form a string. The battery consists of 12 strings. By parallel connection of these strings a battery with the following data will be obtained:

Number of cells:	432
Length:	900 mm
Width:	1100 mm
Height:	400 mm
Weight overall:	320 kg
Capacity:	630 Ah
Open circuit voltage:	72 V
Internal resistance:	39.9 m Ω
Maximum current:	900 A
Maximum power:	32.4 kW
Operating voltage:	36 V
Energy at max. power:	22.7 kWh
Discharge time at max. power:	0.7 h
Efficiency ($E_{out} : E_{in}$) at charge time \geq 10 hours:	0.45
Maximal charging voltage:	105 V
Two hours current:	315 A

Two hours power:	18.7 kW
Operating voltage	59.4 V
Two hours energy:	37.4 kWh
Efficiency ($E_{out} : E_{in}$) at charge time \geq 10 hours:	0.75
Five hours current:	126 A
Five hours power:	8.4 kW
Operating voltage:	67.0 V
Five hours energy:	42.2 kWh
Efficiency ($E_{out} : E_{in}$) at charge time \geq 10 hours:	0.9

4.3 Insulation

The double walled casing of the battery containing the heat insulation between the walls consists of two parts. Both parts are fixed at the rack of the vehicle. The battery is designed such that the upper part has a super insulation and is welded to the rack of the vehicle. The lower part bears the modules.

Conventional insulation is used for the lower case. This part can be disconnected from the rack for maintenance purposes.

The replacement of module can be performed in a few minutes. The casing with the insulation is necessary to keep the battery at operating temperature for a period of time of approximately 24 hours during which the battery might not be charged or discharged. If the battery is not operated for several days it must be heated up before utilization.

5. SAFETY

The most severe hazard for a cell is cracking of the electrolyte tube. Cells have been in operation the outer casing of

which remained undestroyed when such a case occurred. However further safety tests are necessary to get statistical evidence for a high probability to have save cells.

Shock tests with single cells have shown that no damage occurs up to accelerations of 150 g.

Safety tests with complete batteries will be performed in the next years. This tests include experiments concerning failure propagation in the battery and severe accidents where the battery casing and cell casings are mechanically destroyed.

6. LIFE CYCLE

Our present cells have been operated up to 400 cycles. The average life cycle amounts to 250 cycles. It is expected that the average life cycle can be increased to 600 cycles in 1986 and more than 1000 cycles in the nineties.

7. BATTERY PRICES

Mass production is scheduled to start in 1986. According to our present estimations a battery price of approximately 10000 to 15000 DM may be achieved at this time.

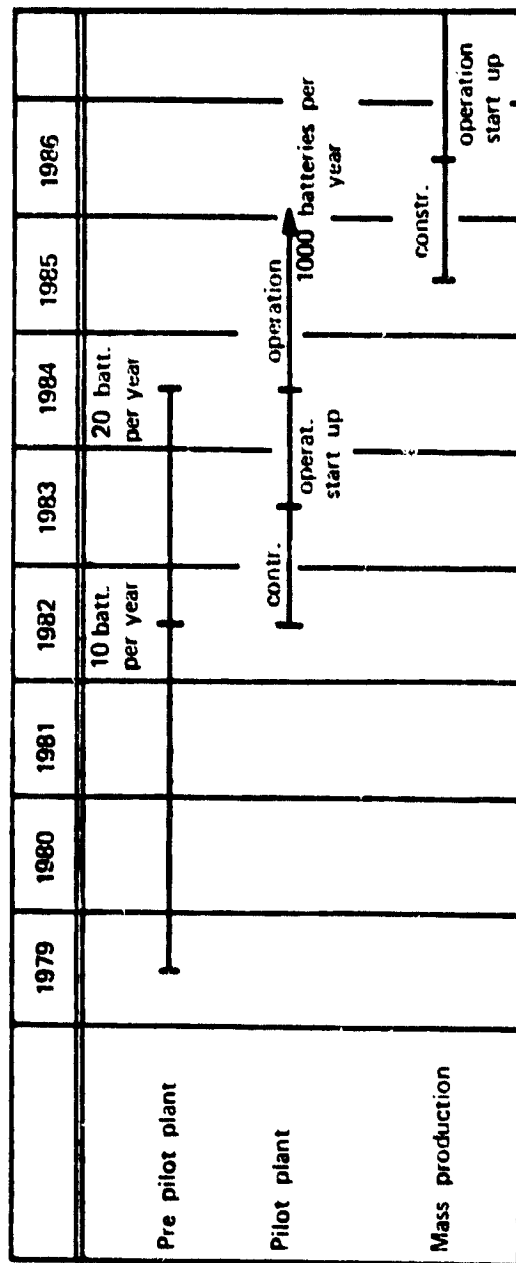
It is expected that this price will decrease in the nineties to a value between 5000 and 8000 DM.

8. MANUFACTURABILITY

We expect that the pilot plant production can be started in 1984 and that the mass production can be started in 1986.

The following Table A.1-1.1 shows the time schedule for the Na-S battery production.

TABLE A.1-1.1- TIME SCHEDULE FOR THE Na/S BATTERY PRODUCTION



LITERATURE

- (1) W. Fischer u. B. Hartmann:
Die Natrium/Schwefel-Batterie. Ein Speicher für die Elektrotraktion und den Spitzenlastausgleich. ASR-Digest für angewandte Antriebstechnik, Heft Sept. 1978, 6. Jahrgang.
- (2) W. Fischer und H. Meinhof:
Neue Ergebnisse mit Natrium/Schwefel-Batterie und Aspekte für ihren praktischen Einsatz. Elektrische Energie-Technik; 24. Jahrgang, 1979, Nr. 1.
- (3) Information of FIAT, Febr. 1979.

APPENDIX A.1-2

A.1-2a Final Report No. 0566 July 13, 1979

A.1-2b Final Report No. 103 July 21, 1979

SUBCONTRACT MAGNETI MARELLI - CRF

UNDER JPL CONTRACT No. 955187

"NEAR TERM HYBRID PASSENGER VEHICLE DEVELOPMENT PROGRAM"

PHASE I

1. INTRODUCTION

For the purposes of the "JPL" Hybrid Vehicle project, Magneti Marelli has made available to FIAT, the leader of the group, its direct experience in the field of electrochemical accumulators.

This report summarizes the position in June 1979 concerning the choice made from the range of batteries suitable to the requirements, and discusses some of their electrical characteristics which can now be achieved on a large scale production basis.

In the light of results obtained in the laboratory on technical cells, the report forecasts the results obtainable using the same battery types, by 1985.

2. CHOICE OF THE BATTERY

The first type of battery to be considered was the Lead-Acid one, partly because we are familiar with this type but mainly because today it is one of the very few road traction battery systems produced industrially and therefore available at a competitive price and a known degree of produced reliability. Its design characteristics are by now so "firm" that the Lead-Acid battery is virtually the point of reference for all other types in more or less advanced stages of development.

Magneti Marelli has also started to develop the Nickel-Zinc type, after carefully investigating the possibilities of achieving performance levels clearly superior to those of the Lead-Acid type, in the near term and within a reasonable investment of resources.

3. LEAD-ACID BATTERY

Among the various types available for the "JPL" project, the one considered was a polypropylene monobloc battery specially designed for electrically-propelled road vehicles weighing less than 2 t approximately.

3.1. Physical characteristics

The space occupied (see Fig. A.1-2.1) is much the same as that of the Golf Cart type of battery and the present weight, 29 kg approximately, enables the battery to readily moved by one person using the special handgrips provided in the cover.

Also in the cover is a system of channels which, when the modules of the complete vehicle battery are connected together, enable the gases released to be suitably vented. This avoids the heavy corrosion which normally occurs in the battery container due to the out flow of sulphur and caused by the escaping gas, and to release safely the explosive H_2/O_2 mixture through a unique exit equipped with a flame interruption device.

The same channels can be used to top up the cells with distilled water. The construction of the cover is such that the ingress of water into a given cell is stopped once the desired level is reached; in this way all cells have the same electric level when the topping-up operation is complete.

3.2. Electrical characteristics

The 12V (nominal) battery module has a nominal capacity of 90 Ah when discharged in 5 hours; its nominal specific discharge energy at this rate is therefore 37 Wh/kg approximately.

Maximum specific power is 140 W/kg approximately and the duration is therefore about 400 effective cycles.

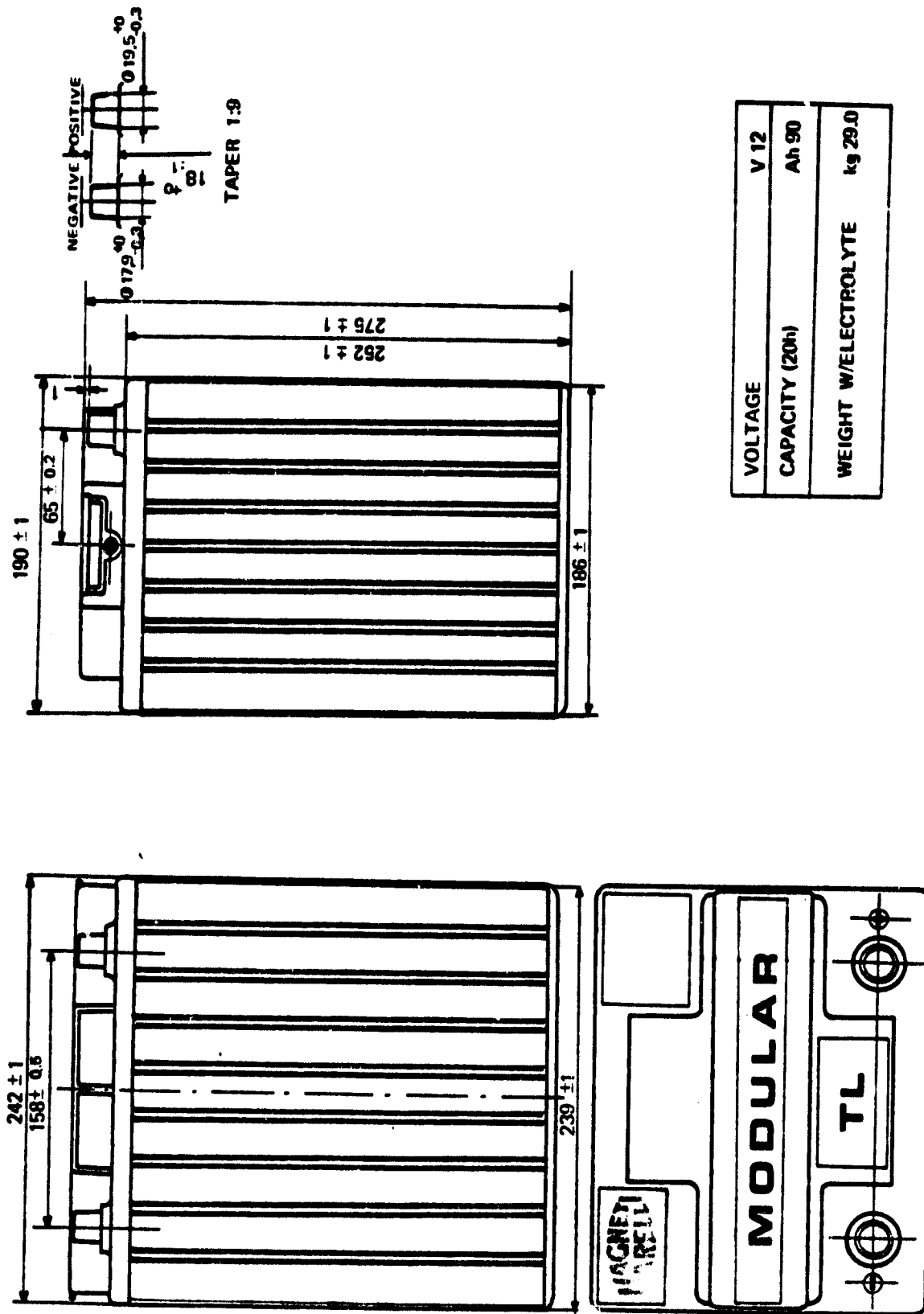


FIG. A.1-2.1- BATTERY SIZES

Results obtained in the laboratory on technical cells show that the performance of these battery modules can be improved, bringing about an increase in the specific energy and the deviation without affecting the specific power. The specific energy is noticeably increased (4.3 Wh/kg approximately in 5 hours) by decreasing the overall weight of the battery module has been kept to 25 kg.

The duration is increased to approximately 600-700 effective cycles. On Fig. A.1-2.2 the relationships between specific energy obtainable and peak power availability, for various mean discharge power levels are shown.

4. NICKEL-ZINC BATTERY

Magneti Marelli has started a research and development program on Nickel-Zinc batteries, which are considered as the most promising for near term traction applications.

At present our efforts are concentrated on producing single Zinc and Nickel electrodes; encouraging results have already been obtained, especially concerning duration in terms of cycles. We believe that future batteries shall have energy densities above 65 Wh/kg and peak power levels of 140 W/kg with a service life equating to that of present Lead-Acid types.

Research at Marelli is not yet sufficiently advanced to permit the supply of technical cells for Phase II of the project, nor to permit us to foresee large-scale production by 1985. For information only, we can state that our intention is to build a prototype Nickel-Zinc battery in a container similar to that used for the present Lead-Acid type (see para. 3), in order to achieve complete physical interchangeability between the two. The Nickel-Zinc battery will have a capacity of 340 Ah approximately and will weigh 23.7 kg; with a specific energy of about 70 Wh/kg approximately.

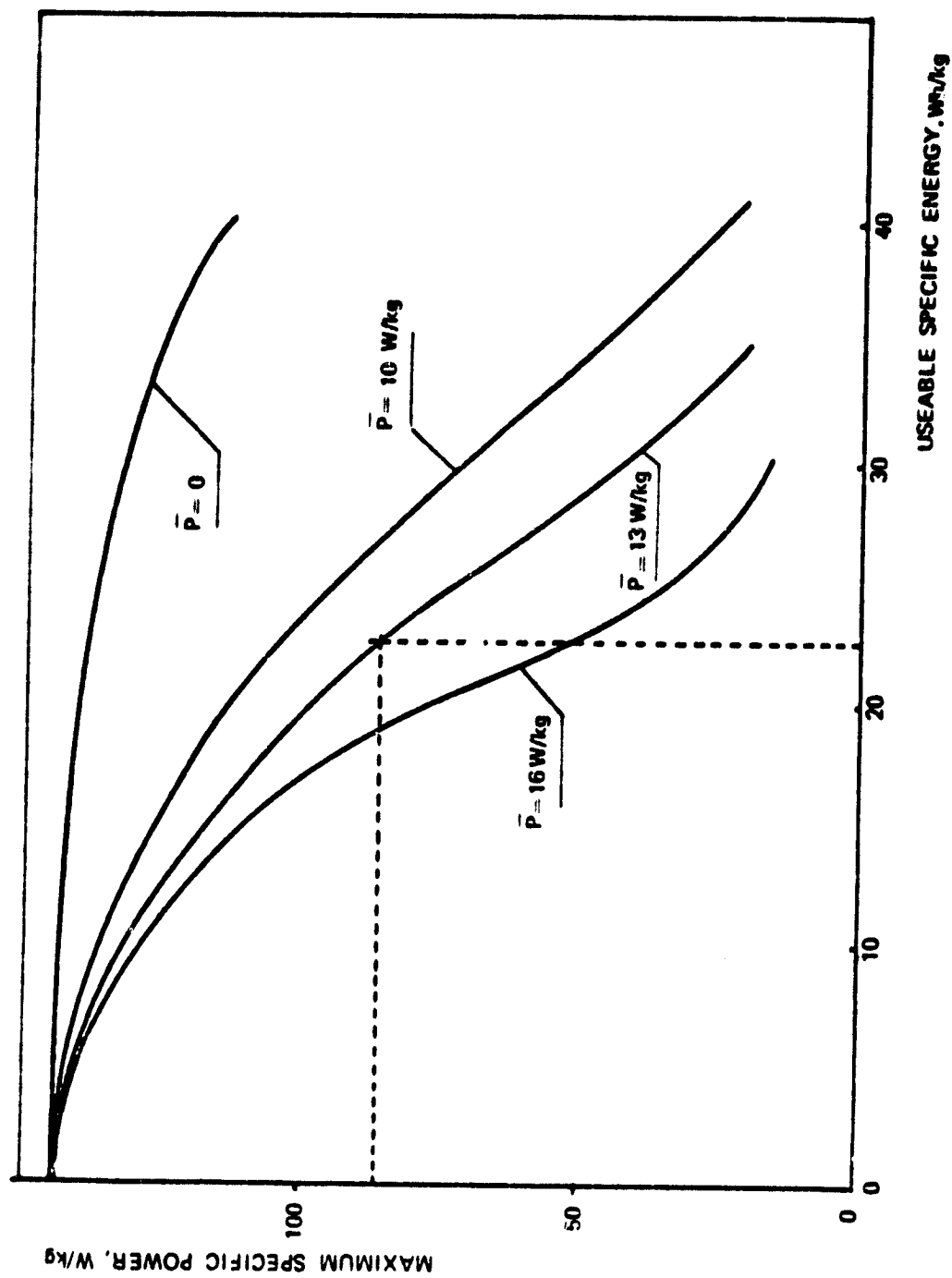


FIG. A.1-2.2 — MAXIMUM POWER VS USEABLE SPECIFIC ENERGY AS A FUNCTION OF AVERAGE POWER.

5. CONCLUSIONS

For the "JPL" Hybrid Vehicle project, Magneti Marelli have examined two types of battery, i.e. the Lead-Acid type and the Nickel-Zinc type.

The first type is already produced industrially and is known to be reliable. A new version of the modular battery has been designed, which can be manufactured in the near future, based on the results of laboratory tests on technical cells.

These results indicate that the battery may well be suitable for use on the specified type of vehicle.

For the Nickel-Zinc type, on the other hand, the present state of the art does not allow us to provide useable batteries within the time scale of the project. Nevertheless, the results obtained with single electrodes enable us to foresee batteries being produced in the future having the following characteristics:

- energy density over 65 Wh/kg
- peak power of approximately 140 W/kg
- duration comparable with that of present Lead-Acid types which would fulfil better the requirements of the JPL Hybrid Vehicle.

1. OBJECT OF PHASE I

Magneti Marelli have been given the task of identifying the possible types of power control that can be used on a hybrid vehicle.

After a preliminary study, Magneti Marelli have decided to adopt a type of power control and corresponding auxiliary equipment that are suitable for a separately excited DC motor.

This characterization has led to a preliminary design for the power circuits and for the battery charger together with an evaluation of weights, dimensions and efficiency.

As far as the power circuitry is concerned, a preliminary design has been made as well as the definition of weight and dimensions of each unit constituting it.

2. POWER CONTROL CHARACTERISTICS

After an evaluation of the various electric system alternatives, the Ni-Zn battery -DC motor combination has been selected by C.R. FIAT.

This choice implies a battery voltage of 96 V and a maximum available power of 38 kW.

Since the maximum power must be supplied even at low battery voltage, the maximum current is about 500 A.

During braking, the current can be about of the same value since the DC motor has commutating poles.

The field current reaches a maximum of 16.5 A at a voltage of 48 V and it must be possible to invert its direction in the shortest time for the braking phase. Braking must be regenerative down to zero speed, thus requiring a voltage boosting for speeds that are less than the basic one.

There must be a braking torque control, similar to that relative to the drive torque so as to modulate braking when the motor operates as a generator.

Ripple must be within 20% of the maximum current (i.e. 100 A peak-to-peak).

During field control operation a mechanical contact shall be able to short circuit the main chopper in order to reduce losses.

It is also necessary to guarantee operation in case of on board computer failure, by deriving a signal directly from the pedal unit.

3. CHOICE OF CONTROL DEVICE TYPE

Based upon previous experiences and evaluations carried out by Magneti Marelli in the design of control devices for electric vehicles, a control device has been chosen consisting of an armature chopper and of a field chopper-inverter. This choice, supported by many practical realizations, has proved to be the most valid and feasible.

The evolution and availability of high power transistors has made it possible to select these for the realization of both choppers, thus allowing an increase in the maximum working frequency and therefore the elimination of the smoothing inductance.

For regenerative braking, provision has been made so that additional choppers are not needed.

Regenerative braking is in fact obtained by modifying the circuit configuration so as to cut off the power supply to the motor (Fig. A.1-2.3). Adoption of a relay has advantageous since it is deenergized when zero current flows through the contacts so that there is no limitation to the number of opening/closing operations it can perform. This choice also allows to use the same armature chopper during normal running and braking conditions.

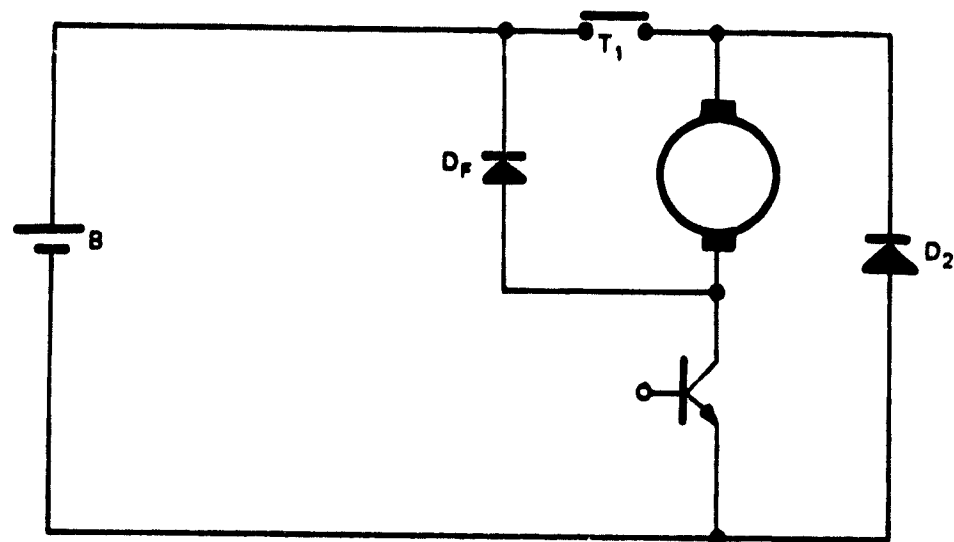


FIG. A.1-2.3 — ARMATURE CHOPPER ELECTRIC DIAGRAM

The control operates mainly by maintaining the armature current I_A within a range that includes a preset value of I_{SET} . The width of this range decreases non-linearly when I_A decreases.

This type of control, which is performed by means of a current feed-back, makes it possible to avoid the use of internal oscillators and frequency controls, by letting the system itself perform the function of oscillator, limited in this by appropriate non-linearities.

The same type of control is also applied to the field current I_F - as from Fig. A.1-2.4. Ripple, though, is maintained at much lower percentage values.

This control has been possible by using a type of electric motor with a field value calculated for a voltage of 48 V. From this it follows that, by supplying a voltage of 96 V, currents are produced which tend to values higher than I_{Fmax} and therefore allowing chopper operation also in the neighborhood of I_{Fmax} . Another advantage is that field inversion times are reduced by half.

4. OPERATIONAL DESCRIPTION

With reference to the block diagram of Fig. A.1-2.4, the on board computer sets a value of armature current I_{SET} .

The armature current oscillates between two threshold values: when the upper threshold is exceeded the chopper transistors are inhibited, whilst a value of current smaller than the lower threshold value makes the chopper conduct. The control thus establishes a ripple equal to 90 A peak-to-peak at a maximum frequency of 2 kHz and a current of 500 A.

For a 100 A current, a ripple value of 30 A peak-to-peak is set, resulting also in a maximum frequency of 2 kHz, because of the increased armature inductance.

This type of operation is valid until the basic motor speed

is reached; over this speed the control of the motor is performed by varying the field current.

The field control is obtained in similar way to the armature control; however field control implies a much lower ripple percentage value (0.1 A over 16.5 A maximum field current) resulting also in a much lower frequency value (300 Hz).

The electric diagram of the armature chopper is given in Fig A.1-2.3.

When the relay T_1 opens the polarity across the motor collector terminals reverses but the armature current maintaining its direction. Fig. A.1-2.5 shows the configuration corresponding to regenerative braking for speeds greater than the basic one ω_b .

The field must also be reversed and shall be controlled so as to limit the I_A and modulate the braking torque.

For values below the basic speed, the armature voltage is no longer capable of supplying current to the battery so that a voltage boosting must be produced in the motor coil, as given in Fig. A.1-2.6.

This circuit arrangement has been designed by Magneti Marelli that have also filed an Italian Patent.

The on-off pulses for the chopper are generated by the same logic which operates a comparison, with hysteresis, between the preset value of current and the actual current in the motor.

A more detailed operational description of the regenerative braking with reference to the block diagram of Fig. A.1-2.4 is given below.

The values of current preset by the on board computer become negative. The absolute values of these are compared with the armature current I_a . The sign detected by an ad hoc comparator, modifies the field reference current bringing it to its maximum negative value. The braking current goes to zero in a time interval shorter than that required for field inversion; thus, there is a very short elapse of time in which the armature current I_a is zero.

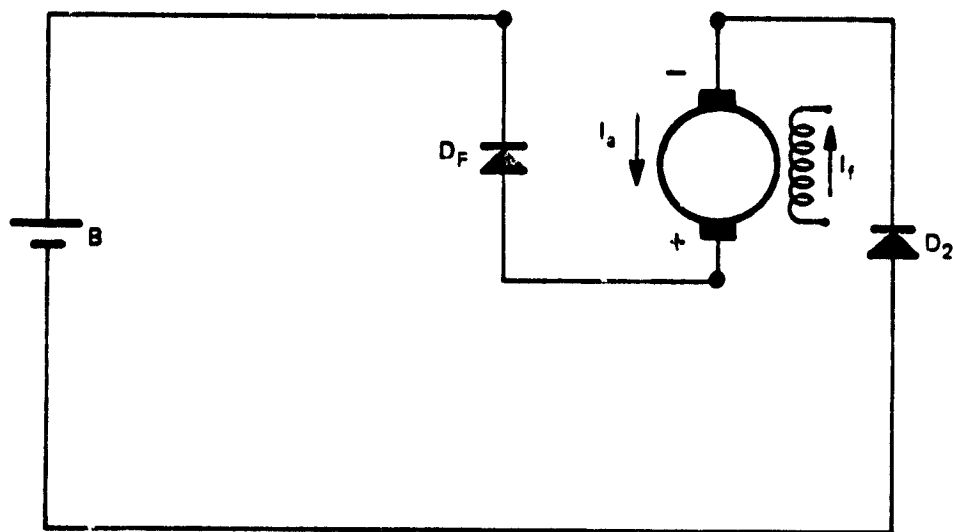


**FIG. A.1-2.5—ARMATURE CHOPPER ELECTRIC DIAGRAM REGENERATIVE BRAKING
CONFIGURATION FOR SPEEDS GREATER THAN THE BASIC ONE**

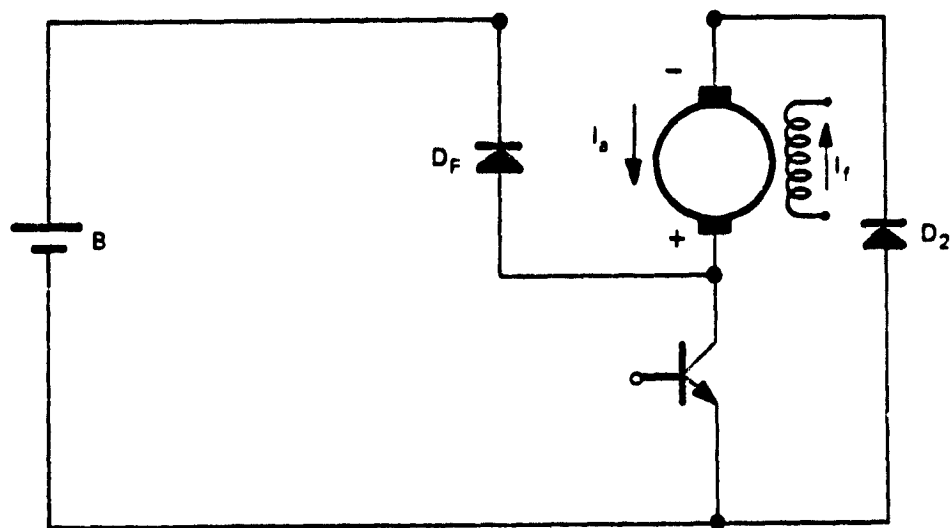


FIG. A.1-2.6 — ARMATURE CHOPPER ELECTRIC DIAGRAM. REGENERATIVE BRAKING CONFIGURATION FOR SPEEDS LOWER THAN THE BASIC ONE

It is during this time corresponding to $I_a = 0$ that the relay opens.

The on board computer, during inversion, shall maintain the value of I_{set} at zero until the field current has reversed and reached a prefixed threshold. Once this transient has extinguished and for speeds greater than ω_b , the armature current I_a settles at an absolute value greater than I_{set} and the $K(I_a - I_{set}) > 0$ error modulates the field weakening.

Therefore, during regenerative braking, for speeds greater than ω_b , the armature current I_a is controlled by varying the field current.

For values of speed below ω_b , the $(I_{set} - I_a)$ positive values short-circuit the motor armature by means of the main chopper; negative values of $(I_{set} - I_a)$ inhibit the chopper and the overvoltage which is produced allows transfer of the energy stored in the armature coil to the battery. This type of operation has proved successful for the more recent types of choppers produced by Magneti Marelli.

5. ARMATURE CHOPPER AND FIELD CHOPPER-INVERTER

For the realization of the main chopper, the Toshiba Giant Transistor 2SD648 have been considered which have the following characteristics:

Monolithic Darlington

400 A maximum continuous collector current

300 V V_{CEO} (SUS)

$T_{on} = 1 \mu s$ typical

$T_{off} = 2 \mu s$ typical.

Two transistors in parallel have been used, thus involving a considerable chopper oversizing with respect to the specifications. This oversizing might be reduced by the availability on the market of analogous components or by the

production of a specific component manufactured, on request, by a specialized American Company. The maximum frequency has been set to 2 kHz so as to satisfy the TR constraints.

With reference to Fig. A.1-2.7, the use of two transistors in parallel implies the need for a current coupling that guarantees equal power dissipations in each transistor.

This is obtained by means of a mutual inductance so that transistor thermal run-away is avoided.

During operation at values above ω_b , i.e. when the duty-cycle is equal to 1, a by-pass relay short-circuits the chopper thus increasing efficiency and avoiding differences in currents that might occur during steady state functioning.

The two transistor bases are independently supplied by two drivers one of which can be inhibited by an OFF signal during battery charging operation (see Fig. A.1-2.7).

The two bases are protected by voltage limiters (clampers) that prevent the base voltage from going below -0.5 V.

The collectors of the two transistors will be fitted with antispikes devices.

Four transistors have been used for the field-chopper, with the following characteristics:

- 18 A maximum continuous current
- 200 V V_{CEO} (sus).

In this way mechanical contacts are avoided for field inversion, thus increasing the overall reliability. Also, it allows to control chopper and field inversion operation. By alternatively switching on and off the two diagonals, chopper and current inversion operations are obtained in the shortest time possible.

Energy transfer to the battery is still performed via the two diodes down to zero current, whilst the transistors are inhibited although their bases would enable them to conduct.

At the end of energy transfer to the battery, the reverse voltage on the transistors reduces to zero and the transistors begin to conduct up to the preset value of reverse current; at this point, chopper operation begins again.

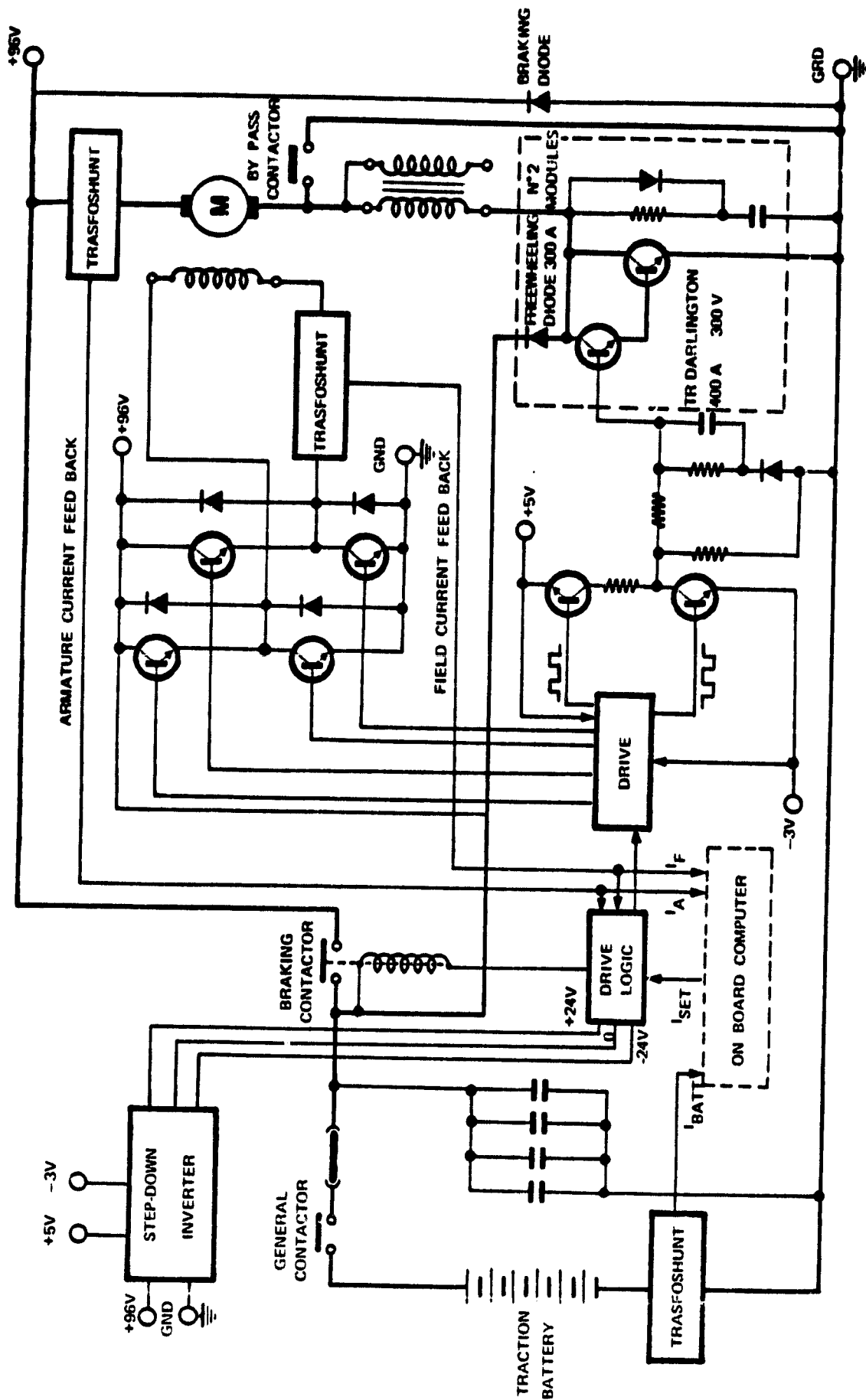


FIG. A.1-2.7 ARMATURE AND FIELD CHOPPER CIRCUIT

6. AUXILIARY EQUIPMENT

Main battery charger - Fig. A.1-2.8.

With reference to the battery charger circuit of Fig. A.1-2.8, the line voltage is rectified and chopped so as to obtain an average voltage value which is less than the minimum battery voltage.

After filtering, this voltage is applied to the main chopper via coil L_2 . Only one power transistor is forced to conduct whilst the other is kept inhibited by the driver. At this point, via the chopper, coil L_2 begins to store energy; the armature current I_a starts increasing and when it reaches the upper threshold value the chopper opens and the energy stored in L_2 is transferred to the battery. When I_a reaches the lower threshold value the transistor is forced to conduct again. This type of operation is the same as for regenerative braking operation for values below ω_b . A negative I_{set} information is sent from the on board computer based upon the actual I_{batt} .

7. EVALUATION OF WEIGHTS, DIMENSIONS AND EFFICIENCY

The most relevant elements as far as weights and dimensions are concerned are:

- No. 2	heat dissipators for the power transistors, designed for a forced air speed of 4 m/sec	
	Dimensions (mm)	Weight (kg)
	177 x 127 x 128	5.6
- No. 3	500 A relays:	
	170 x 130 x 90	1.9
- No. 4	1000 μ F, 200 V capacitors	
	120 x 52 \emptyset	
- No. 2	600 A trasfoshunts	
	150 x 130 x 80	2.5

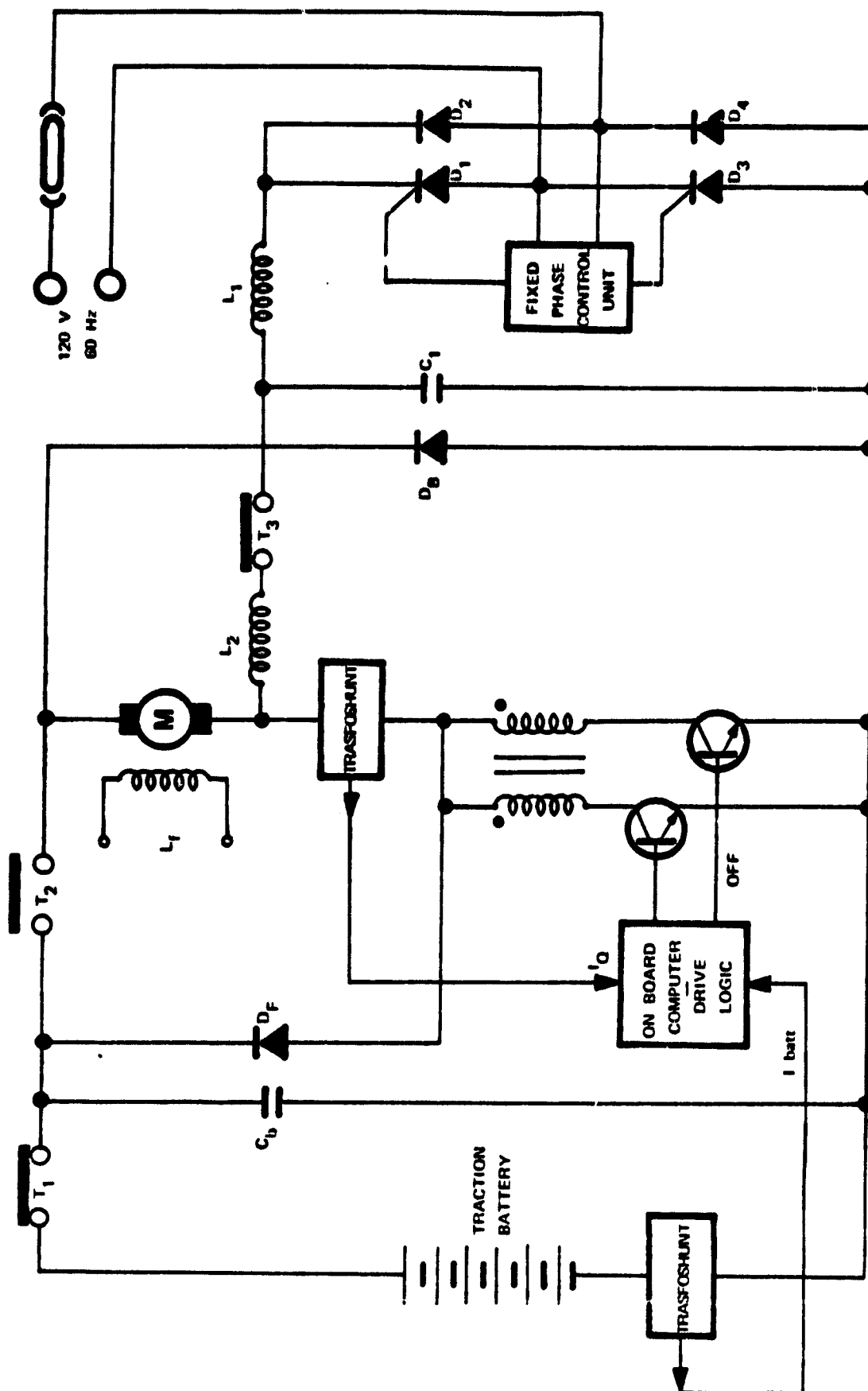


FIG. A.1-2.8 BATTERY CHARGER CIRCUIT

Overall dimensions (mm)

200 x 300 x 400

Total weight (kg)

22

The addition of container, control cards and connections bring to final overall dimensions of:

400 x 350 x 250 mm

and to a final total weight of

27 kg

The battery charger dimensions are:

150 x 100 x 200 mm

and the weight, including coils, capacitors and relay is:

4 kg

The field chopper expected efficiency is 0.96 under control worst condition i.e. with a duty cycle equal to 50% and an armature current of 500 A.

Battery charger efficiency is expected to be around 0.94.

APPENDIX A.1-3

Final Report No. CS 167/79 May 24, 1979

SUBCONTRACT PININFARINA - CRF

UNDER JPL CONTRACT No. 955187

"NEAR TERM HYBRID PASSENGER VEHICLE DEVELOPMENT PROGRAM"

PHASE I

PRELIMINARY DEFINITION OF THE VEHICLE ARCHITECTURE

General philosophy of body design

As far as the present state of the art is concerned relative to aerodynamics, a two-volume body design has proved more efficient than the three-volume type, geometric conditions being equal.

The general architecture of the vehicle body is as shown on drawing X, where account has been taken of mechanical parts and battery dimensions, number of passengers, capacity of the trunk and law regulations.

Drawing X (Fig. A.1-3.1)

It shows by means of three view, 1:5 scale, a first approach to the design that takes a previous research on aerodynamics by Pininfarina as a starting point and relative to a high-performance 4-passenger car, called "STUDIO CR 25".

Such a choice has been made because, for what concerns dimensions the body shape was capable of being adapted to the JPL design without deterioration in aerodynamic parameters.

Drawing J - 1:5 scale (Fig. A.1-3.2)

Definition by means of 4 views of the body shape considered as best (among the various ones presented as an alternative to this one) from functional aerodynamic, esthetic and legal points of view.

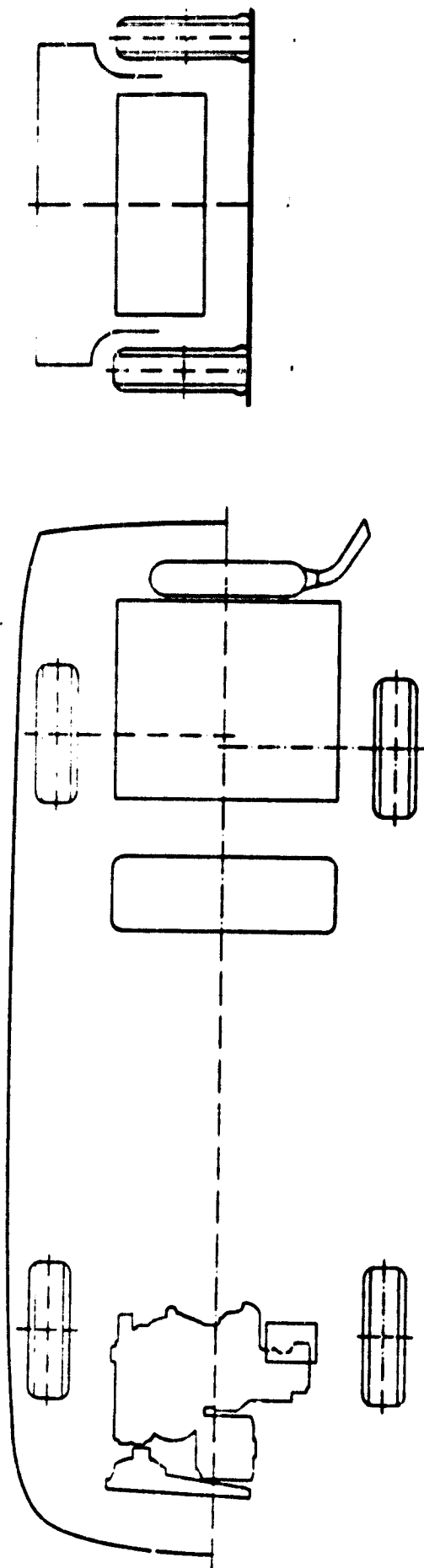
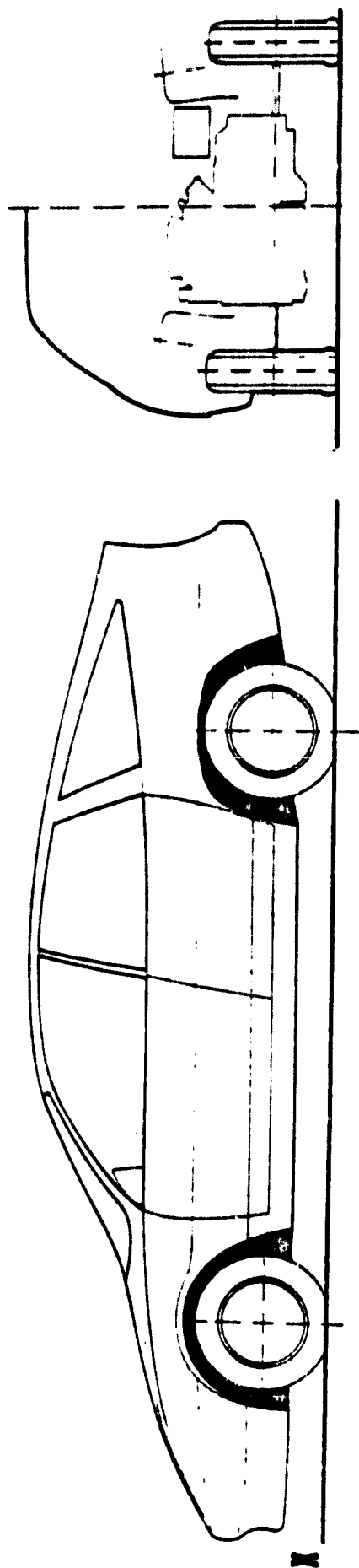


FIG. A.1-3.1 - BODY SHAPE - THE FIRST SOLUTION

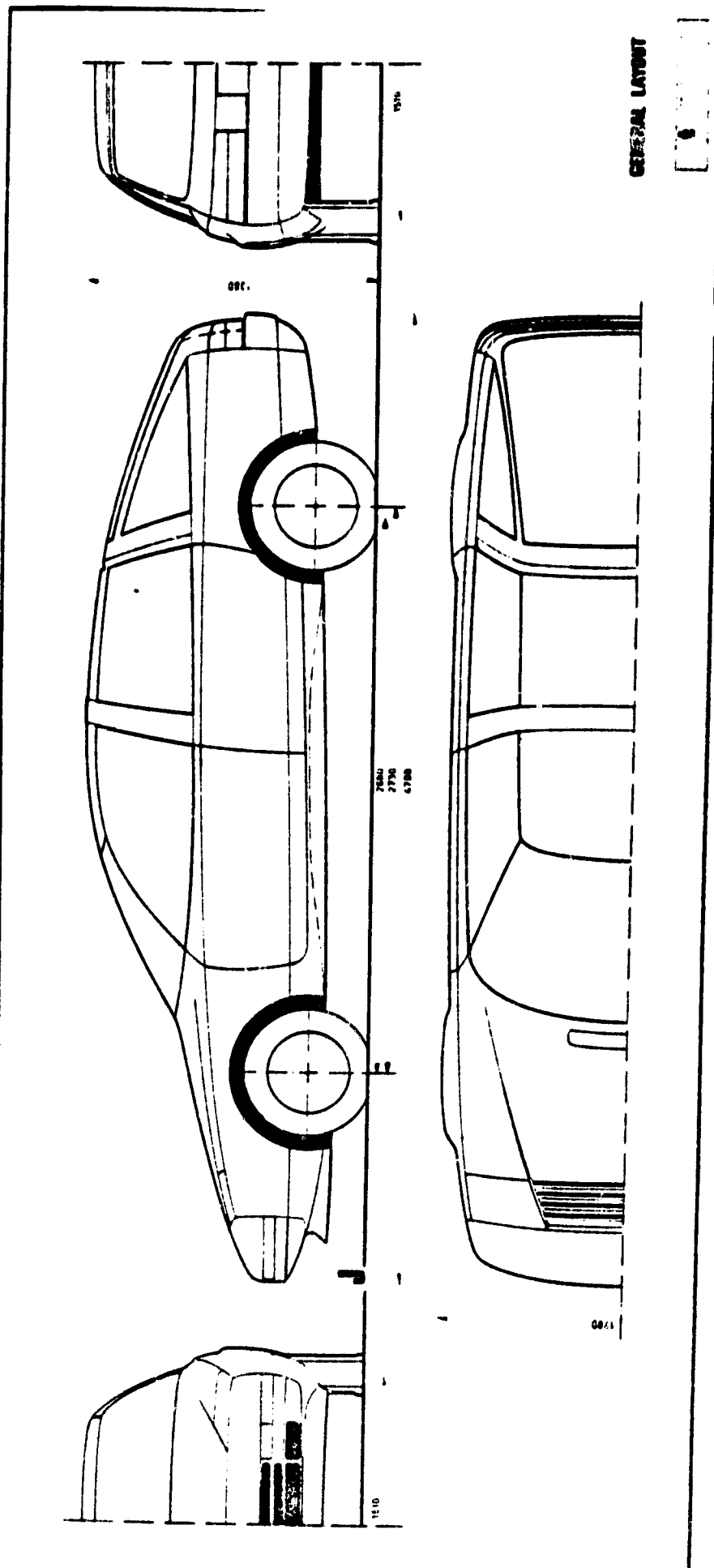


FIG. A.1-3.2 — BODY SHAPE — THE SELECTED SOLUTION

Drawing J with profile views (front, rear and three quarter front and rear) (Fig. A.1-3.3/4/5)

Drawing J - 1:5 scale - Four views showing the position of the "typical sections" (Fig. A.1-3.6).

Figures A.1-3.7 to A.1-3.17 - 1:1 scale showing the "typical sections".

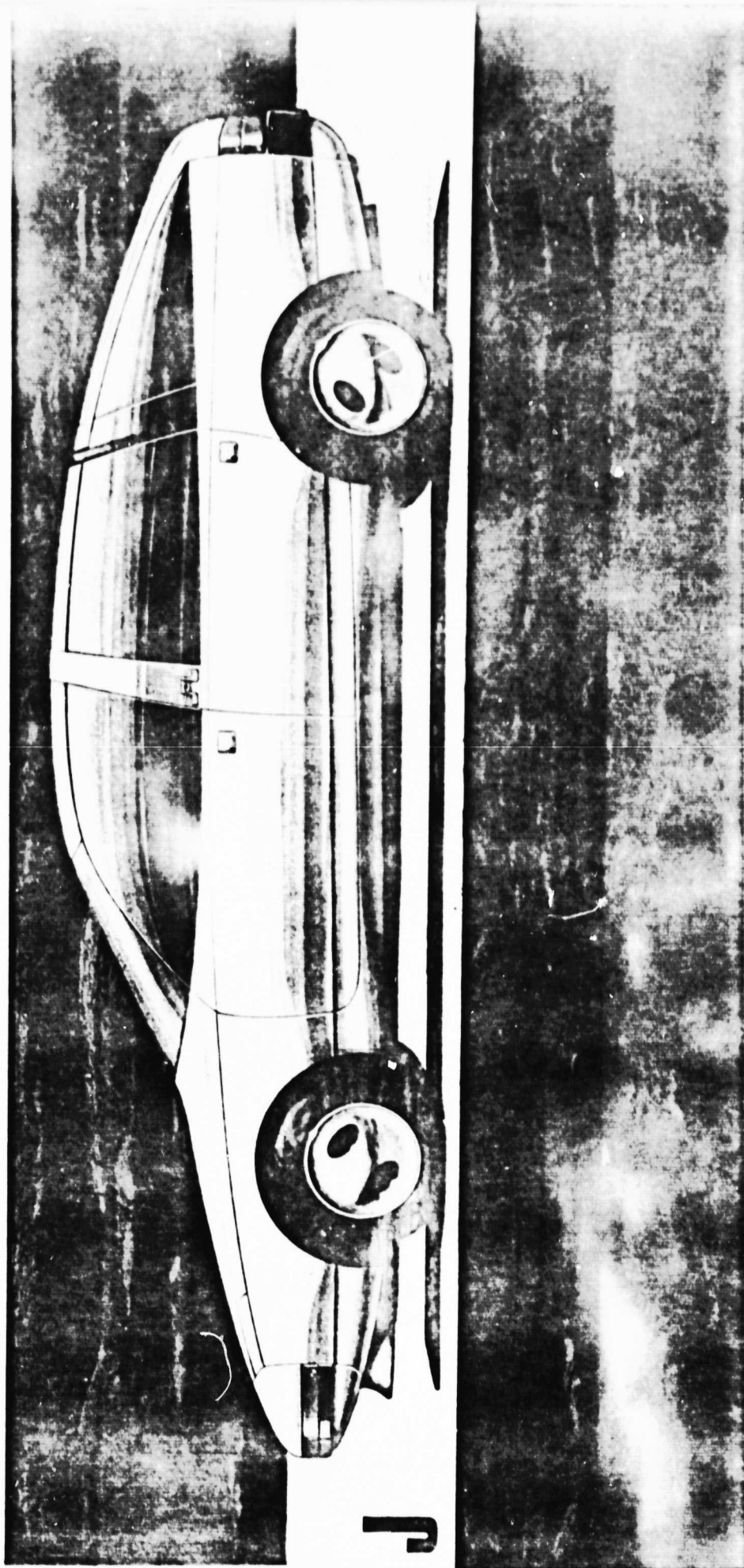


FIG. A.1-3.3 - BODY SHAPE - LATERAL VIEW

ORIGINAL PAGE IS
OF PL

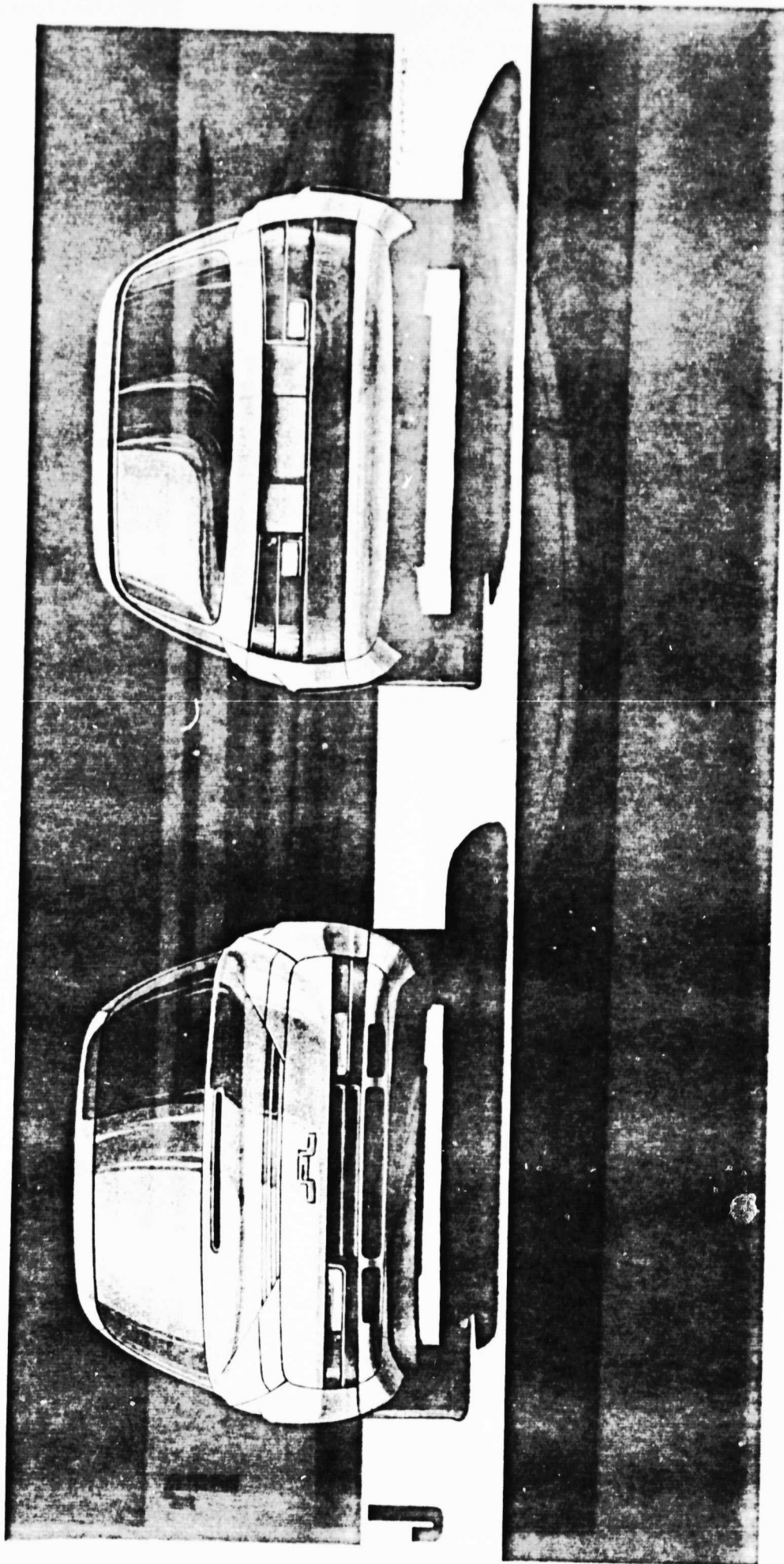


FIG. A.1-3.4 - BODY SHAPE - FRONT AND REAR VIEWS

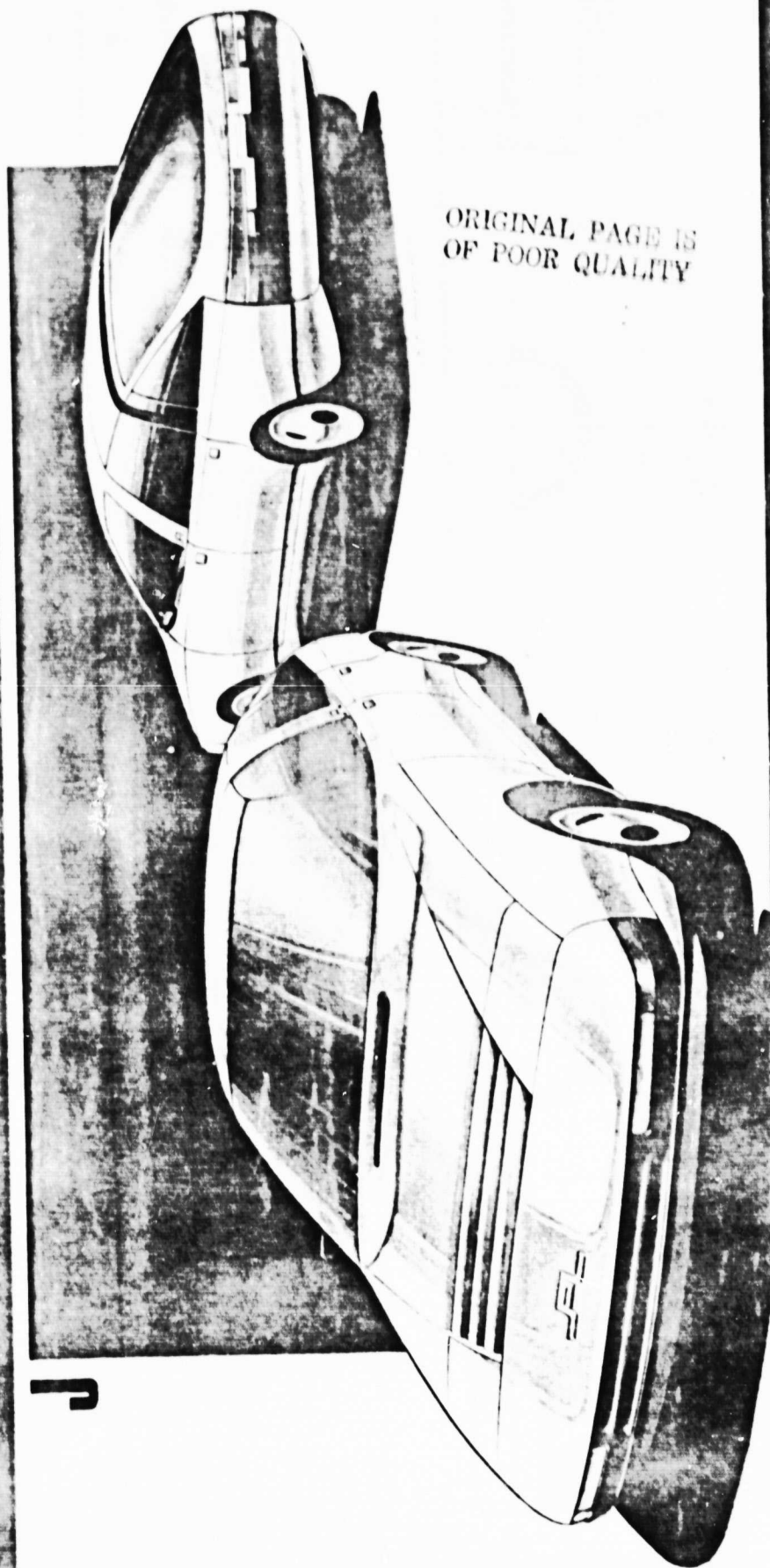


FIG. A.1-3.5 - BODY SHAPE - THREE QUARTER FRONT AND REAR VIEWS

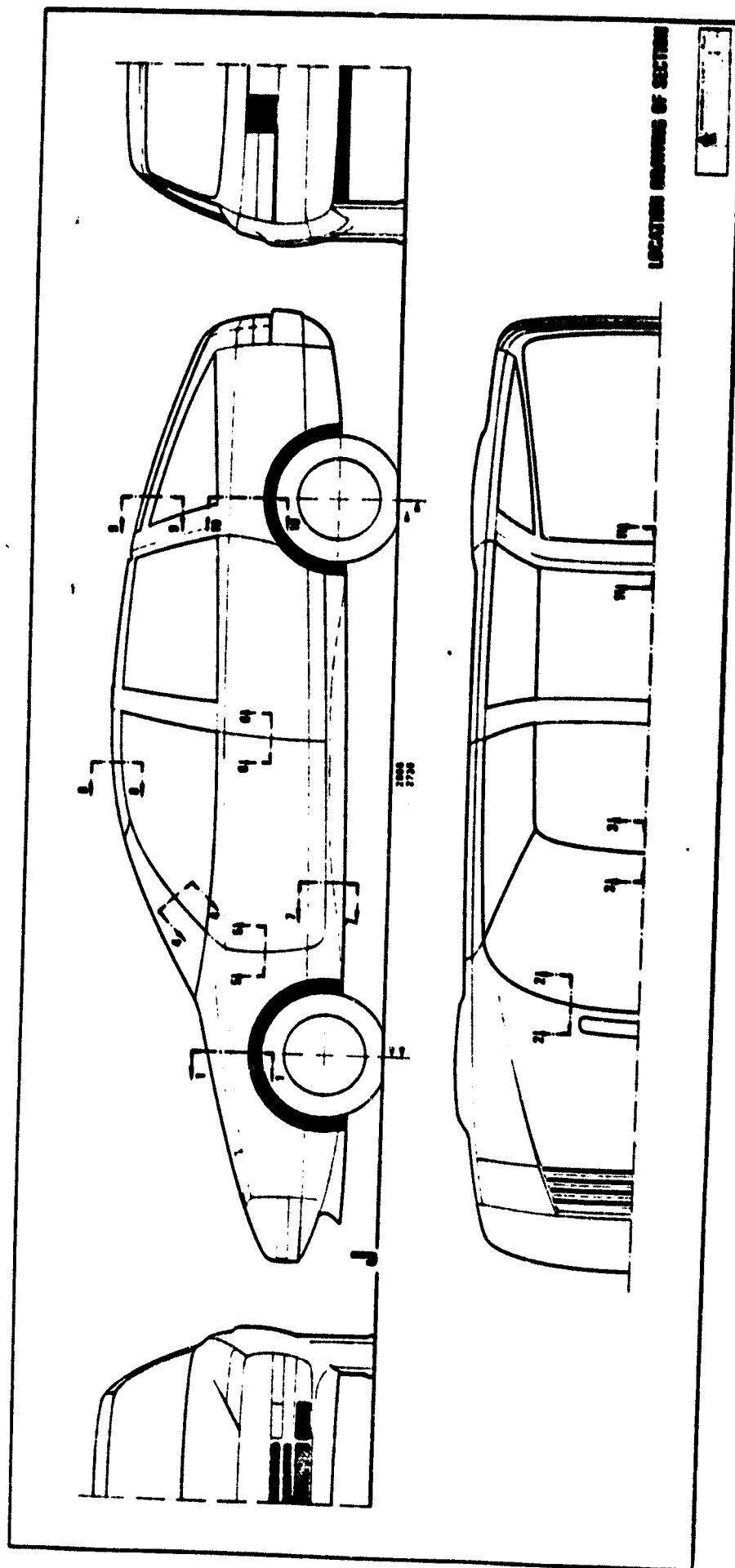


FIG. A.1-3.6 - BODY SHAPE - TYPICAL SECTIONS

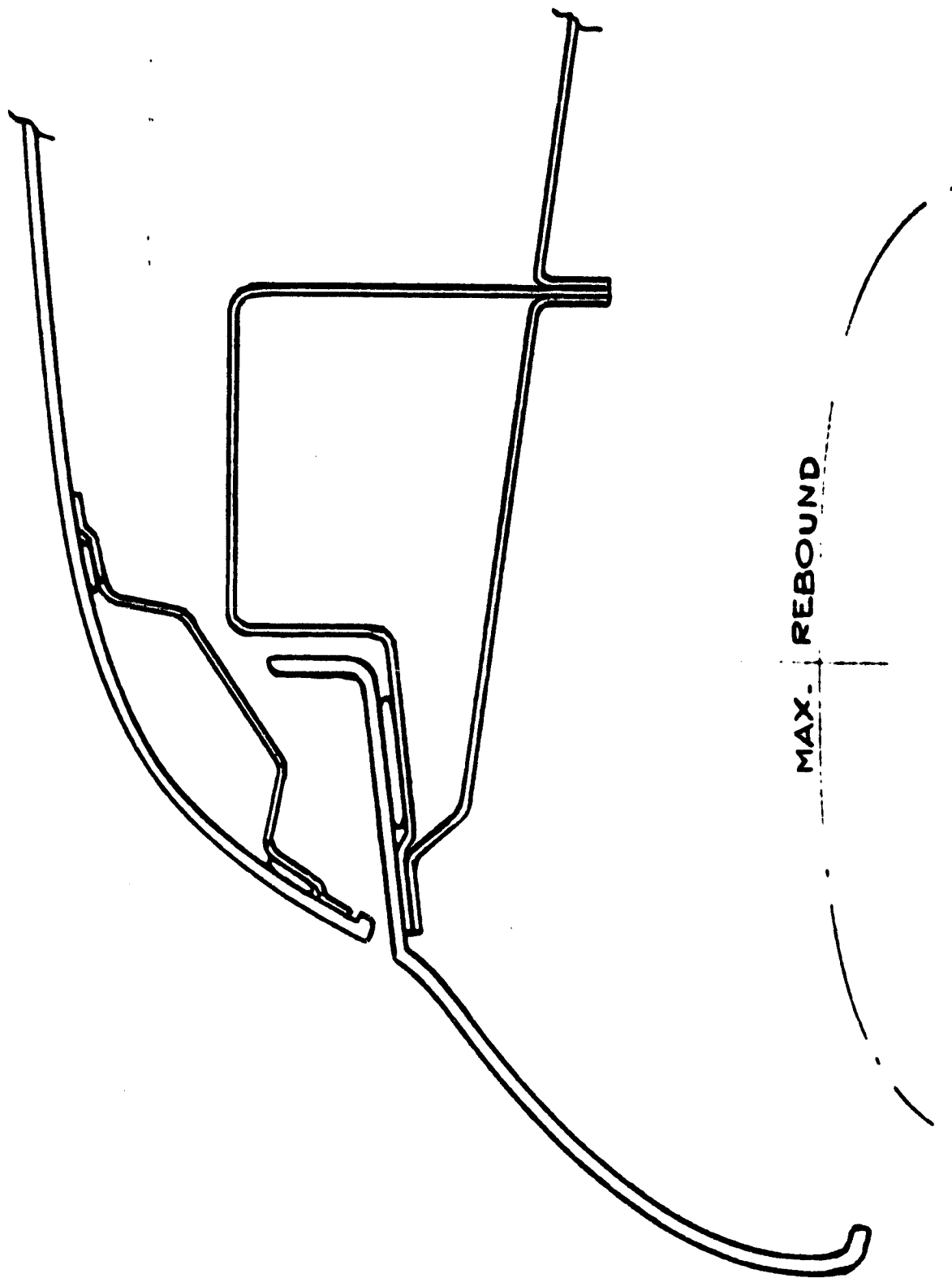
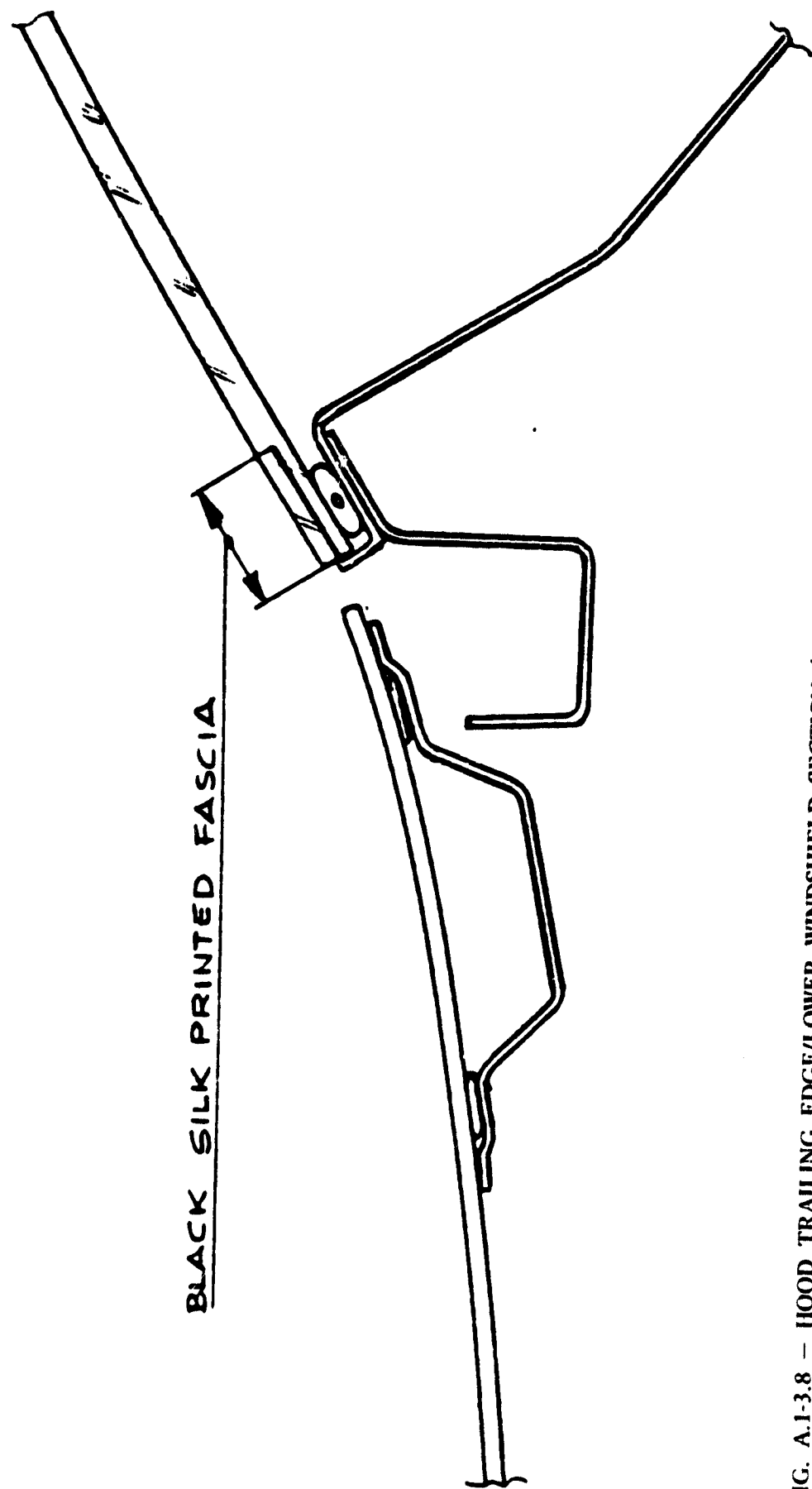


FIG. A.1-3.7 - HOOD/WING SECTION ON FRONT WHEEL CENTER LINE (DISREGARDING SHOCK-ABSORBER)



BLACK SILK PRINTED FASCIA

FIG. A.1-3.8 - HOOD TRAILING EDGE/LOWER WINDSHIELD SECTION (AT SIDE OF AIR INTAKE)

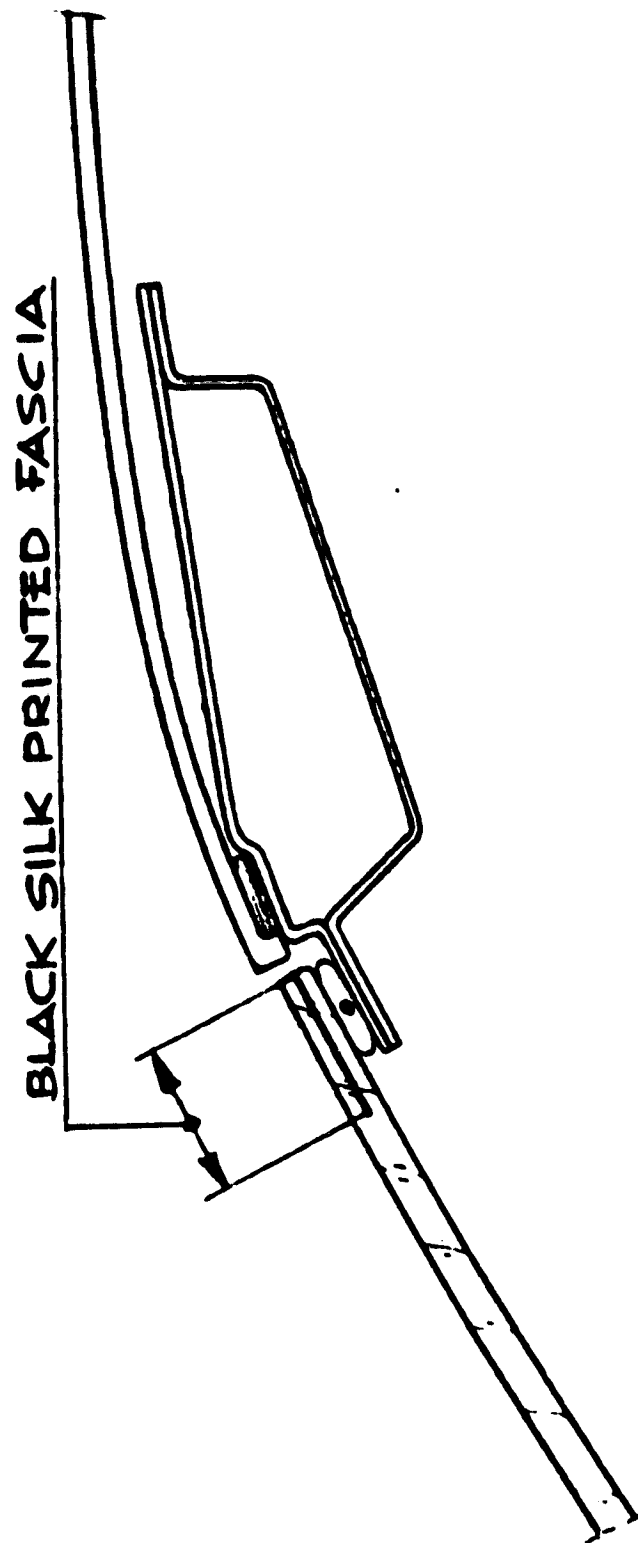


FIG. A.1-3.9 - UPPER WINDSHIELD CENTER SECTION

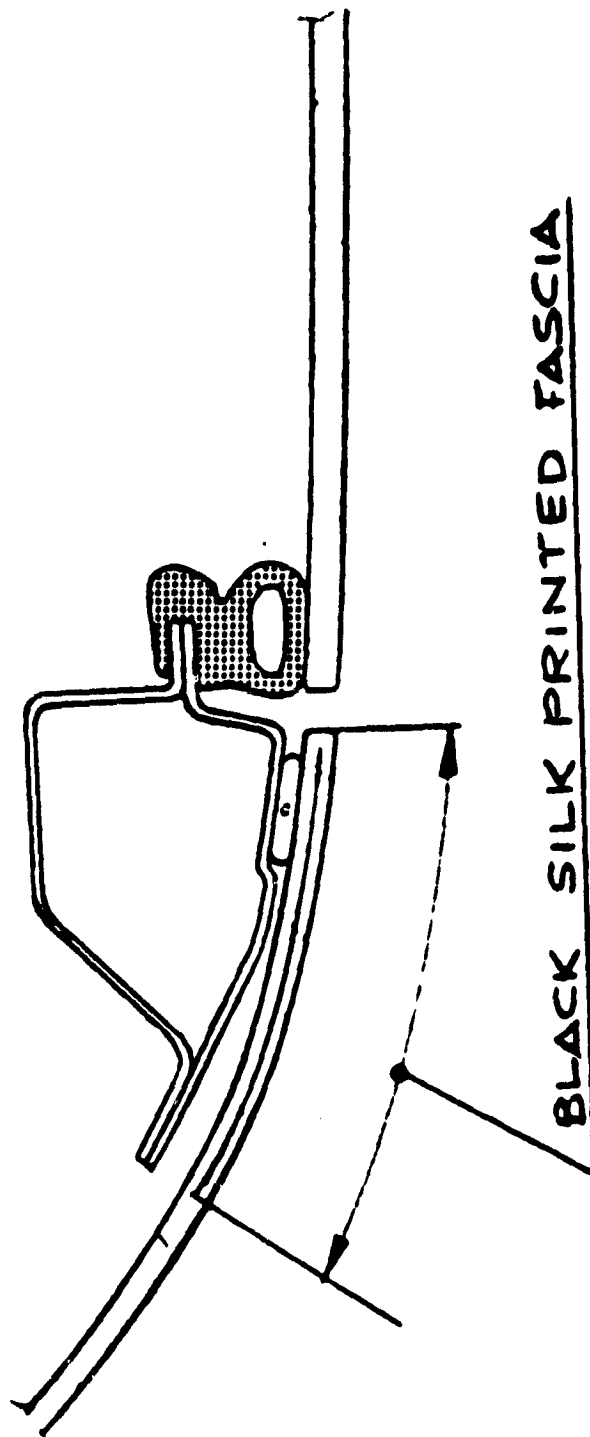


FIG. A.1.3.10 -- "A" PILLAR SECTION

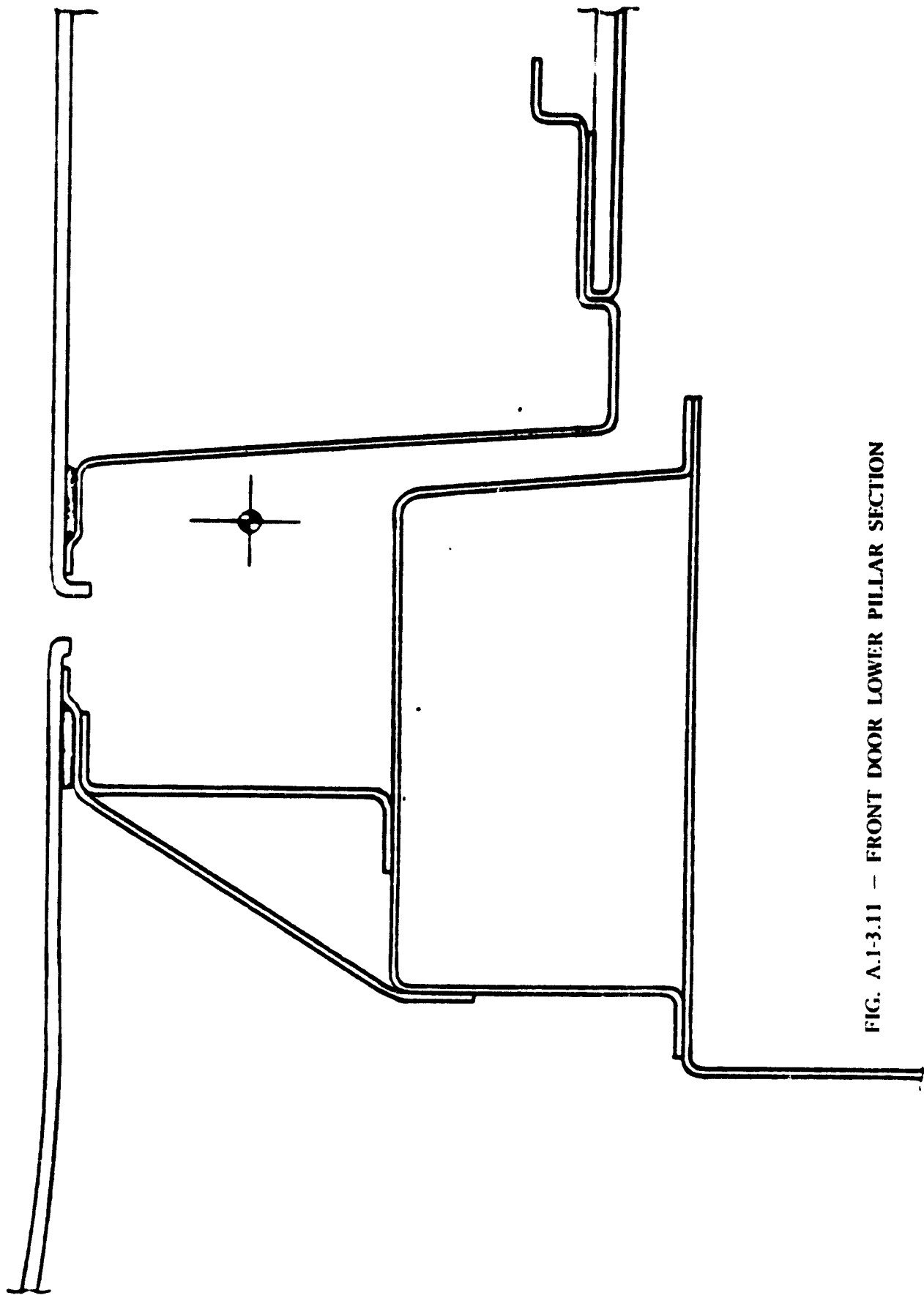


FIG. A.1-3.11 - FRONT DOOR LOWER PILLAR SECTION

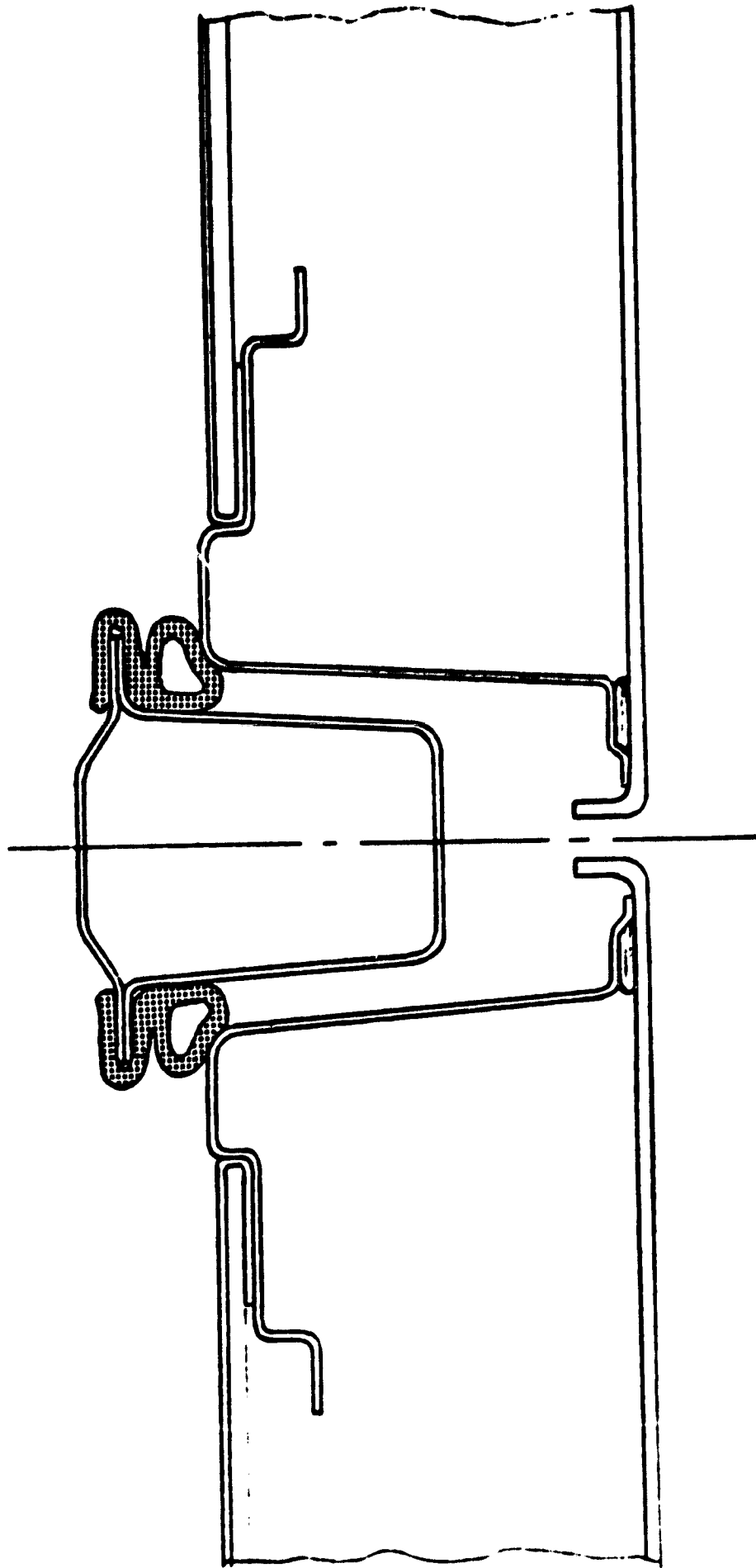


FIG. A.1-3.12 - LOWER CENTER PILLAR SECTION

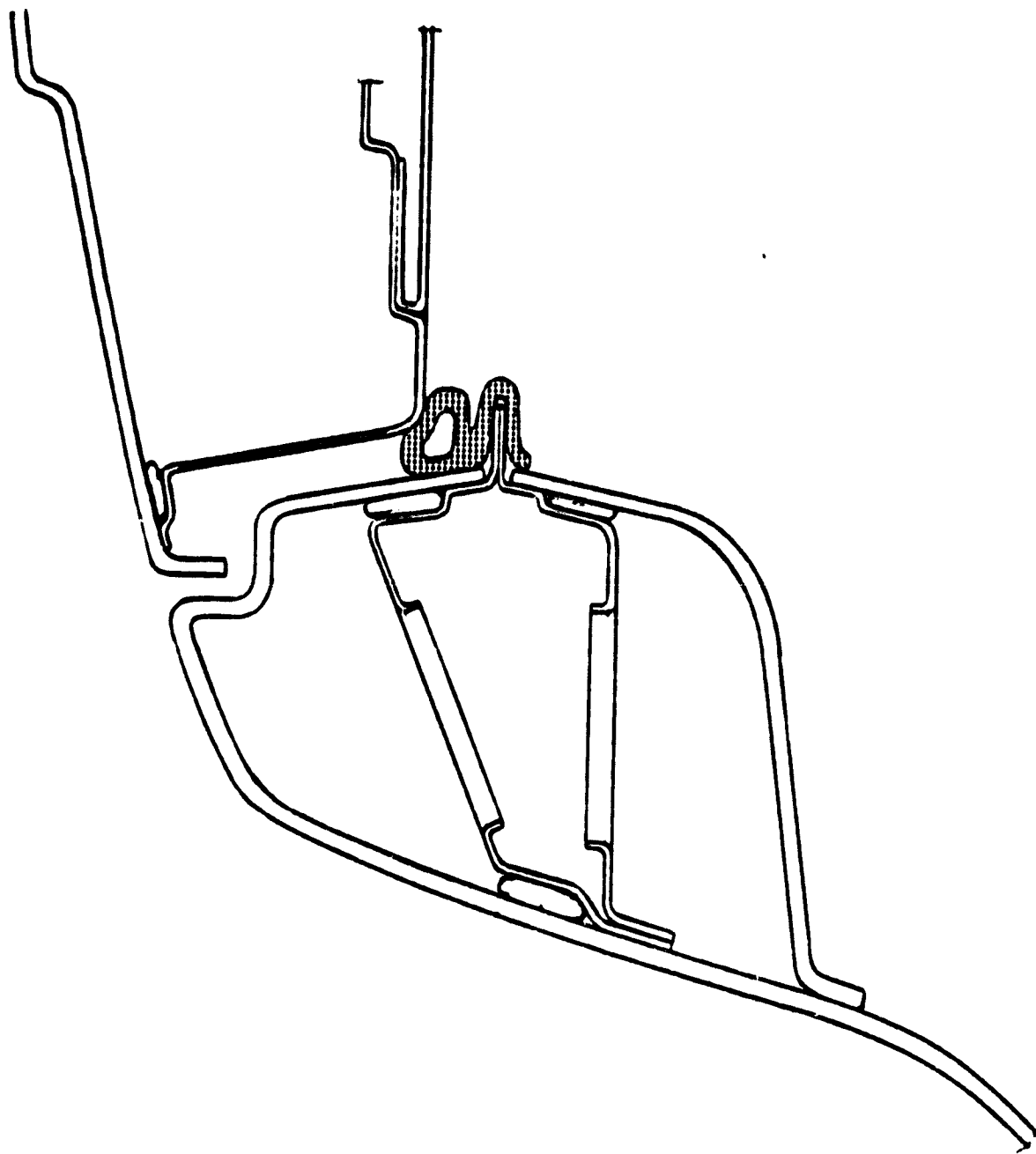


FIG. A.1-3.13 - SILL/ROCKER PANEL & LOWER DOOR EDGE SECTION

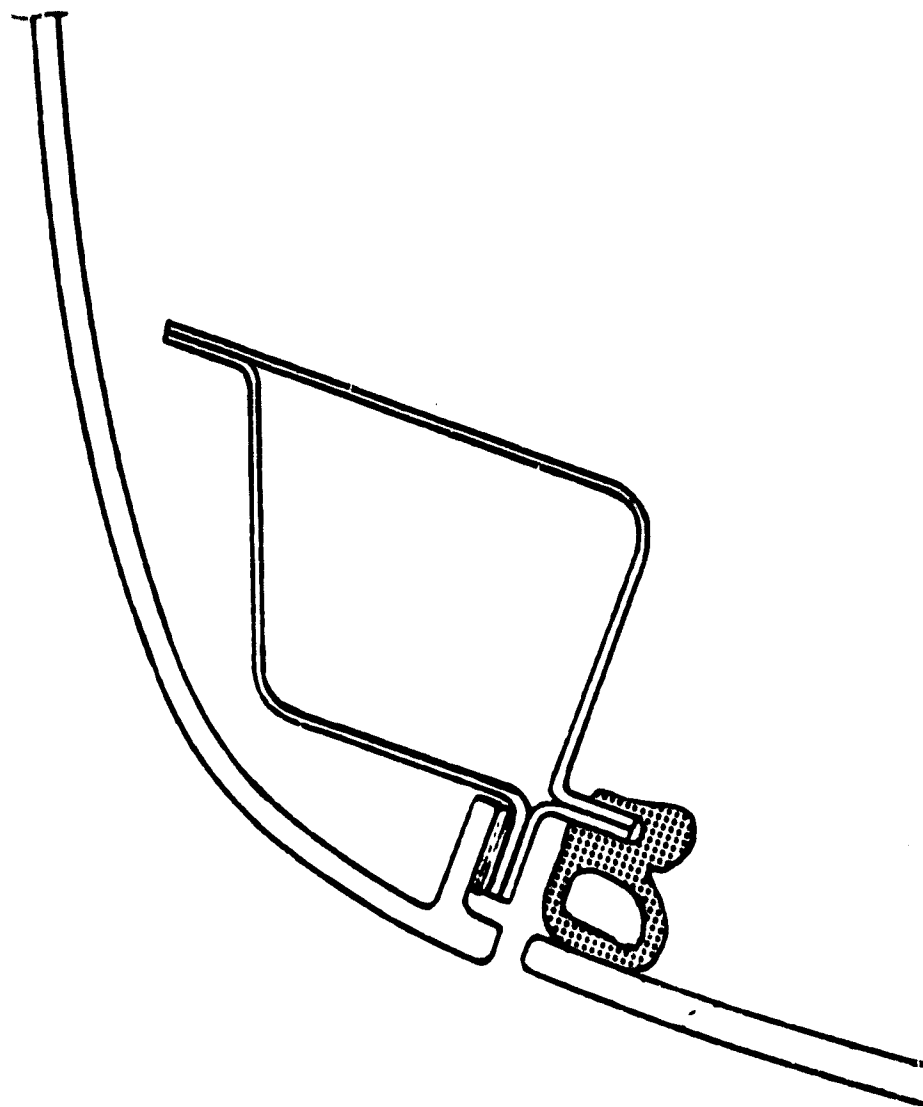


FIG. A.1-3.14 -- ROOF/UPPER DOOR EDGE SECTION

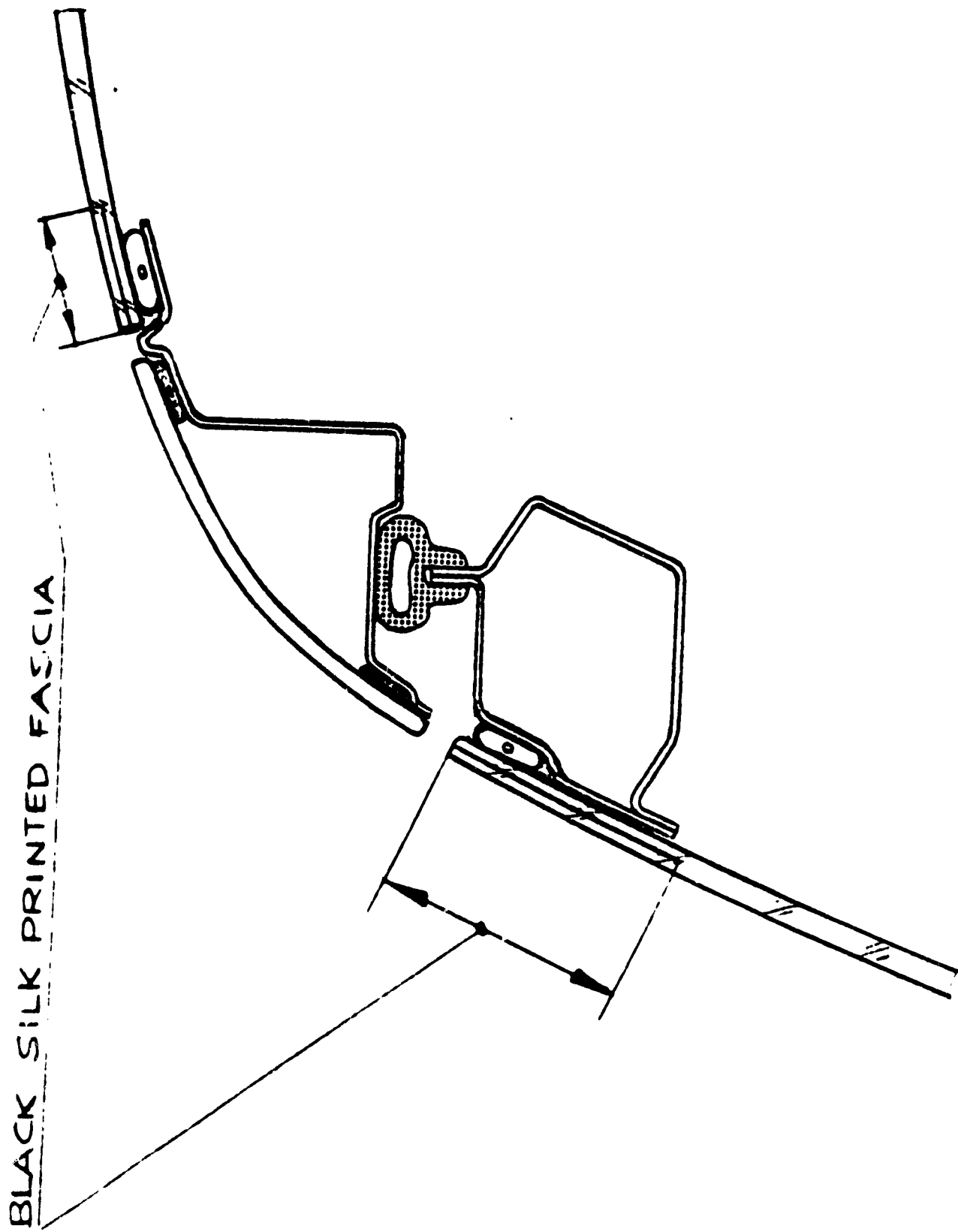


FIG. A.1-3.15 - FIFTH DOOR SIDE SECTION

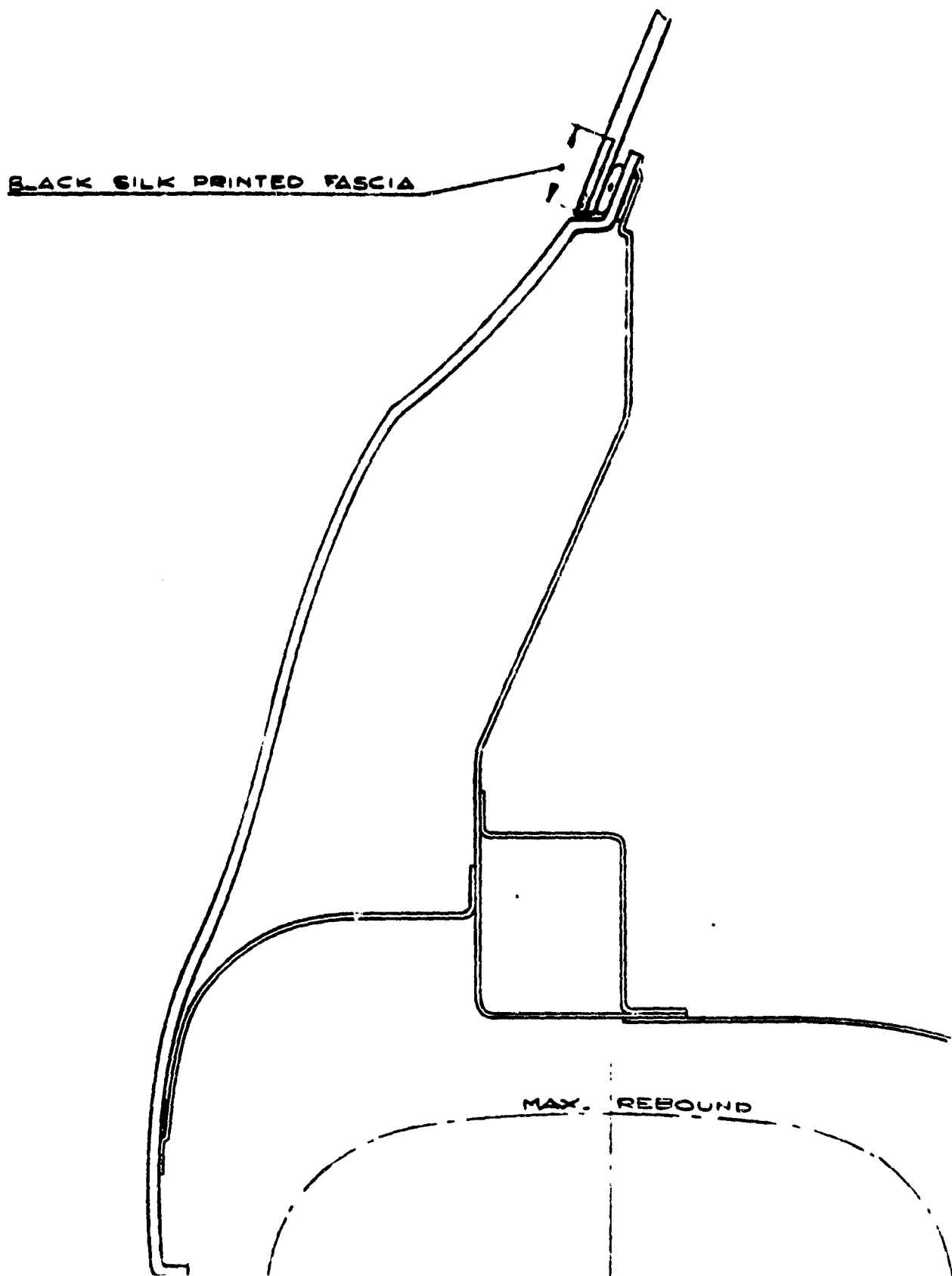


FIG. A.1-3.16 - REAR WING SECTION ON REAR WHEEL CENTER LINE

BLACK SILK PRINTED FASCIA

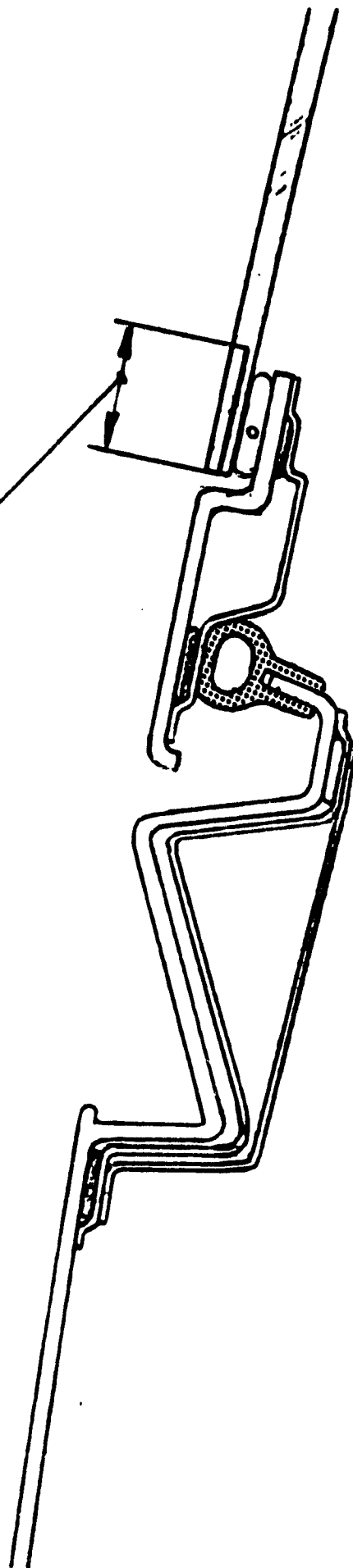


FIG. A.1-3.17 - FIFTH DOOR CENTER SECTION

ORIGINAL PAGE IS
OF POOR QUALITY

APPENDIX A.1-4

Final Report No. RT 143 May 24, 1979

SUBCONTRACT PIRELLI - CRF

UNDER JPL CONTRACT No. 955187

"NEAR TERM HYBRID PASSENGER VEHICLE DEVELOPMENT PROGRAM"

PHASE I

Projected characteristics of tires to be produced according to the state of the art technology of the '80 s and particularly suitable for Internal Combustion Engine vehicles and for the "Hybrid Vehicle"

1. INTRODUCTION

A preliminary evaluation of the characteristics of the tires that will be produced in accordance with the state of the art technology of the '80s can be made taking account of the tire evolution trend in these last decades and also of:

- 1) the technological innovation that takes advantage of the new developments in terms of materials and techniques
- 2) the vehicle evolution
- 3) the market trend evolution.

This trend can be extrapolated for the next 5-10 years, bearing in mind that points 2) and 3) will play a greater role than in the past in relation to the problems of energy cost increase.

As far as vehicles are concerned, i.e. the internal combustion engine type and the hybrid type, reference is made to vehicles capable of reaching a maximum speed of 130 km/h and the design of which aims at a drastic reduction in consumptions; it is assumed, also, that in both cases all the other performance characteristics are comparable (accelerations, comfort etc.).

In particular the hybrid vehicle proposed by FIAT will have the following characteristics:

Curb weight	1600 kg
Capacity (5 persons + baggage)	420 kg
Total weight	2020 kg

The following have been assumed as reference characteristics for the tires used on such vehicles:

Vertical stiffness
Cornering stiffness
Road holding on wet surface
Rolling resistance

The above characteristics do not include parameters which are directly connected to tire safety, although this must be perfectly adequate for all the vehicle working conditions.

2. TIRES FOR INTERNAL COMBUSTION ENGINE VEHICLE

2.1 Vertical Stiffness

This is a very important parameter because, together with suspension stiffness, it contributes considerably to the ride smoothness and comfort.

What is actually of interest under this point of view is the dynamic vertical stiffness measured while the tire is rolling, in the area of deflection corresponding to load conditions.

The only important improvement, as far as this parameter is concerned (in the elapse of time that has been considered) has been in passing from bias-ply tires to radial-ply tires (see Fig. A.1-4.1)).

For radial-ply tires, further considerable changes in this parameter are not expected in the future. Anyway an increase in tire pressure results in an energy absorption reduction (Fig. A.1-4.2)) and, therefore, the increase in vertical stiffness which follows will be relevant for obtaining a saving in energy, especially if it is accompanied by appropriate modifications to the vehicle suspension system.

2.2 Cornering Stiffness

The cornering stiffness is a parameter that has kept growing as a function of the tire structure (bias-ply tire, radial-ply tire, etc.). The present trend towards low profile radial-ply tires would have the potential capability of providing a higher value of cornering stiffness; on the other hand, while it is rather doubtful that a further increase of this parameter would result in an appreciable driveability advantage, the structures necessary to achieve this might result in a higher rolling resistance coefficient.

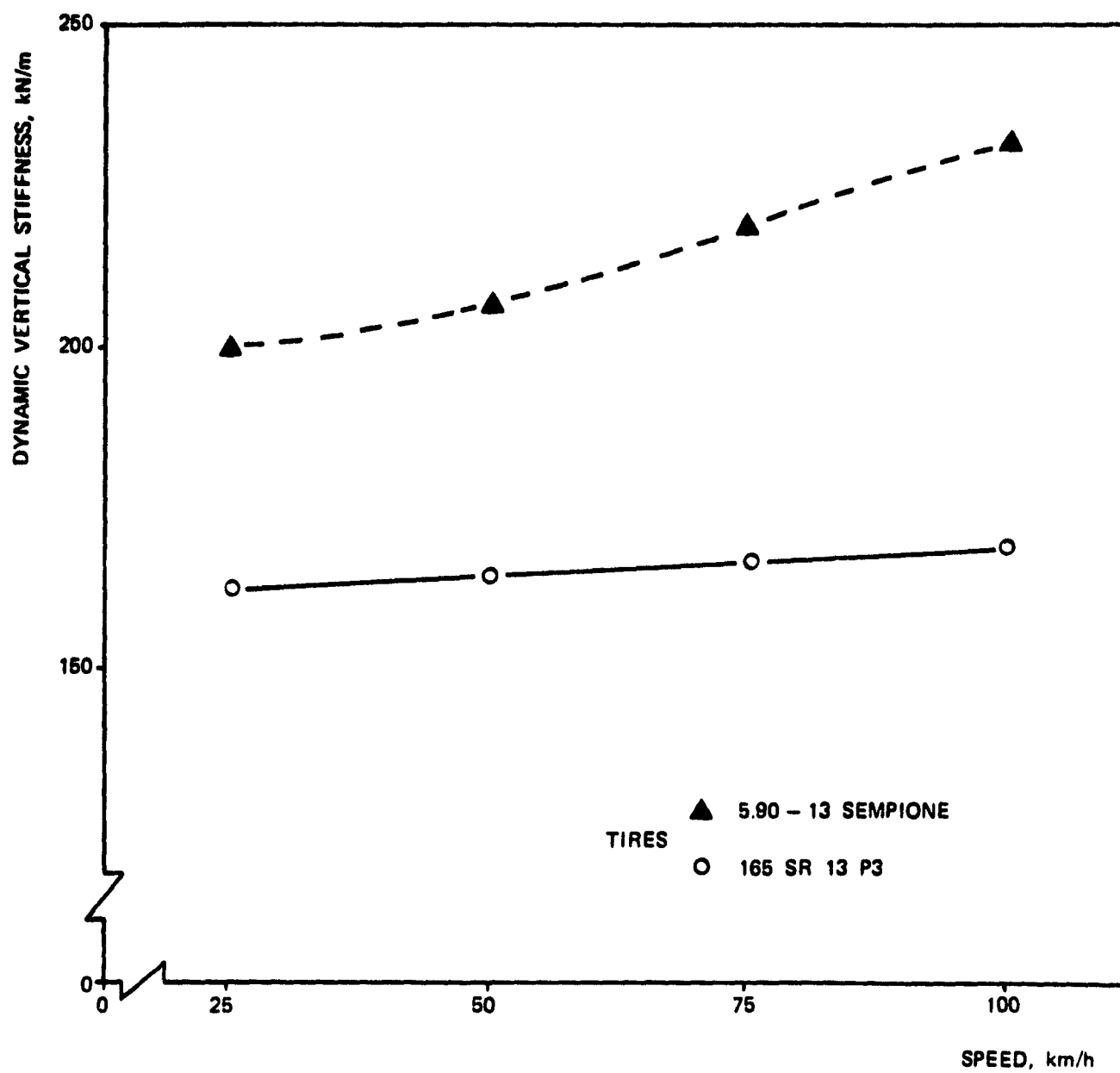


FIG. A.1-4.1- DYNAMIC VERTICAL STIFFNESS VS SPEED FOR TWO DIFFERENT TIRES

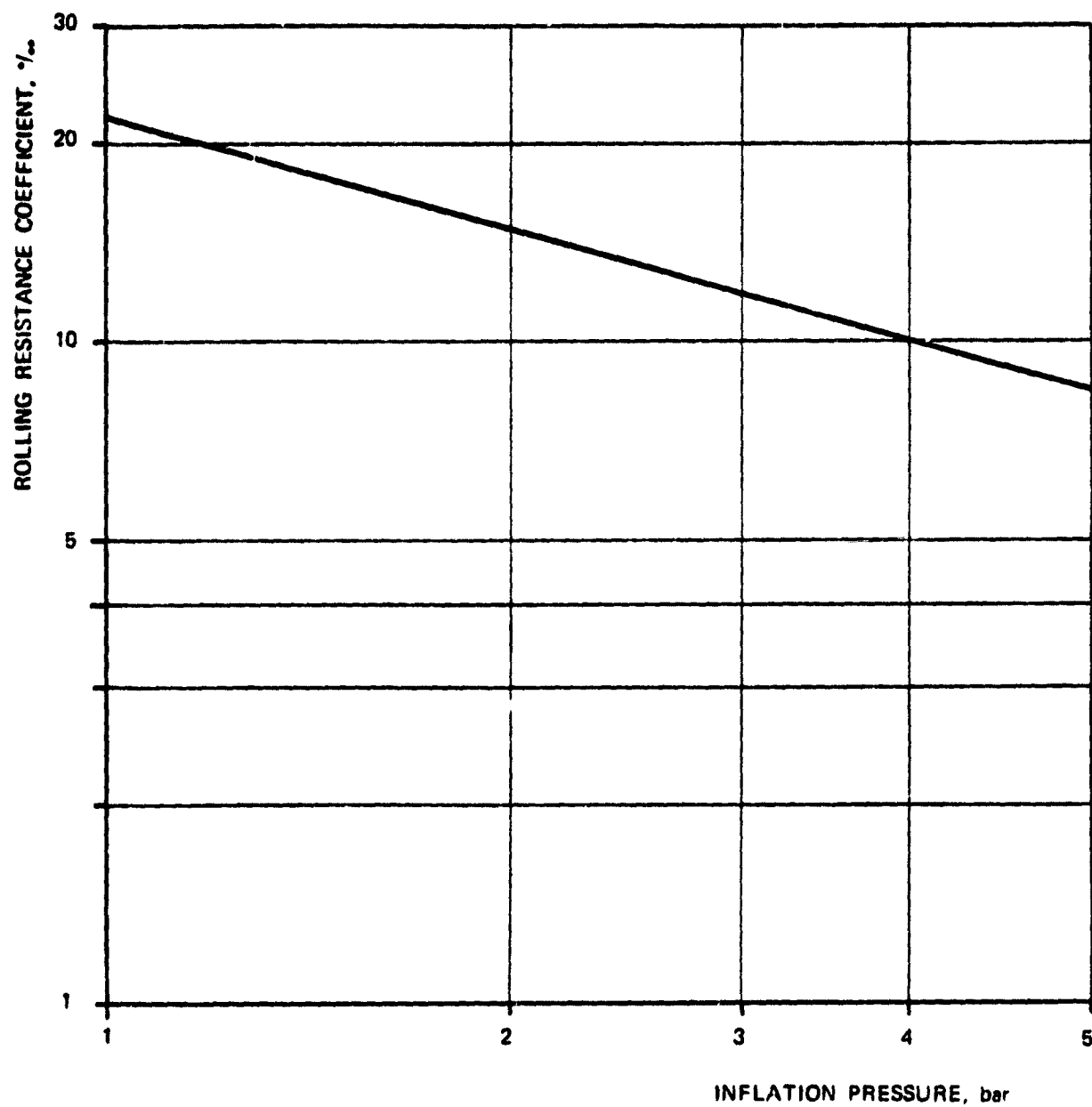


FIG. A.1-4.2 — INFLATION PRESSURE EFFECT ON ROLLING
RESISTANCE COEFFICIENT

Based upon these considerations, a value of tire height/width ratio has been taken as reference which is between 0.70 and 0.60, so that a cornering stiffness can be assumed which maintains the present values (Fig. A.1-4.3).

2.3 Roadholding on wet surface

Although it is rather hard to evaluate this parameter quantitatively, it can be stated that the use of radial-ply tires has improved the vehicle roadholding on wet surface for the fact that for this type of tire it is possible to adopt highly grooved treads.

Another relevant improvement has been in passing from quasi longitudinal grooved treads to transverse treads.

This is particularly important at high speeds, when the loss of traction due to aquaplaning effects becomes relevant.

It is expected that roadholding on wet surfaces at low speeds (in which the tread compound becomes important) will be maintained at its present values, that can be considered acceptable, also in order not to compromise the rolling resistance values which would become higher in case higher traction coefficient compounds are adopted.

Roadholding on wet surfaces at high speeds will instead improve, independently from the rolling resistance coefficient, by properly modifying the tread design.

This forecast, which is bound to such an important factor like safety, remains valid also if the actual speed of vehicles will diminish both for power reduction reasons (due to fuel saving) and for reduction of the speed limits.

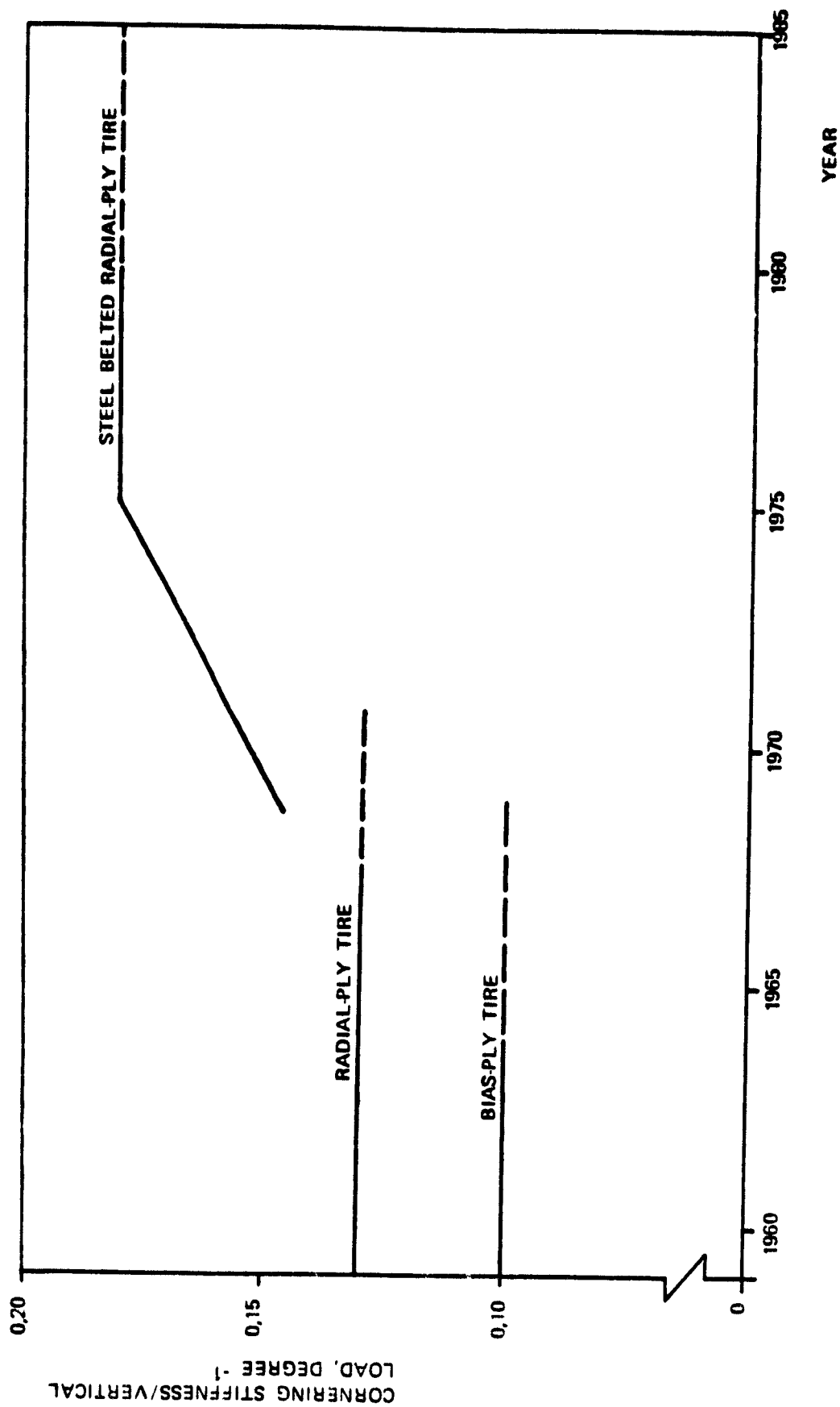


FIG. A.1-4.3 TIME EVOLUTION OF CORNERING STIFFNESS/VERTICAL LOAD RATIO FOR DIFFERENT TIRE TYPE

2.4 Tire dimensions

The tire across dimensions will slightly increase, external diameter and deflection being equal, in view of the introduction of the low profile type tires: this type of tires presents in fact low energy absorption characteristics that are obtainable without sacrificing other properties.

The use of tires of a diameter slightly greater than the present one (cross section and deflection being equal) might imply a further decrease of the rolling resistance coefficient (Fig. A.1-4.4).

It can be assumed, without involving big changes in the vehicle architecture, that appropriately designed cars capable of very low fuel consumption, will be equipped with tires with diameters 10% greater than the present ones.

2.5 Rolling resistance

Also in this case the tire technological evolution has led to an appreciable improvement in terms of rolling resistance (Fig. A.1-4.5).

It can be expected that the values presently reached will further diminish for tires of the 80's, due to improvements that can be obtained on the tire itself and to the adoption of slightly larger diameters (+10%).

3. TIRES FOR HYBRID VEHICLE

The specific characteristics of the tires for the hybrid vehicle will not be substantially different (excluding dimensions which are function of the various loads per axle) from those of the internal combustion engine vehicle (refer to paragraph 1 for reference vehicle characteristics).

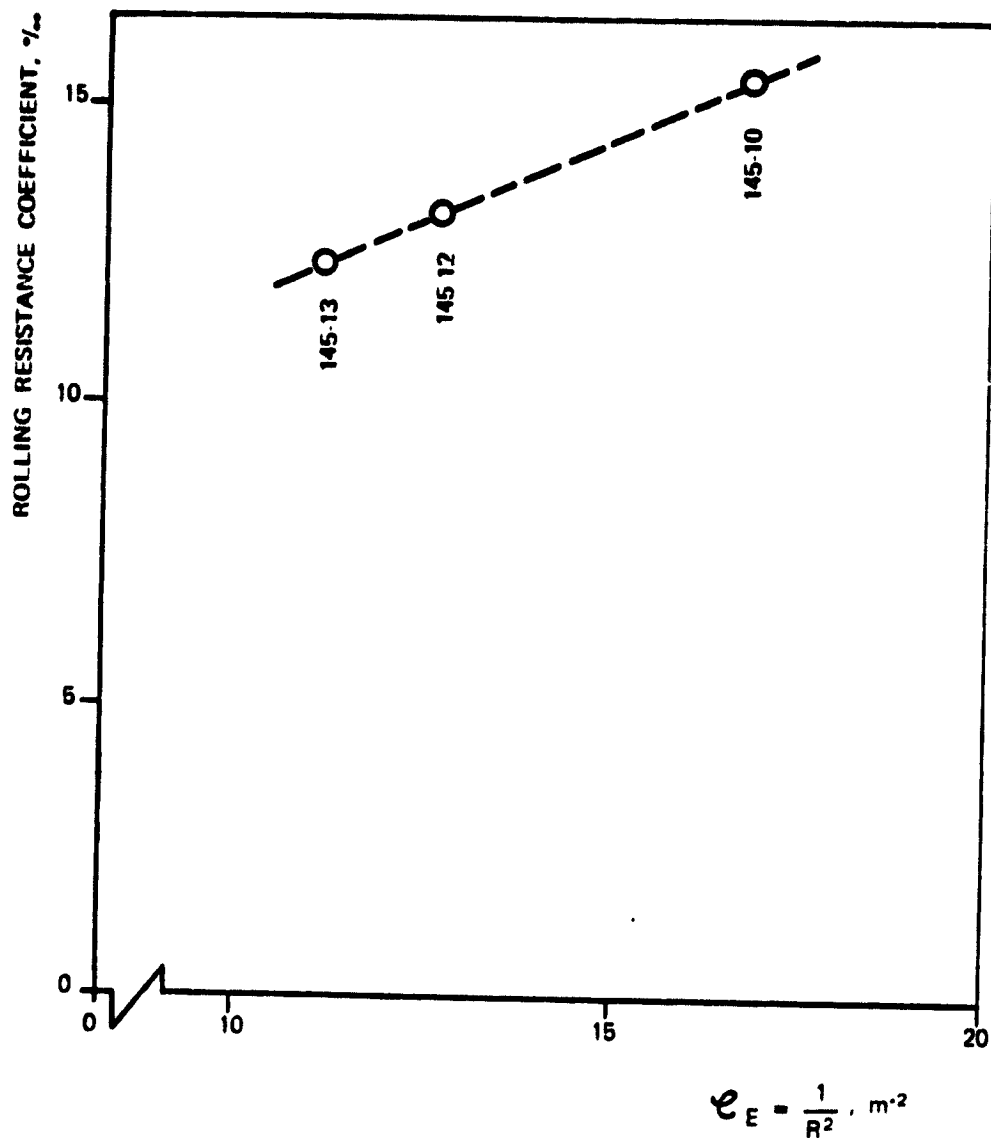


FIG. A.1-4.4 - TIRE RADIUS EFFECT ON ROLLING RESISTANCE COEFFICIENT

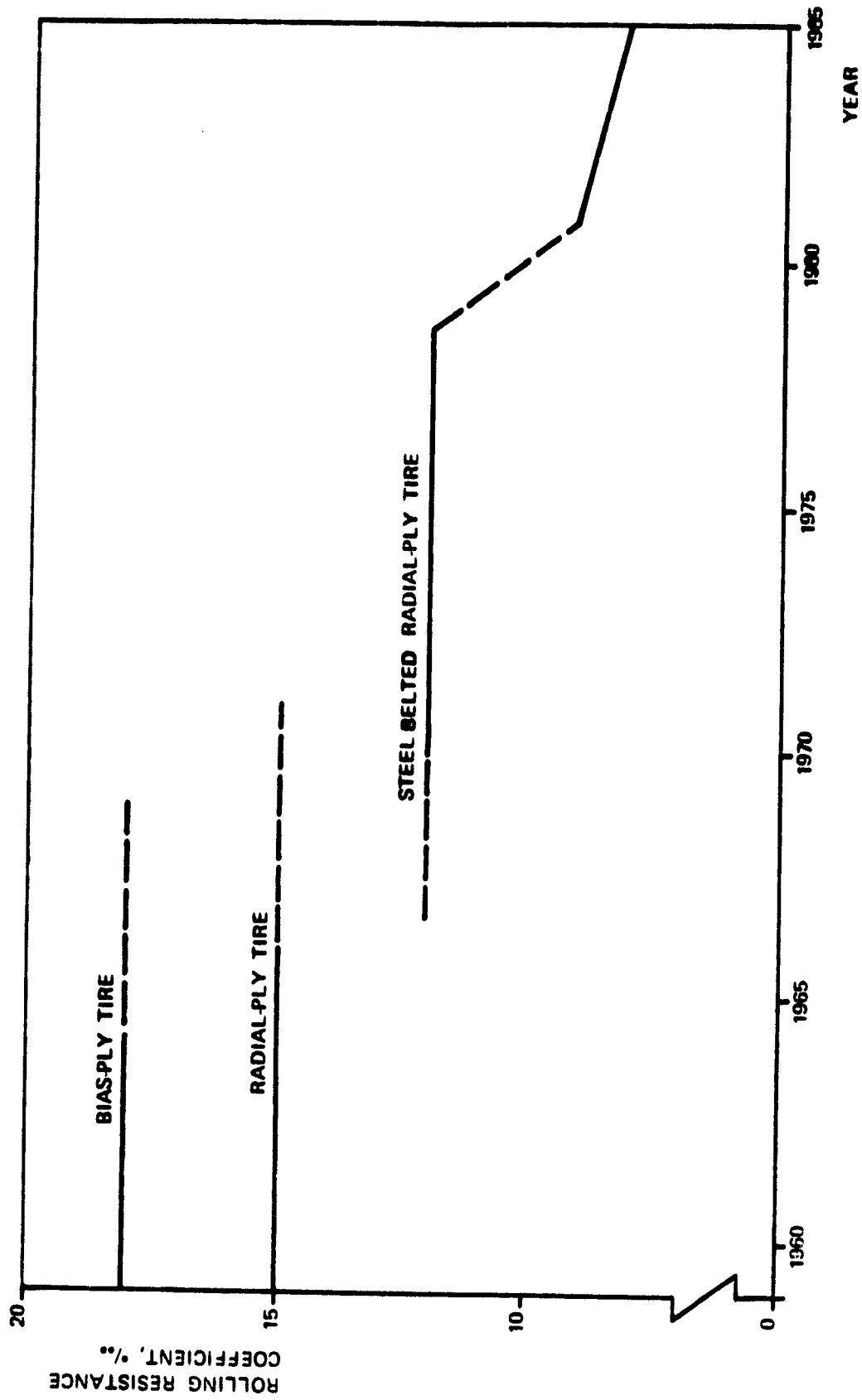


FIG. A.1-4.5 ROLLING RESISTANCE COEFFICIENT VS YEAR AS A FUNCTION OF PLY TIRE TYPE

However the greater overall weight of the hybrid vehicle and, most of all, the smaller ratio between full load weight and weight with driver only, allow, with the same level of comfort, to use a higher inflation pressure. Assuming a 20% increase in inflation pressure, the rolling resistance that can be expected for hybrid vehicle tires will further decrease (Fig. A.1-4.6).

4. COST ESTIMATES

The tires under consideration will have substantially the same weight as the present ones; the use of high-quality materials capable of reducing the rolling resistance will imply a cost increase not greater than 5%.

5. PIRELLI POSSIBLE CONTRIBUTION TO PHASE II OF THE PROGRAM

Pirelli possible contribution to Phase II of the program will consist in supplying prototype tires especially designed and manufactured for the hybrid vehicle.

6. CONCLUSIONS

The state of the art technology of the '80s will result in a large scale production of radial-ply tires and particularly in a broad use of the low profile type tires.

In general, there will be an improvement in tire characteristics due to the inevitable perfectioning of the product, but the preliminary parameters (vertical and cornering stiffness) will maintain their present values. An exception is

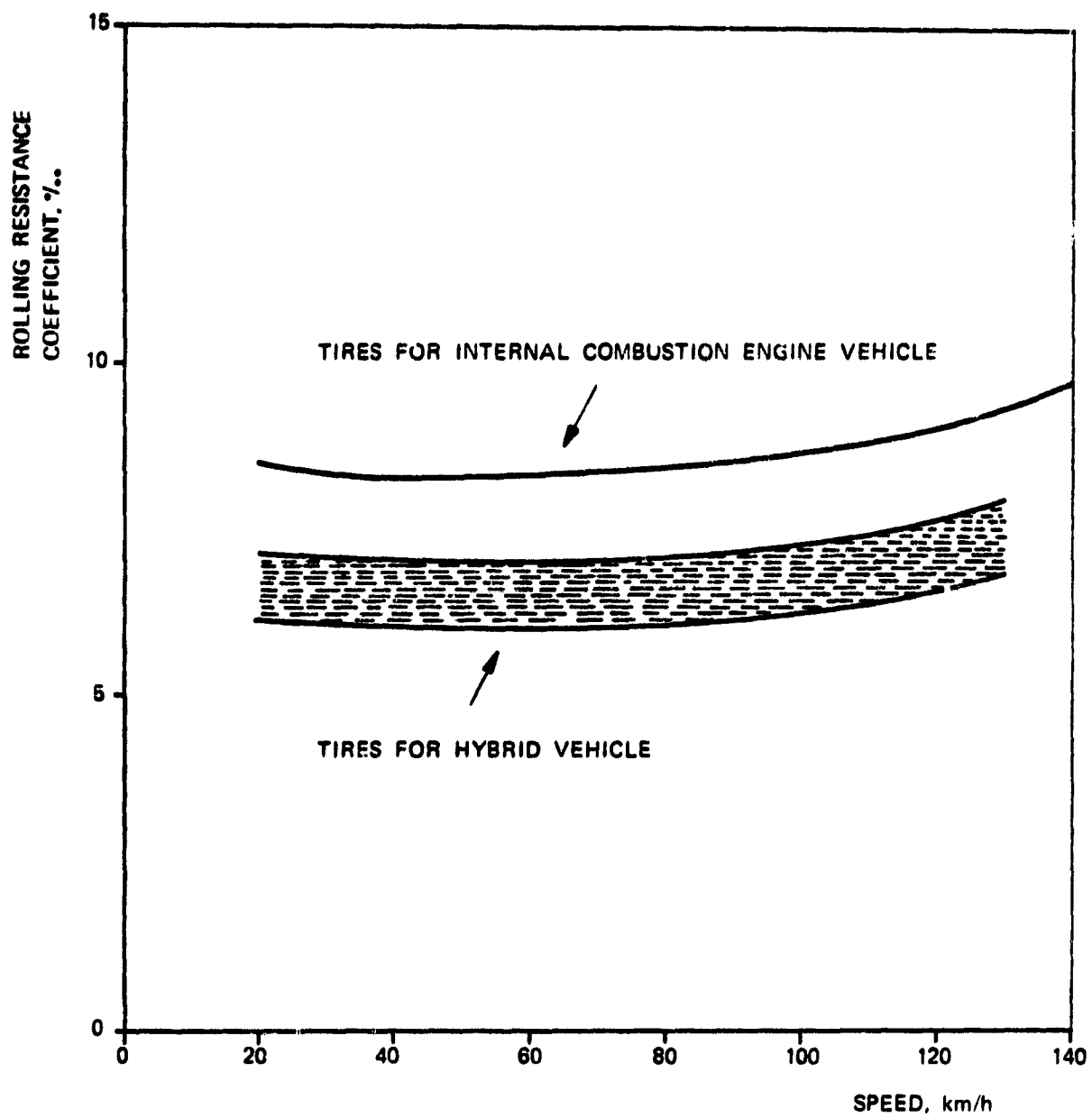


FIG. A.1-4.6 — ROLLING RESISTANCE COEFFICIENT VS SPEED FOR DIFFERENT VEHICLES

represented by the rolling resistance coefficient which, owing to the adoption of slightly larger diameters, will reduce down to a value of 0.8%.

For the hybrid vehicle, because of the greater masses involved and of smaller load variations, it will be possible to adopt higher inflation pressures, so as to reduce the rolling resistance coefficient down to about 0.6%-0.7%.

The overall dimensions will be according to the FIAT proposed limits

\varnothing = 650 mm

Chord = 195 mm

The expected cornering stiffness characteristics are given in Fig. A.1-4.7.

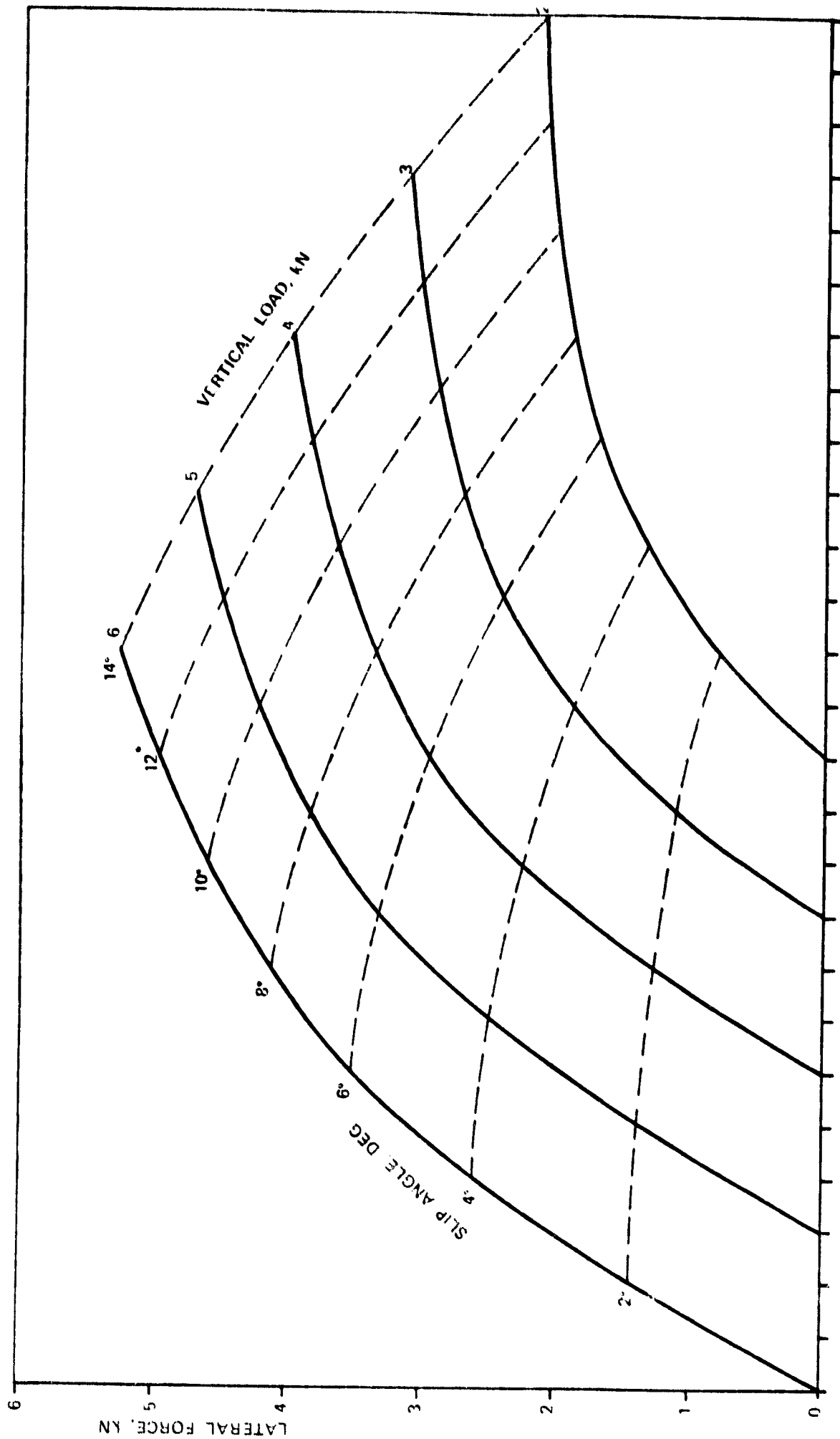


FIG. A1-4-7 CORNERING STIFFNESS CHARACTERISTICS FOR HYBRID VEHICLE TIRES

APPENDIX A.3-1

HANDLING COMPUTER SIMULATION MODEL

The mathematical model is characterized by 11 d.o.f. (degrees of freedom) so distributed:

- 6 d.o.f. associated with the body, considered like a rigid body in which the overall sprung mass is included. They are the 3 body center-of-gravity translations and the 3 body rotations (roll, pitch, yaw)
- 4 d.o.f. associated with the angular velocity of each wheel since different slip ratios are possible
- 1 d.o.f. associated with the steering wheel angle. This degree of freedom exists only for those maneuvers in which the steering wheel is released.

The main input data required by the program are the following:

- vehicle geometry
- sprung and unsprung mass
- moments of inertia
- geometric, kinematic and elastic characteristics of the suspensions
- braking system characteristics
- steering system characteristics
- transmission characteristics (gear, final ratio, torque converter,...)
- tires characteristics
- propulsion system characteristics
- aerodynamic parameters
- maneuver data.

In the frame of the main characteristics, the simulation mathematical model:

- performs a simulation of a vehicle (not necessary having a symmetrical behaviour) with any of the four wheels being either driving or braking or both
- takes into account the non-linearity of the suspension and

- estimates its longitudinal and lateral displacements
- can deal both with independent suspensions and rigid axles; therefore it takes into account effects due to possible anti-pitch and/or anti-roll rods
 - as far as tire are concerned, considers the non-linear relationship between lateral forces and slip angles, normal load and tractive forces. Moreover it estimates camber forces and aligning torques. Vertical and lateral tire flexibilities are instead neglected
 - assumes that the central moments of inertia of the vehicle remains constant during any motion: the interaction of those parts that change position during the maneuver is therefore neglected
 - takes automatically into account the aerodynamic effects due to the vehicle speed
 - can introduce external disturbances such as wind gusts from any direction and external forces and/or torques applied to the center of gravity
 - neglects any effect connected with an irregular road-bed or the lifting of a wheel from the ground.

The model can simulate all the "open-loop" tests (free path).
Among these:

- steering-pad
- steering wheel angle input
- throttle release
- balanced or unbalanced braking during straight forward or cornering motion
- external disturbances
- overtaking (only if steering wheel angle recording is available).

The characteristic outputs of the program are shown in the following pages. Graphs and Tables are relative to one of the maneuvers performed in the frame of hybrid-reference vehicle behaviour comparison.

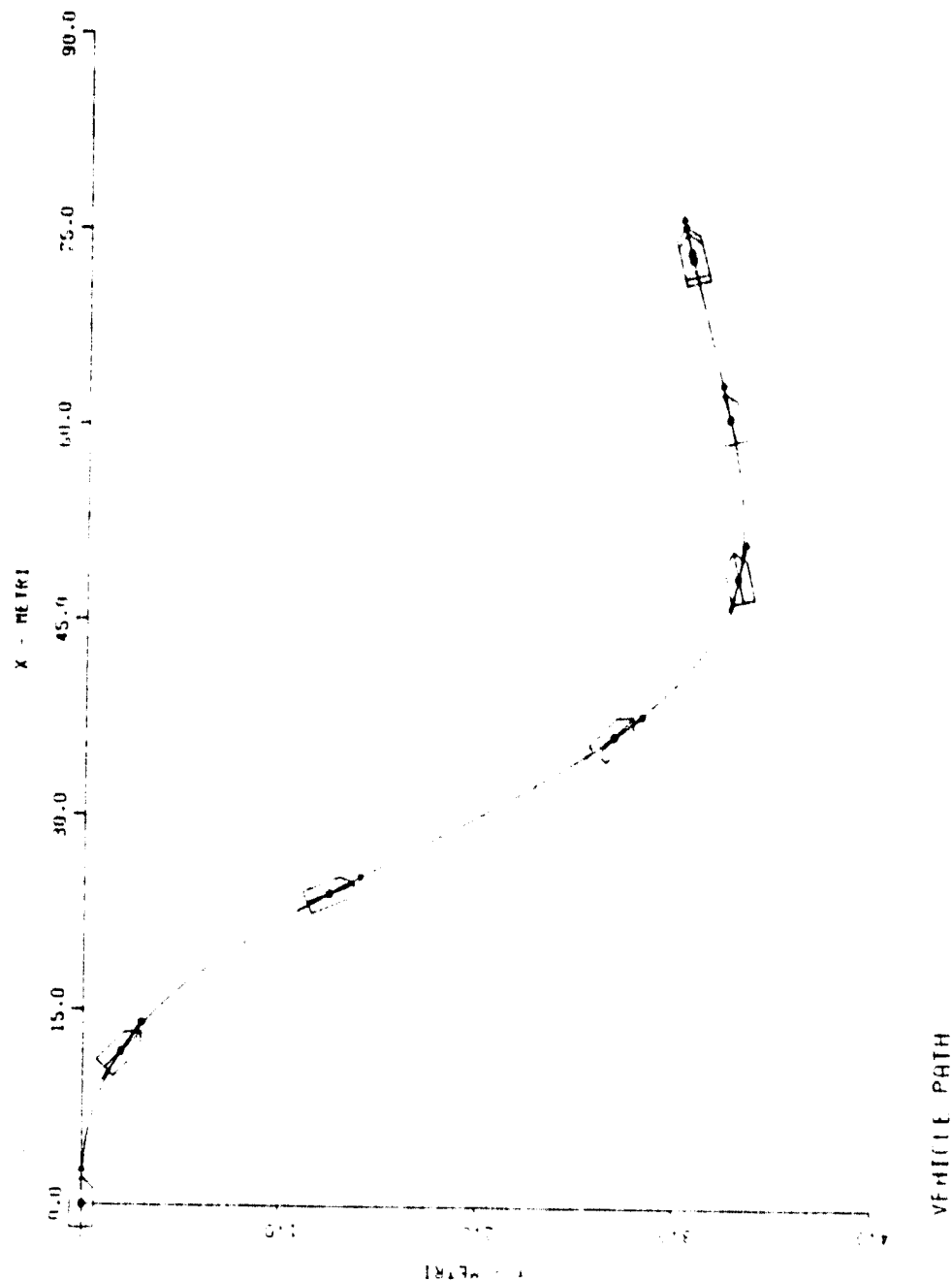
GRAPHS

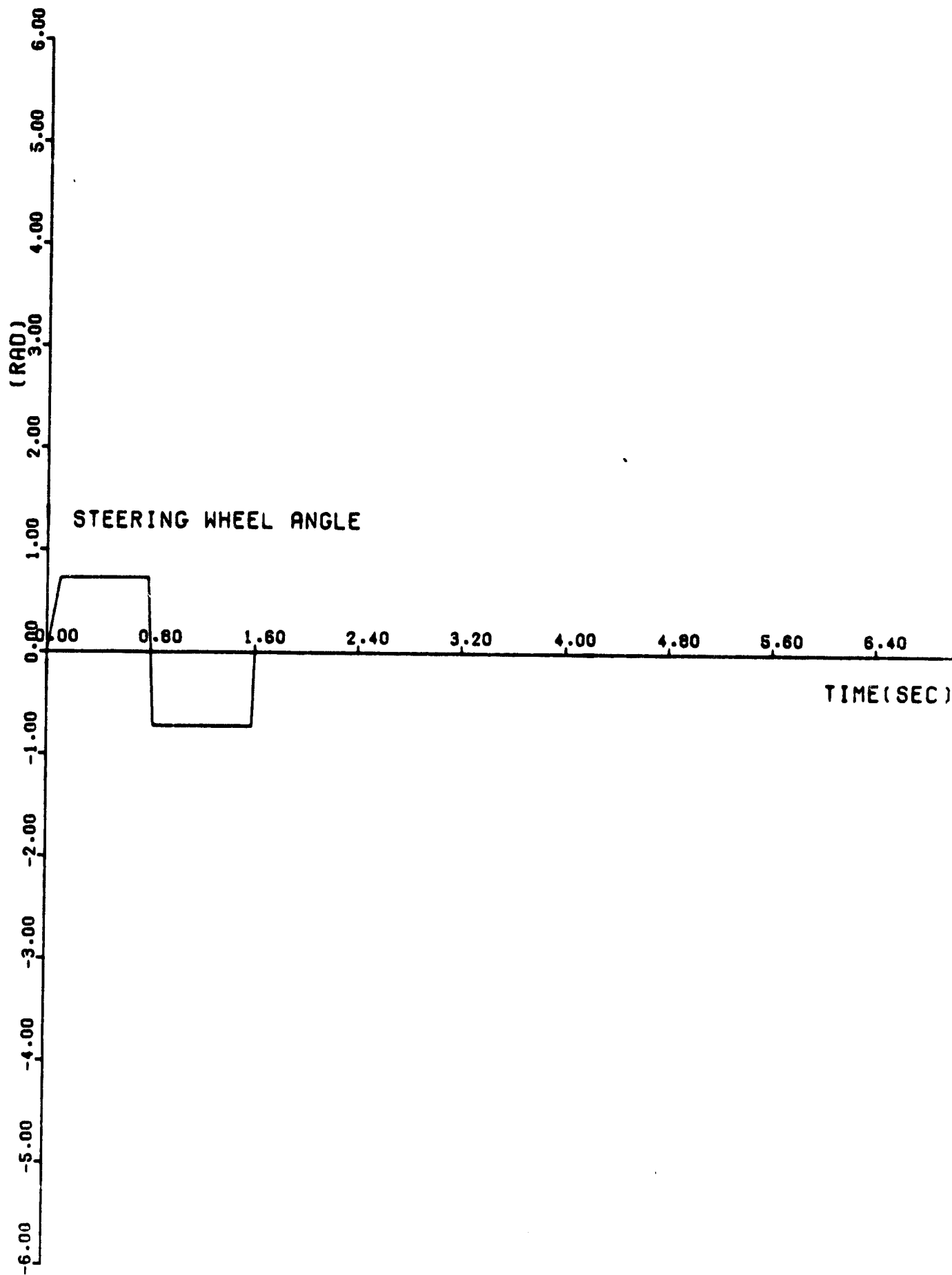
- 1 Vehicle Path
- 2 Steering Wheel Angle vs Time Input Law
- 3 Roll Angle Output vs Time Output Plot
- 4 Pitch Angle Output vs Time Output Plot
- 5 Sideslip Angle vs Time Output Plot
- 6 Yaw Angle vs Time Output Plot
- 7 Yaw Rate vs Time Output Plot
- 8 Yaw Acceleration vs Time Output Plot
- 9 Curvature vs Time Output Plot
- 10 Lateral Acceleration Output Plot
- 11 Four Wheels Normal Load vs Time
- 12 Four Wheels Slip Angle vs Time
- 13 Four Wheels Lateral Force vs Time
- 14 Four Wheels Self-Aligning Torque vs Time

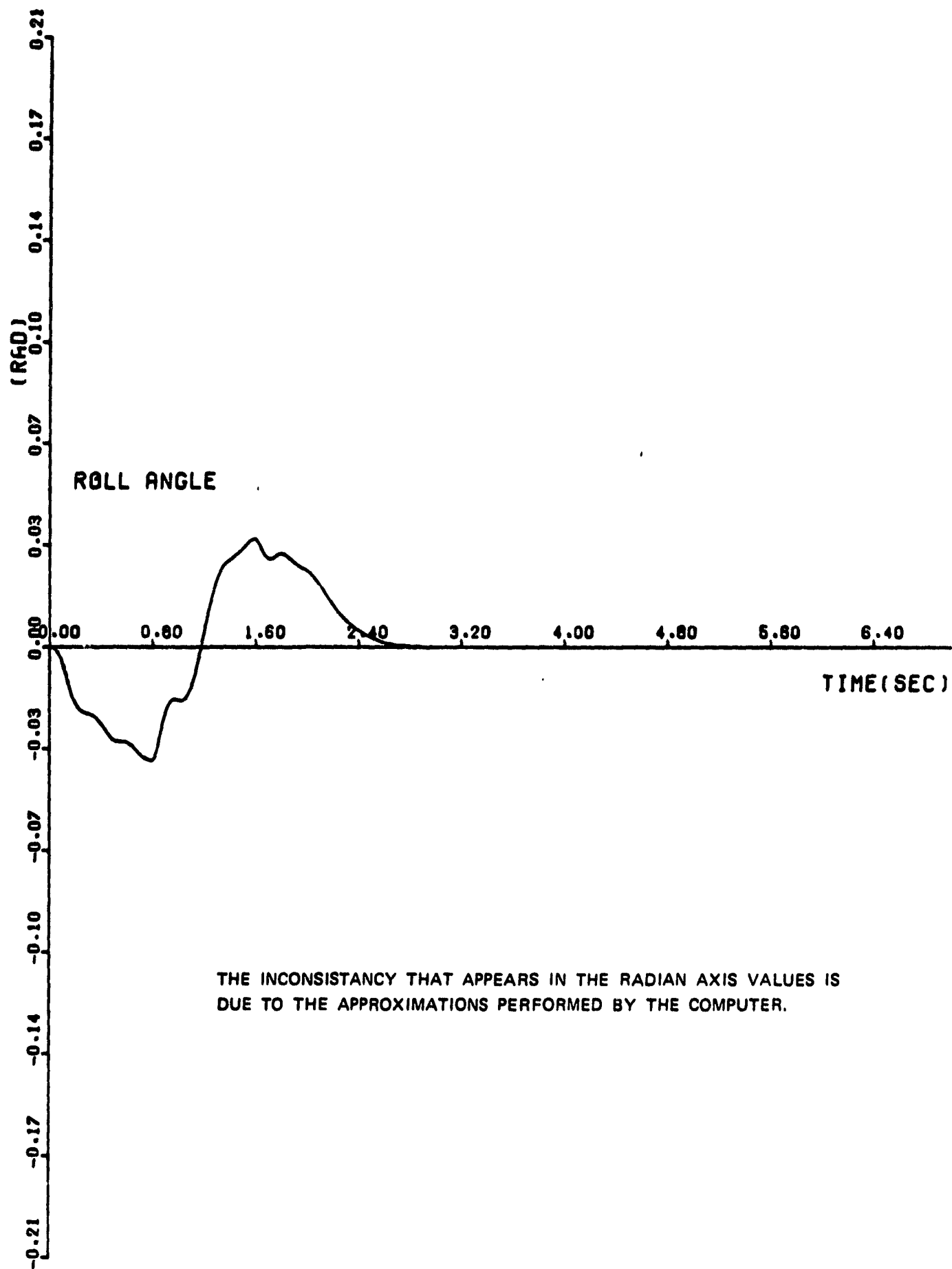
TABLES

- 15 Hybrid Vehicle Output Data During Lane Change Maneuver At 55 MPH For Various Instants (Time Difference Between Two Consecutive Instants = 0.1 Sec).

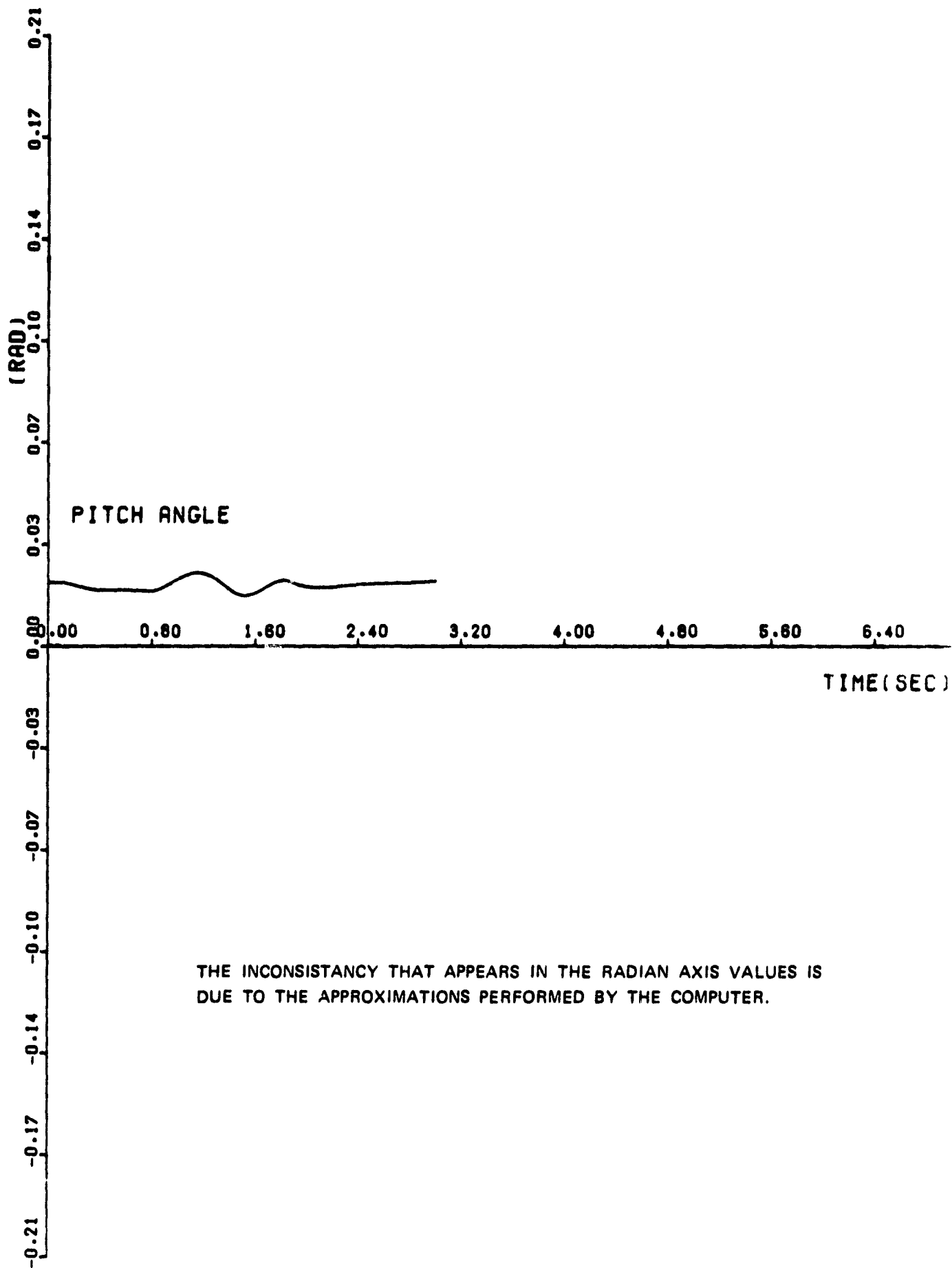
*** HANDLING ***

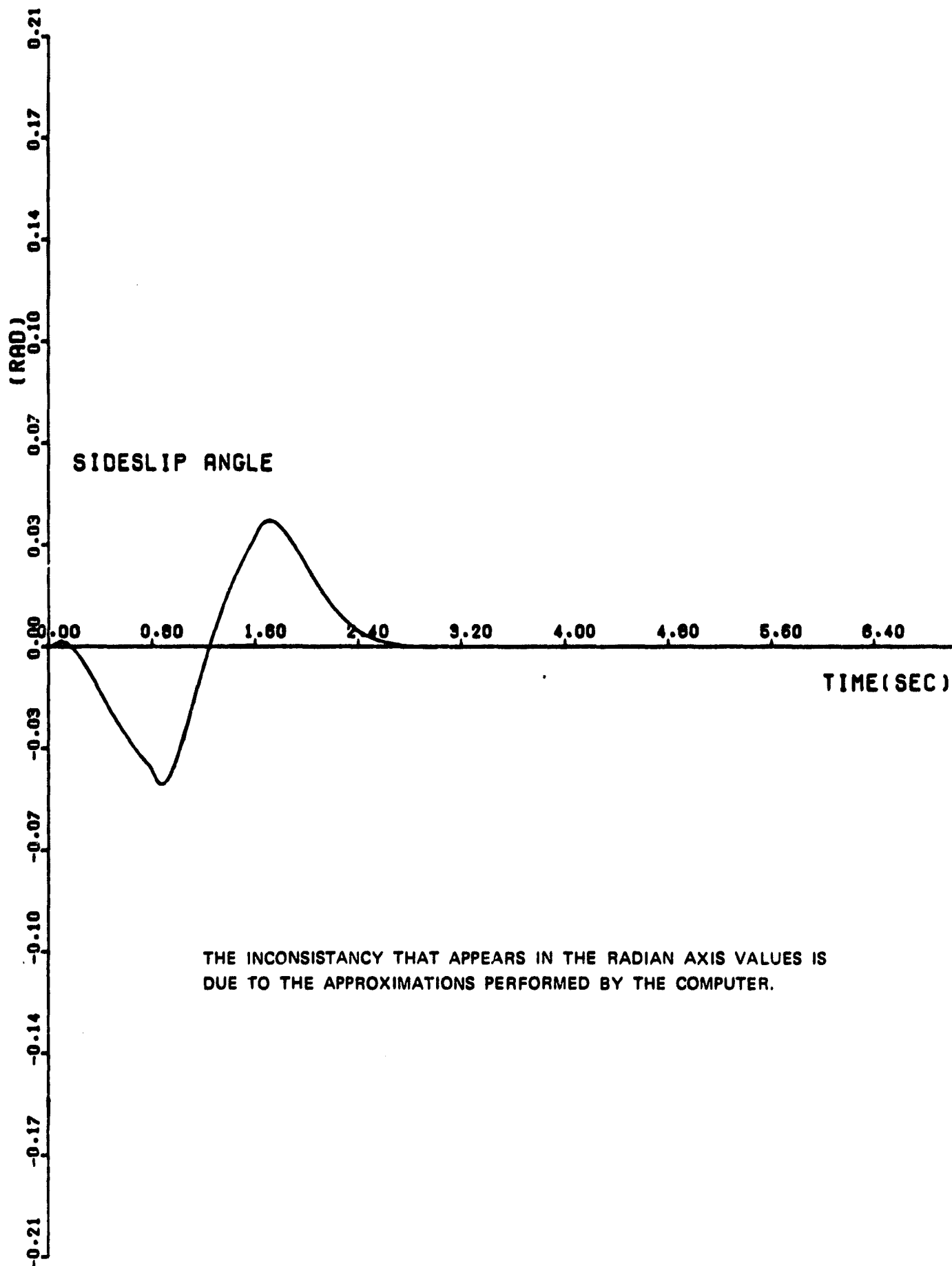




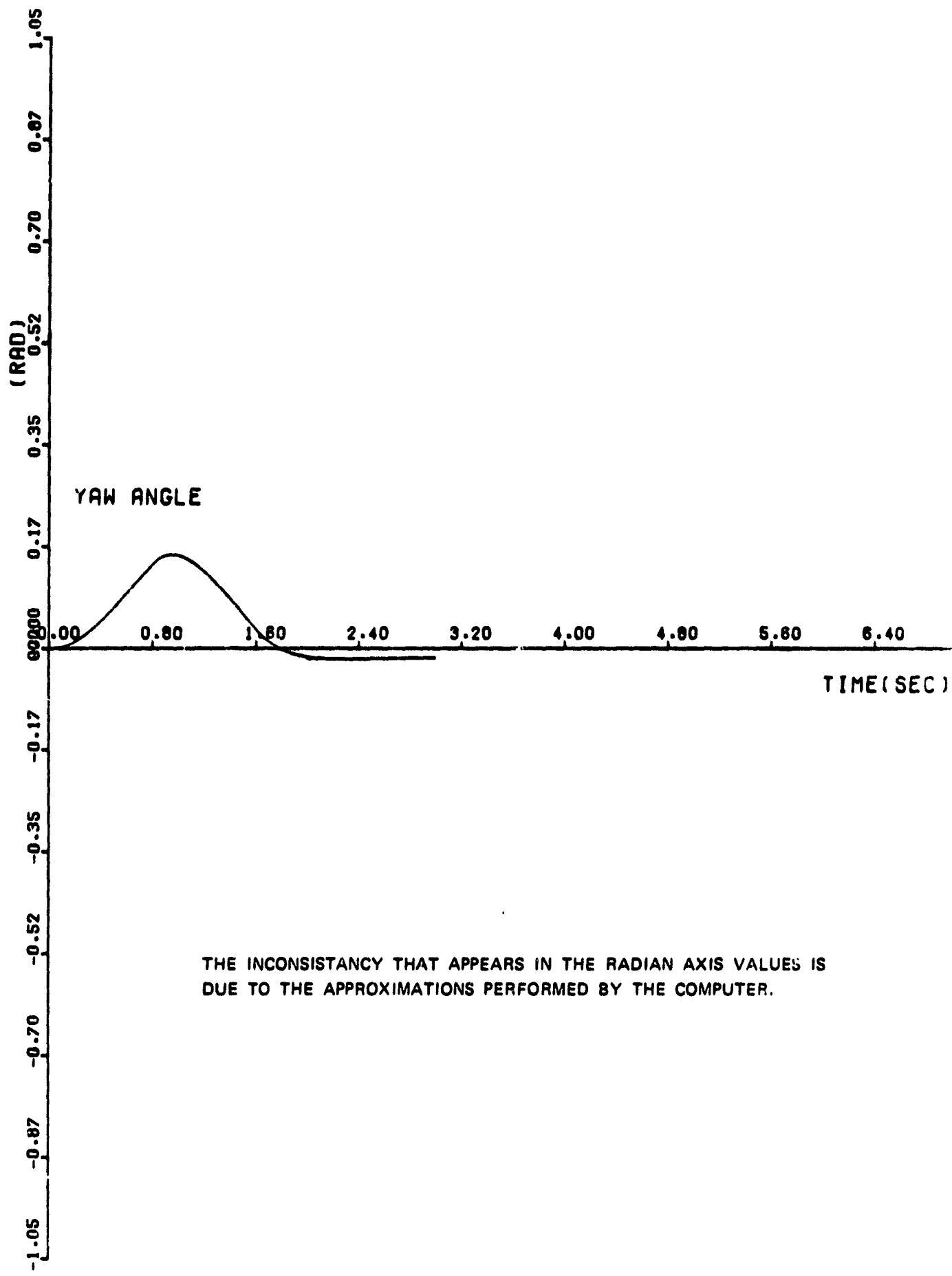


THE INCONSISTANCY THAT APPEARS IN THE RADIAN AXIS VALUES IS
DUE TO THE APPROXIMATIONS PERFORMED BY THE COMPUTER.

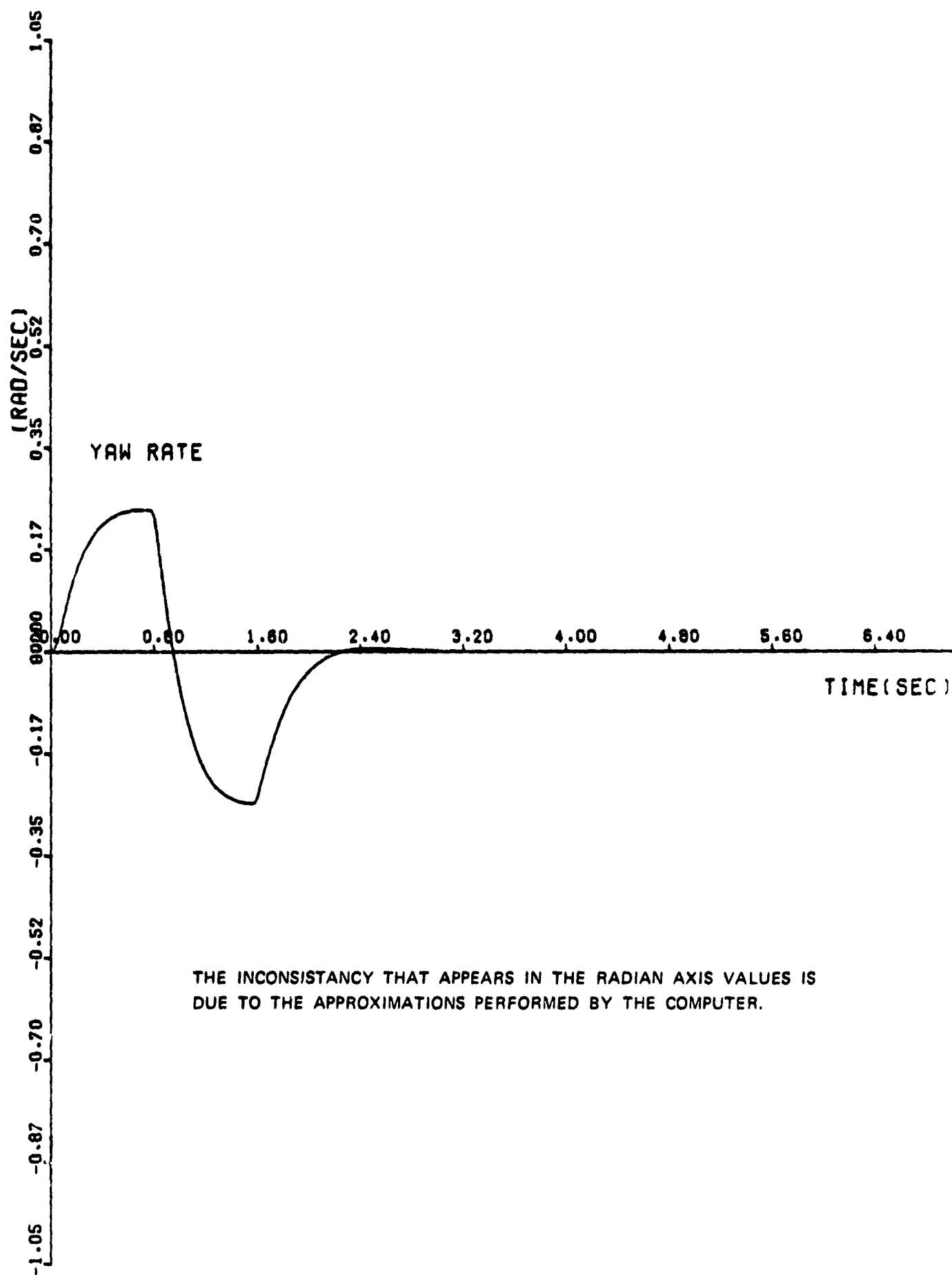


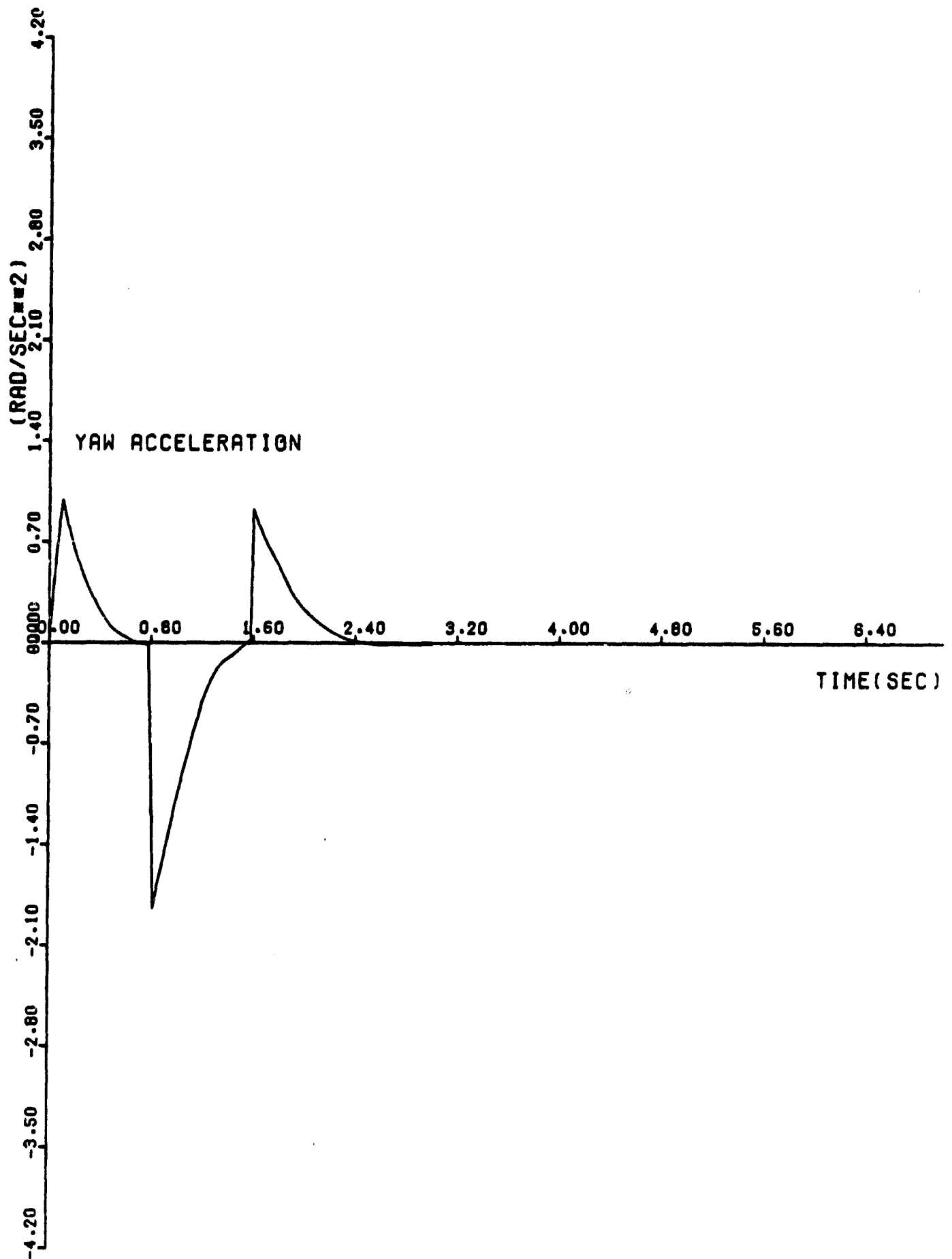


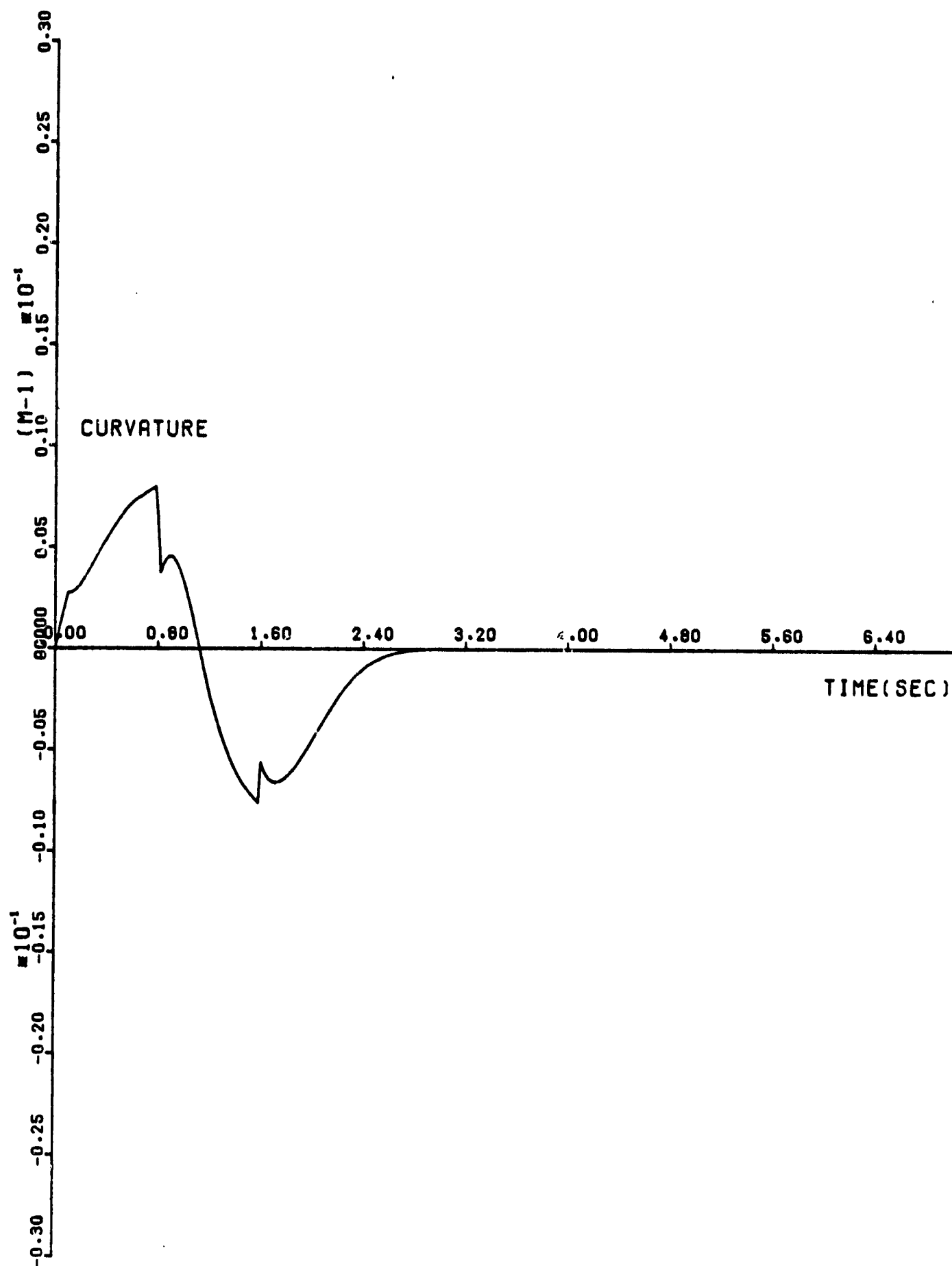
THE INCONSISTANCY THAT APPEARS IN THE RADIAN AXIS VALUES IS
DUE TO THE APPROXIMATIONS PERFORMED BY THE COMPUTER.

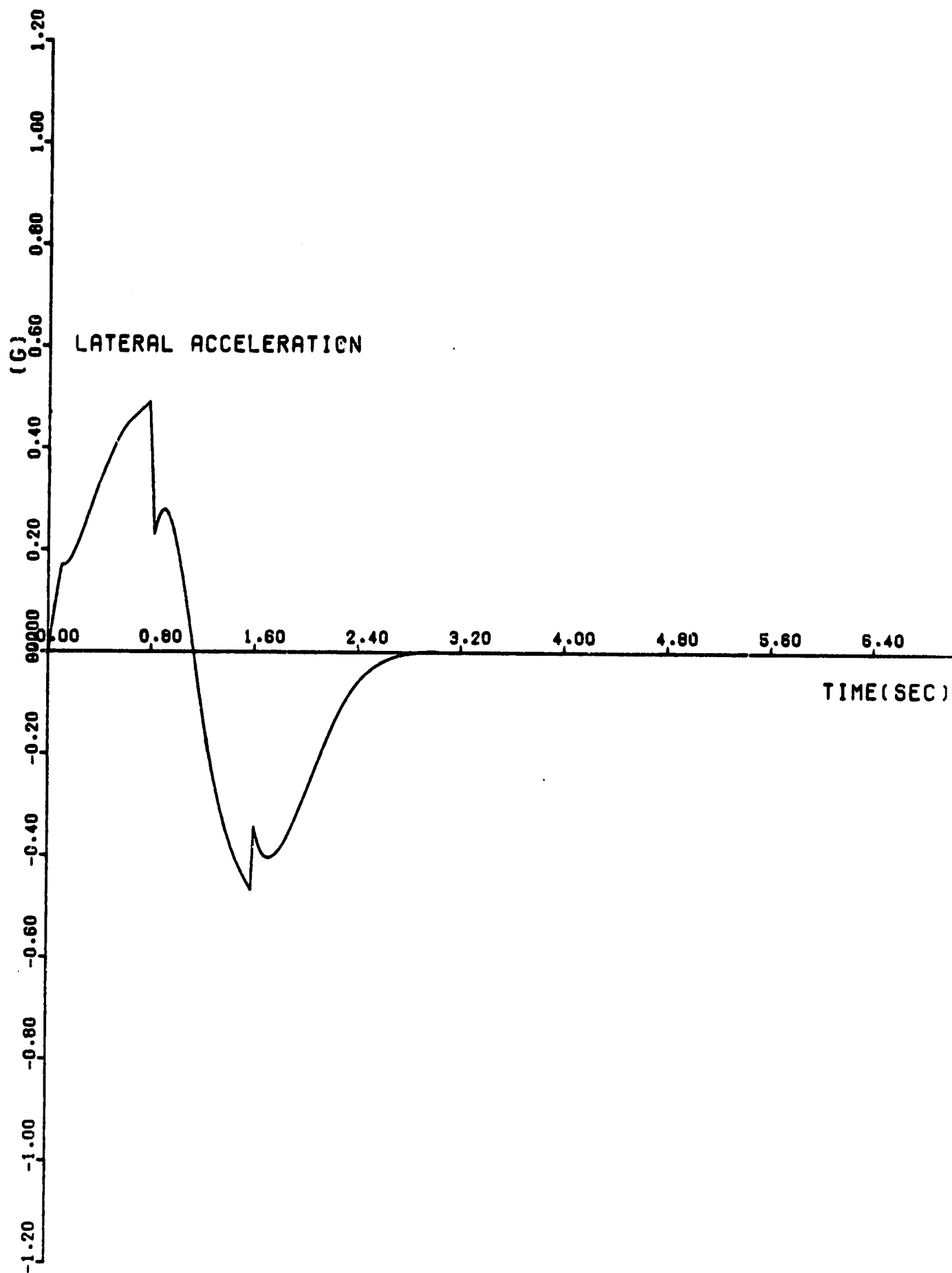


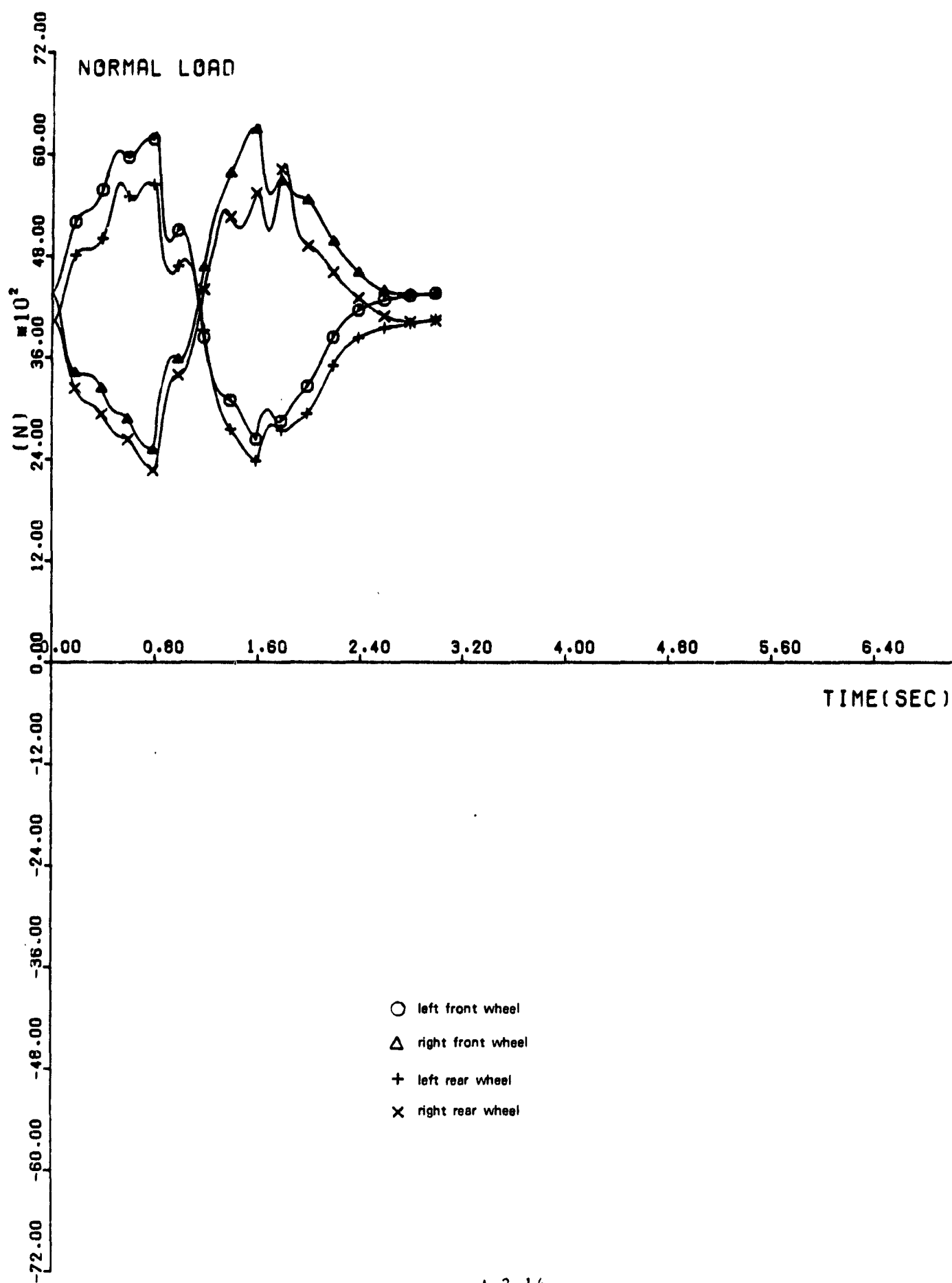
THE INCONSISTANCY THAT APPEARS IN THE RADIAN AXIS VALUES IS
DUE TO THE APPROXIMATIONS PERFORMED BY THE COMPUTER.

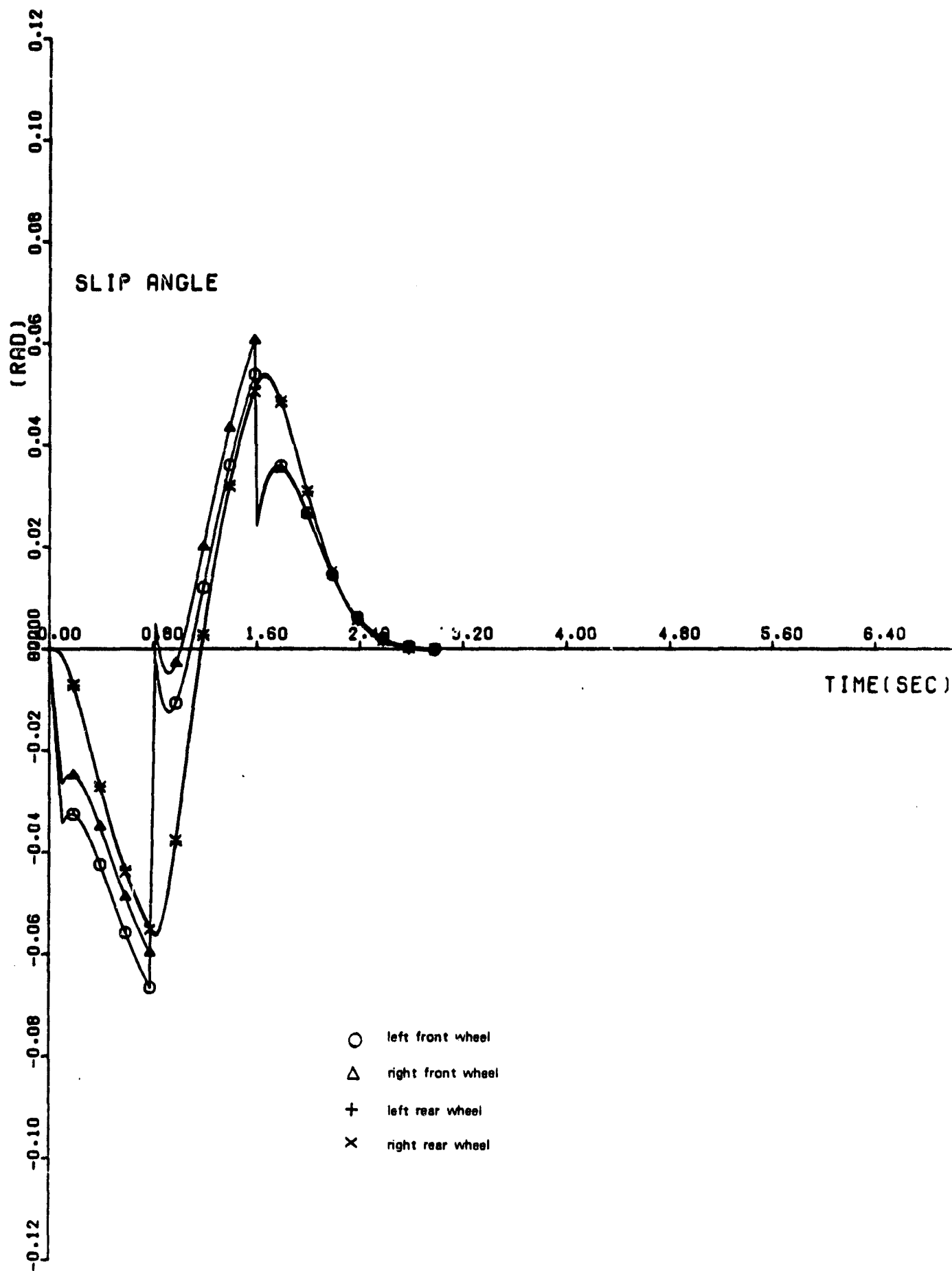


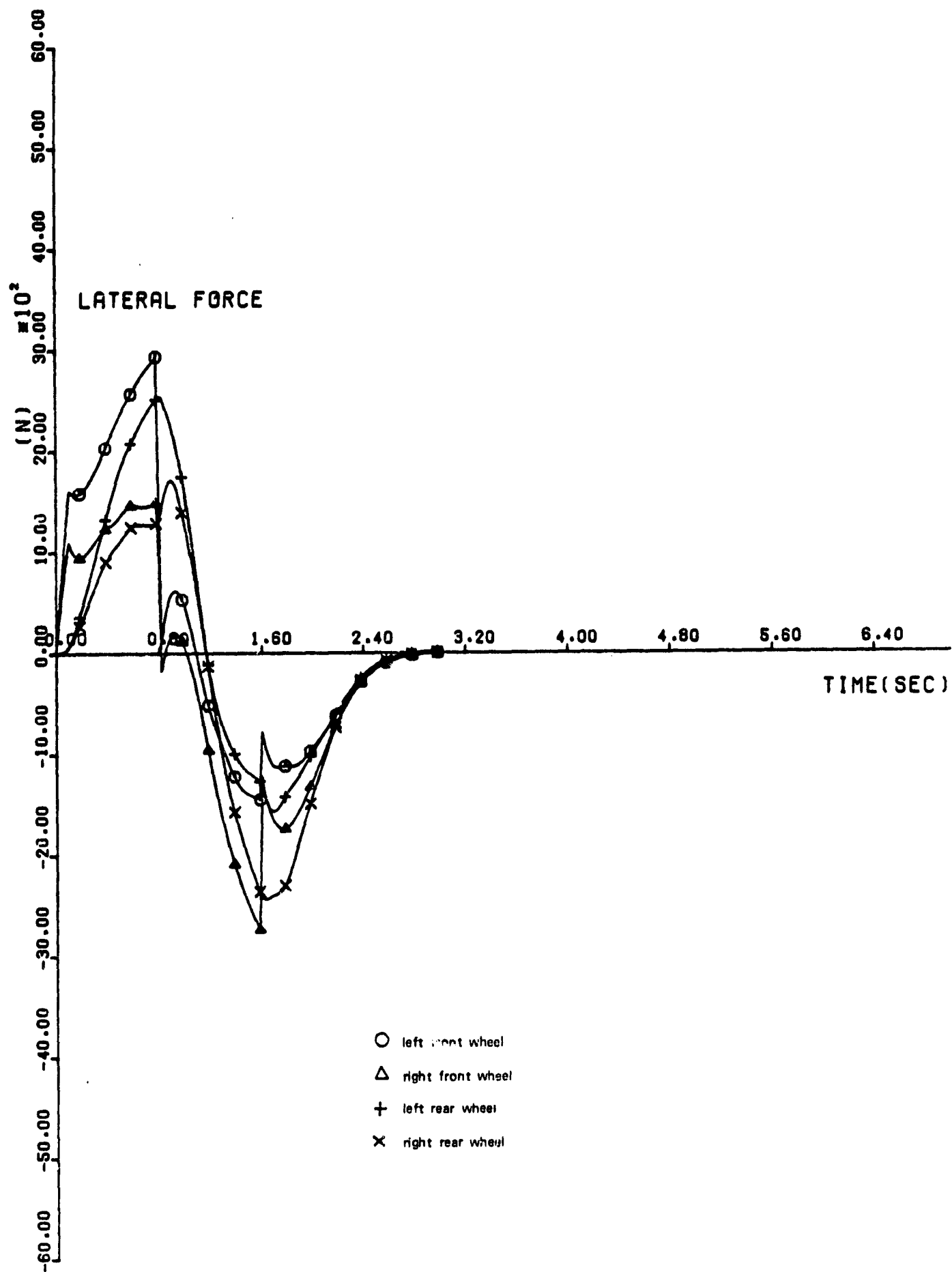


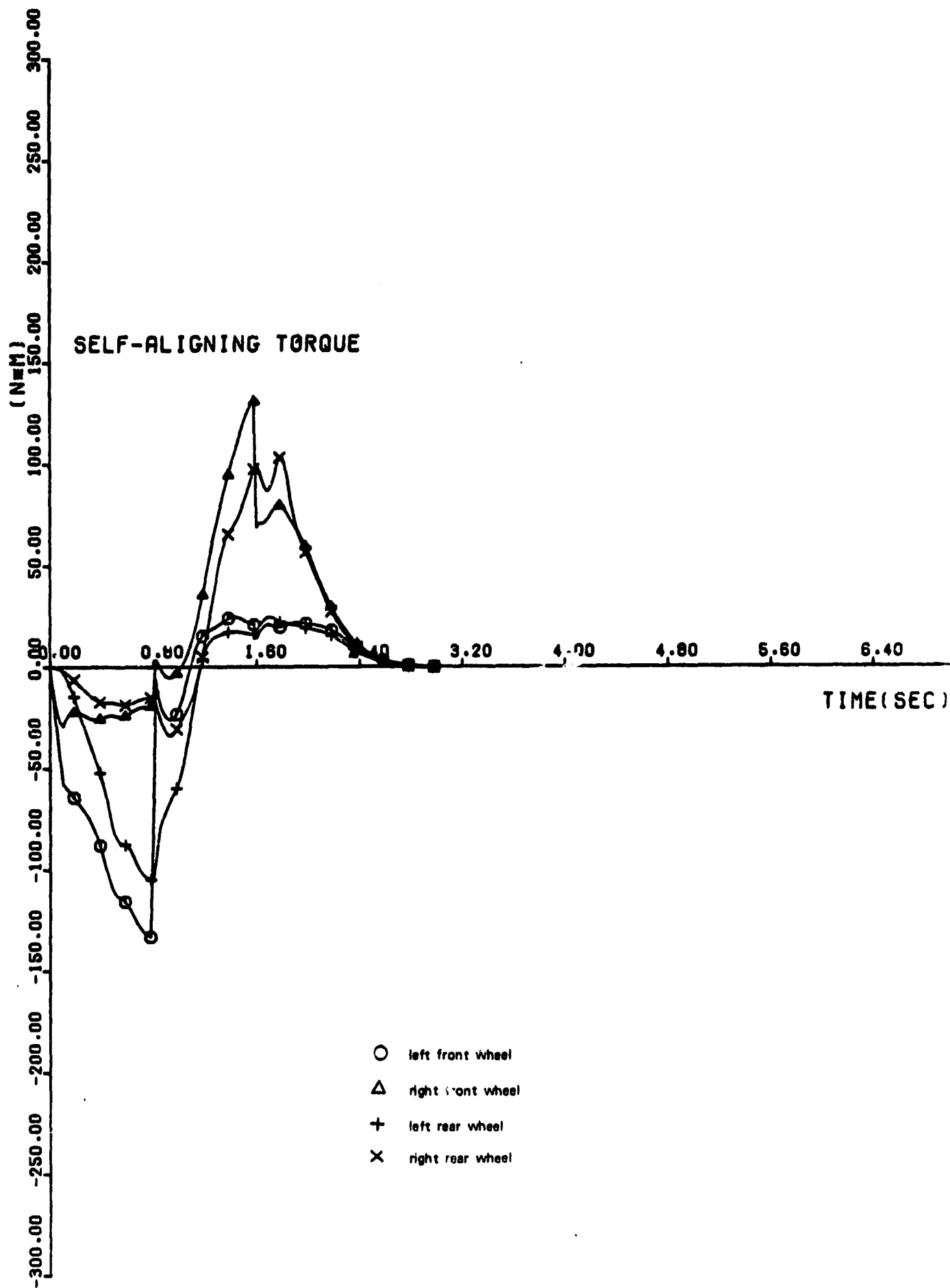












RISULTATI ALL' ISTANTE T = .70000									
VELOCITA' KM/H = 00.3478 RAGGIO EFFETTIVO = 130.368									
ACCELERAZIONE LATERALE = .470901 G CONTINGENZA EFFETTIVA = .476947									
SSSSS V E I C O L O SSSSS									
X	= 17.1886	VINX	= 24.4578	ATMX	= -.555931				
Y	= .533158	VJNY	= 2.01946	ATNY	= 4.50891				
Z	= .362728-01	VINZ	= -.196923-01	ATNZ	= .300337-01				
	= .767105-02	VMOX	= 24.5201	AMOX	= -.155220-01				
VELOCITA'	= 24.5411	VMOY	= -.925930	AMBY	= 4.61044				
RAGGIO	= 130.368	VMOZ	= .412601	AMBZ	= .201310				
PASSO INT.	= .200000-01	PSTAR	= -.441303-01	PPINTOS	= .330064				
CONTINGENZA	= .470901	OSTAR	= -.104700-01	OPUNTOS	= -.109267-01				
INDICE ESV	= 6.92956	RSTAR	= .241039	RPUNTOS	= -.151579-02				
SSSSS ANGOLI VELOCITA' DISSSS									
ANGOLI DI:	VELOCITA' DI:	ANGOLI DI:	ANGOLI DI:	VELOCITA' DI:	ACCELERAZIONI DI:				
ASSETTO VERO	= -.370003-01	-2G 7P 30.0S	13G 51P 36.5S	-110940-02					
ASSETTO MIS.	= .000000	0G 0P .0S	0G -5P 0.7S	.000000					
IMBARCATA	= .119470	6G 50P 42.5S	-2G 15P 55.1S	.000000					
RECCHEGGIO	= .100212-01	1G 5P 23.4S	0G 0P .0S						
ROLLIN	= .371104-01	-2G 7P 36.2S							
VOLANTE	= .723750	41G 20P 4.2S							
SSSSS RUOTE SSSSS									
ANT.SIN.	POST.SIN.	ANT.DES.	POST.DES.						
STERZO	387906-01	.310216-01	.000000						
DERIVA	-.625916-01	-.557261-01	-.510672-01						
CONVENENZA	-.586900-03	.572092-04	-.140513-03						
CAMPANATURA	.217500-03	.161650-01	-.100017-01						
CAMP. RTF. AL SUOLO	-.415171-01	-.202000-01	-.600121-01						
SCUOTIMENTO	.392011-01	.007490-01	.363227-01						
VELOCITA' SCUOTIM.	.109371-01	.667402-02	-.504631-01						
VFL. DEF. LAT. PNEUM.	.000000	.000000	.000000						
CARTO SCUOTIMENTO	5566.77	5110.32	2113.52						
LATERALE	2006.29	2360.54	1266.50						
LONGITUDIN.	240.740	-66.7176	-20.2045						
QUOTA PESO+CAR. SCUOT.	6150.30	5636.70	2372.60						
MOMENTO AUTOALLIN.	-128.636	-100.417	-16.0332						
RFS. AL ROTOL.	24.9100	22.3976	0.07930						
FLENANTE	.000000	.000000	.000000						
VFL. CENTRO RUOTA	24.6537	24.6033	24.3453						
VFL. ROTAZ. RUOTA	01.6845	00.7062	79.6386						
SCORRIMENTO	.104300-01	-.315630-02	-.220000-02						
SSSSS P I L O T A R G T O SSSSS									
VELOCITA' DI ROTAZ.	449.745	4204.74	POTENZA DI ROTOLAMENTO = 7.03462						
COPIA	34.5440	3.52131	POTENZA AERODINAMICA = 9.31000						


```
*****  
*          RISULTATI ALL' ISTANTE T = 2.30MPA          *  
*          *****                                     *  
*          *  
*          *  
*****  
* VFLUITTA' KM/H      = 89.1250      RAGGIO EFFETTIVO   = -631.712    *  
* ACCFLRAZIONE LATERALE = -.0674M9-MIG CONTINGENZA EFFETTIVA = -.066073-MIG *  
*****  
*          $$$$$$ V E I C O L O $$$$$$                *  
*****
```

X	56.24R3	VINX	24.47R3	AINX	5552R2-01
Y	3.3P209	VINY	-234130	AINY	-94900R
Z	3R1708-01	VINZ	-590R09-02	AINZ	-100R21
CURVATURA	-150330R-02	VHORX	24.4733	AM08X	652367-01
VELOCITA'	24.4704	VMORY	2210K5	AM0VY	-940R20
RAGGIO	-631.712	V40BZ	502609	AM0RZ	-987491-01
PASSO INT.	200000-01	PSTAR	-390117-01	PPHNT03	16612R
CONTINGENZA	-964903-01	QSTAR	463445-02	QPHNT03	-434380-02
INDICE FSV	474439-02	RSTAR	232920-02	RPHNT03	-376449-01

	ANGOLI DI:	SSSS ANGOLI	VEICOLI	SSSS	ANGOLI DI:	VELOCITA' DI:	ACCELERAZIONI DI:
		VELOCITA' DI:					
ASSETTO VERO	-004101-02	-			00 30P 23.00	-	
ASSETTO MIS.	-000000	-			00 0P -00	-	
IMBARCATA	-104062-01	.237219-00		-10 3P 16.60	00 0P 9.30		.376116-01
200650-01	.461245-00			10 11P 43.70	00 10P 31.50		
101660-02	-307622-01			00 31P 34.00	-26 16P 41.60		
000000	-000000			00 0P -00	00 0P -00		.000000

SSSSS R U O T E SSSS			
	ANT. SIN.	POST. SIN.	
STERZO	.000000	.000000	POST. DFS.
DERIVA	.006134-02	.059207-02	.000000
CONVERGENZA	.002100-05	.115034-03	.070073-02
CAMPANATURA	.466961-03	.102296-01	.004200-03
CAMP. RIF. AL SUOLO	.220000-01	.352430-01	.101532-01
SCUOTIMENTO	.510030-02	.609460-01	.227115-01
VELOCITA' SCUOTIM.	.171941-01	.293214-01	.741721-01
WFL. DEF. LAT. PNEUM.	.000000	.000000	.201950-01
CARTON SCUOTIMENTO	.3600.02	.3370.97	.000000
" LATERALE	.401.003	.165.035	.3002.00
" LONGITUDIN.	.262.710	.48.1220	.417.441
QUOTA PESO+CAR. SCUOT.	.0069.17	.3741.05	.54.9020
MOVIMENTO AUTALLIN.	.12.0671	.10.4077	.4005.60
" RFS. AL ROTOL.	.15.0001	.13.6695	.14.9416
" FRENANTE	.000000	.000000	.16.5600
WFL. CENTRO PUNTA	.24.4002	.24.4002	.000000
WFL. PORTA. PUNTA	.01.6600	.70.0076	.24.4760
SCUOTIMENTO	.172163-01	.343026-02	.01.2000
			.127349-01
			.332000-02

VELOCITA' DI ROTAZ.	SSSE P I L O T A C C I O SSSE	POTENZA DI POTOLAMENTO =	CV
448.120	= 4279.31 GIRI/1'	• POTENZA DI POTOLAMENTO =	6.98724 CV
34.7888	= 3.54583 KGM	• POTENZA AFRONTAMENTA =	9.24408 CV
POTENZA	= 21.1865 CV		
FANFALLA	.318696		
COPPIA VOLANTE	-1.42795	• PISIN TANTE FORZE EXT. RADIC.	.000000
MARCIA INSERITA	3	• PISIN TANTE MOM. EXT. MARIC.	.000000
DESS-CIRC-FREMIANTE	.000000	• PISIN TANTE COMP. VELLOC. VENTIN	.000000

RISULTATI ALL' Istante T = 2.5000

VELOCITA' KM/H = 80.1665 DACCIO EFFETTIVO = INFINITO
ACCELFRAZIONE LATRALE = -.335605-016 CONTINGENZA EFFETTIVA = .000000
SSSSS V E I C O L O SSSSS
X = 61.1449 VINI = 24.4001 AINX = .525354-01
Y = 3.24211 VINI = -.354134 AINY = -.330326
Z = .354700-01 VINZ = -.166213-01 AINZ = .124704-01
CURVATURA = -.540408-03 VMORX = 24.4853 AINXV = .500364-01
VFLCITA' = 24.4907 VMORV = .760355-01 AMORV = -.329307
RAGGIO = -1020.14 VMORZ = .510674 AMORZ = .140110-01
PASSO INT. = .200000-01 PSTAR = -.210309-01 PPUNTOS = .700697-01
CONTINGENZA = -.335915-01 USTAR = .100005-02 QPUNTOS = -.147703-01
INDICE FSV = .100654-01 RSTAR = .502961-02 QPUNTOS = -.237004-02

SSSSS ANGOLI VEICULO SSSSS
ANGOLI DI: VELOCITA' DI: ACCELERAZIONI DI:
ASSETTO VERN .307262-02 ANGOLI DI: PG 10P 33.05
ASSETTO MTS. .000000 PG 10P .09
IMBARDATA -.175320-01 PG 10P 16.45
RFFCMEGGIO .215423-01 PG 10P 3.45
ROLLIN .330439-02 PG 10P 21.65
VOLANTE .000000 PG 10P .05
PG 17P 10.15
PG 6P 0.05
-16 15P 3.15
PG 0P .05

SSSSS R U O T E SSSSS

ANT. SIN. POST. SIN. ANT. DES. POST. DES.
STERZO .000000 .000000 .000000 .000000
DIRIVA .333193-02 .267592-02 .333193-02 .267592-02
CONVERGENZA .100464-05 .100232-03 .463214-05 .953005-04
CAMPAURA .521792-03 .100003-01 .023020-03 .100003-01
CAMP. RTF. AL SUOLO .210793-01 .310585-01 .210585-01 .264036-01
SCUOTIMENTO .590056-02 .634450-01 .100592-01 .002033-01
VFLCITA' SCUOTIM. .200056-02 .100000-02 .347073-01 .290603-01
VEL. DEF. LAT. PNFUM. .000000 .000000 .000000 .000000
CARTON SCUOTIMENTO .3010.19 3004.02 3755.52
LATERALF .153.931 -150.514 -132.599
LONGITUDIN. 251.153 -49.0000 -52.4030
QUOTA PFSO+CAP.SCUOT. 4241.02 3910.44 4445.19
MOMENTO AUTOALLIN. 5.35200 3.50065 5.07833 4.40025
RFS. AL ROTOL. 15.0376 14.3001 16.7411 15.4731
EPIEVANTE .000000 .000000 .000000 .000000
VFL-CENTRO RUNTA 24.4943 24.4042 24.4042 24.4042
VFL-ROTAT. RUNTA 01.5076 00.0000 01.3903 00.0000
SCUOTIMENTO .157019-01 .334214-02 .136756-01 .336550-02

SSSSS P I L O T A C G T O SSSSS

VELOCITA' DI ROTAZ. 440.230 420.37 GRT/1' .000000
COPPIA 34.7001 3.5415 KGM .000000
POTENZA 15504.4 21.1017 CV .000000
FARFALLA .310005 .000000
COPPIA VOLANTE -.530005 .000000
MARCIA INSERITA 3 .000000
PRESS.CTRC.EPIEVANTE .000000 .000000
POTENZA DI ROTOLAMENTO = 0.01500
POTENZA AERODINAMICA = 0.25300

APPENDIX A.3-2

CURVMAGN COMPUTER SIMULATION MODEL

APPENDIX A.3-3

CURVMAGNCAR COMPUTER SIMULATION MODEL

APPENDIX A.3-4

PRESTMCC COMPUTER SIMULATION MODEL

The CURVMAGN program provides the values of the various magnetic quantities in the different sections in which the magnetic circuit of the DC electric machine is divided. The no-load magnetization curve is plotted, once the geometrical quantities of the magnetic circuit, the magnetic characteristic curve of the laminations and of the iron used are known together with the Lehman diagram at no-load relative to the salient pole and assuming the necessary approximations for what non-linear magnetic phenomena are concerned.

Simulation of the magnetization curve of a DC electric machine has proved to be reliable, after comparison with that obtained by means of the experimental data relative to a DC compensated electric machine.

The CURVMAGNCAR program provides the values of flux distribution in the air gap and draws by means of a plotter the magnetization curve under load conditions for all the values of current considered, once the geometric quantities of the magnetic circuit, the magnetic characteristic of the laminations, the Lehman diagram at load relative to the salient pole, the degree of compensation and the auxiliary poles excitation are known.

The PRESTMCC program provides the mechanical power curves versus motor speed as in motoring as in generating conditions, at different values of armature current with the following input data: supply voltage, geometric and magnetic quantities of the electric machine.

Furthermore this program provides the efficiency map of the motor/generator DC machine.